NEUTRON DOSIMETRY WITH A WATER CALORIMETER

by

Gordon Galloway

A thesis submitted for the degree of Doctor of Philosophy in the Faculty of Medicine, University of Edinburgh.

September, 1986

Preface

The work described in this thesis was carried out at the MRC Cyclotron Unit, Western General Hospital, Edinburgh between October, 1981 and October, 1984. A paper containing some of the results has already been published, a copy of which is bound at the back of this thesis. The research was carried out entirely by the author, and the thesis was composed solely by the author.

Acknowledgements

My sincere thanks go to Professor J R Greening who was responsible for instigating the project and for his guidance and helpful criticism throughout.

I am especially grateful to Mr J R Williams for his continual help and encouragement, and particularly for his assistance with the ionisation dosimetry of the neutron beam.

The help and co-operation of Mr T E Saxton, Mr R Goodall, Mr D B McKay, Mr D Arnott and the rest of the staff of the MRC Cyclotron Unit, Edinburgh is gratefully acknowledged.

For their skill in constructing the equipment I would like to express my thanks to Mr D Terrace and Mr A Hutton.

Thanks for his assistance with the electron beam measurements are extended to Dr D I Thwaites.

I am also indebted to Miss A K Wotherspoon and Mrs M A Galloway for their excellent work in typing the manuscript.

During the course of this work I was in receipt of the Whaitt Research Scholarship from the Faculty of Medicine for which I would like to express my gratitude.

Table of Contents

List of Illustrations

List of Tables

Abstract

In certain situations neutron radiotherapy has potential advantages over conventional X-ray therapy. It has yet to be conclusively proven that neutron therapy is more efficacious than X-ray therapy, and in many institutions worldwide neutron therapy is currently being evaluated. It is important that the dosimetry of neutron beams is consistent so that clinical results from different centres can be compared. Due to the relatively large uncertainties in the measurement of absorbed dose in neutron beams this consistency is difficult to achieve. This work describes the application of a recently developed dosimetry method, namely water calorimetry, to the field of neutron dosimetry.

The concept of absorbed dose and its measurement are discussed. The theory behind radiation calorimetry in general, and specifically water calorimetry, is outlined followed by a review of water calorimetry and calorimeters for neutron dosimetry. The calorimeter, which consists simply of a thermally insulated tank of water, and its construction are described. The temperature rise in the water was detected by a thermistor which was incorporated in a Wheatstone bridge circuit. The merits of different configurations of bridge circuit are discussed and the literature on the subject is reviewed. The circuit employed was an AC bridge having asymmetric, inductive ratio arms. The output of the bridge was detected by a lock-in amplifier and the signal was fed directly to a microcomputer which stored and analysed the data.

Absorbed dose measurements with the calorimeter were made in 4 and 9 MV photon beams, a 10 MeV electron beam and a d(15)+Be neutron beam. Calorimetric determinations of absorbed dose were compared, under identical conditions, with ionisation chamber dosimetry. In the 4 MV

and 9 MV photon beams calorimetric measurements of absorbed dose to water were respectively 4.0 and 4.5% higher than ionisation chamber measurements. In the 10 MeV electron beam calorimetric measurements were 5.5% higher. These differences are due to the heat defect in water which is discussed in detail. In the neutron beam absorbed dose measured with the calorimeter was compared with that measured using an Exradin tissue equivalent ionisation chamber. Doses measured with the ionisation chamber were calculated according to the European protocol for neutron dosimetry. Absorbed dose to tissue measured with the calorimeter was 4.4% lower than that measured with the ionisation chamber. Relative to ionisation chamber dosimetry, dose measurements with the calorimeter were approximately 9% lower in the neutron beam than in the photon beams. The implications of this result, and those from other water calorimeters, are fully discussed.

CHAPTER 1

THE MEASUREMENT OF ABSORBED DOSE

1.1 INTRODUCTION

In radiotherapy it is important to deliver prescribed radiation doses accurately. It is generally accepted that radiation delivered to within 5% of the prescribed dose is clinically acceptable (Moss et al 1973). The major difficulties in attaining this level of accuracy are obtaining reliable patient positioning and the irregular shape of the patient and the target volume. However, it is equally important that the dosimetry of the radiation beam is accurate, in order to deliver the desired dose.

Methods of specifying "radiation dose" have been evolving ever since radiation was first used for therapy. The amount of energy deposited per unit mass, termed the absorbed dose, is the most fundamental way of measuring energy deposition in a material. To completely characterise the energy deposition by a radiation beam, other factors are necessary, such as the type of radiation (X-ray, neutron etc.) and the energy spectrum of the beam. For any radiotherapy beam it is necessary to be able to measure absorbed dose and its spatial and temporal distributions. In the early days of radiation dosimetry it was not absorbed dose, but a unit called the roentgen which was used to quantify the amount of X-radiation. In 1928 the International Commission on Radiation Units and Measurements (ICRU) defined the roentgen, r, as a "quantity" of X-radiation which, in a free air chamber, produced a given amount of charge at STP. This quantity of X-

radiation was not given a name by the ICRU and this rather unsatisfactory situation existed until 1957. In 1957 the ICRU defined the quantity "exposure dose" and the roentgen became the unit of exposure, which was defined for gamma as well as X-radiation (ICRU 1957).

Although exposure gave a measure of the intensity of a photon beam, it was also desirable to measure the amount of energy deposited by a beam when it passed through a material. Thus in 1951 the ICRU stated, "For the correlation of the dose of any ionising radiation with its biological or related effects the ICRU recommends that the dose be expressed in terms of the quantity of energy absorbed per unit mass of irradiated material at the point of interest" (ICRU 1951). In 1954 they gave the name "absorbed dose" to this quantity of radiation and adopted the rad as the unit of absorbed dose (ICRU 1954). This also allowed other types of ionising radiation such as neutron and electron beams to be measured, since exposure, by definition, was only applicable to photon beams. Another limitation on the usefulness of the concept of exposure arises from the fact that the definition states that all the charged particles liberated by photons in the measuring volume are completely stopped in air. This necessitates the use of a free air chamber to measure exposure, with the requirement that charged particle equilibrium exists throughout the sensitive volume. Unfortunately charged particle equilibrium is only attainable for photon energies less than about 300 keV, at which point the size of the free air chamber becomes prohibitively large.

Absorbed dose, however, is a much more useful concept, being valid for all types of radiation and at all energies. The ICRU's first definition of absorbed dose was simply that it was the "quantity of

energy" absorbed per unit mass of the irradiated material at the point of interest and the rad was assigned the value 100 ergs/gram (ICRU 1954). This rather vague definition was made more precise by the ICRU in 1962 when it defined the absorbed dose, D, as "the quotient of ΔE_D by Δm where ΔE_D is the energy imparted by ionising radiation to the matter in a volume element; Δm is the mass of matter in that volume element" (ICRU 1962). This defined D as a macroscopic quantity which had to be averaged over the volume occupied by Δm. As the mass Δm (and the volume which it occupies) becomes smaller, the random statistical fluctuations in the value of D become larger, because the nature of the interaction is to deposit energy in discrete steps. Strictly speaking this defined D as a stochastic variable and not a continuous function of space and time, so terms such as absorbed dose gradient and absorbed dose rate could not be defined.

This has been resolved in the current ICRU definition (ICRU 1980) by defining the "energy imparted", ε, by ionising radiation to a mass dm as,

$$\varepsilon = \sum R_{in} - \sum R_{out} + \sum Q \qquad (1.1)$$

where $\sum R_{in}$ is the radiant energy incident on the volume, $\sum R_{out}$ is the radiant energy emerging from the volume and $\sum Q$ is the sum of all changes in rest mass energy of nuclei and elementary particles which occur in the volume (the $\sum R$'s do not include any rest energies). Absorbed dose is then defined as

$$D = \frac{d\bar{\varepsilon}}{dm} \qquad (1.2)$$

where $d\bar{\varepsilon}$ is the mean energy imparted by ionising radiation to the mass dm. This definition of ε ensures that only energy transferred from the radiation beam to the material, and not from any other source, is included in the absorbed dose. Also the specific energy, z, is defined as $z = \varepsilon/m$ and is a stochastic quantity. Absorbed dose is then rigorously defined as

$$D = \lim_{m \to 0} \bar{z} \qquad (1.3)$$

where $\bar{z}$ is the mean or expectation value of z. Thus absorbed dose is a continuous function which is defined at a point and therefore has a gradient and a rate. The SI unit of absorbed dose is the Gray (1 Gray = 1 J/kg = 100 rads).

1.2 METHODS OF ABSORBED DOSE MEASUREMENT

The dosimetry of clinical neutron beams is universally carried out with cavity ionisation chambers. Current protocols recommend the use of ionisation chambers constructed of tissue equivalent (TE) plastic, flushed with TE gas, for the determination of absorbed dose to tissue in fast neutron beams (Broerse et al 1981, AAPM 1980). Ionisation chambers have a high sensitivity and are therefore capable of very precise measurements. They are convenient instruments to use as measurements can be made quickly and easily. In neutron dosimetry it is necessary to employ a homogeneous chamber which is why TE chambers flushed with TE gas are used (see chapter six). Other combinations have also been used such as polyethylene chambers flushed with ethylene gas and polystyrene chambers flushed with acetylene gas. Ionisation chambers are generally not used as absolute instruments, but are calibrated in a known radiation field. Such a calibration is used to

determine the mass of gas within the cavity, which is otherwise difficult to determine accurately. This method also avoids the large uncertainty in the absolute value of W_N, the average energy required to produce an ion pair in the gas, in the neutron beam. The calibration and use of a TE ionisation chamber is discussed fully in chapter six. The neutron beam from the MRC cyclotron in Edinburgh is produced by a beam of 15 MeV deuterons impinging on a beryllium target; the notation d(15)+Be will be used. At this energy the uncertainty in determining absorbed dose to tissue with a TE ionisation chamber is 6.5% (Mijnheer and Williams, 1981).

Calorimetry is the only truly absolute method of determining neutron absorbed dose. It has the fundamental merit that it measures energy deposition directly, by measuring the heating produced by a radiation beam. The response of a calorimeter is independent of neutron energy and additional information, such as the average energy required to produce an ion pair or neutron cross section data, is not required. Unfortunately calorimetry is relatively insensitive due to the small amounts of energy deposited by medical therapy beams. Calorimeters are slow and cumbersome to use and are therefore not suitable for routine use. They are more useful as standard instruments against which other secondary dosimeters can be calibrated. Calorimeters for neutron dosimetry have generally been constructed with isolated TE plastic absorbers. Absorbed dose to the plastic is obtained by measuring the temperature rise produced in the absorber by the radiation beam. The accuracy to which absorbed dose to tissue can be measured with such a calorimeter is similar, or marginally better, than that attainable with a TE ionisation chamber.

Recently a radically different type of calorimeter, known as the water calorimeter, has been developed. It was first described by Domen (1980) who used it to measure absorbed dose in a cobalt-60 gamma ray beam. Essentially a water calorimeter consists of a large thermally insulated tank of water in which a thermistor is suspended. Absorbed dose to the water, at the position of the thermistor, is obtained from the temperature rise experienced by the thermistor and the specific heat of water. Domen (1982) measured absorbed dose rates in water of 100 cGy min^{-1} with a precision of about 0.5%. To date there have been no reports of other investigations in which a water calorimeter has been used for neutron dosimetry.

Ionisation chambers and calorimeters are the two principal instruments used to measure absorbed dose in a neutron beam. There are several other methods but they are all significantly less accurate and are therefore not suitable for clinical dosimetry. Proportional counters constructed of TE plastic have been used in neutron dosimetry. In theory it is possible to discriminate between the neutron component and the gamma ray component of absorbed dose with a proportional counter. However, this is difficult to achieve in practice. The purity of the gas within the counter has also been a problem. The overall uncertainty in measuring neutron absorbed dose with a proportional counter is greater than 10%. Geiger-Muller counters are not suitable for measuring neutron absorbed dose but are useful for measuring the associated photon component, in conjunction with an ionisation chamber. They have a very low sensitivity to neutrons which makes them ideal for this purpose.

Activation methods have been used to measure neutron absorbed dose but are more useful for determining neutron spectra, by making use of

the different thresholds of nuclear reactions. Neutron fluence can be measured with an activation detector but the calculation of absorbed dose requires an accurate knowledge of spectral composition, kerma factors and cross-section data. For fast neutrons the uncertainty in determining absorbed dose is large because of the uncertainty in these basic data. Fission chambers, where the ionisation caused by fission fragments is detected, have also been used. With this method it is possible to discriminate against gamma rays because the energy deposited by the fission products is much greater than that deposited by the accompanying gamma rays.

Photographic emulsions and thermoluminescent materials can be used, although both of these methods are more sensitive to gamma rays than to neutrons. The sensitivity to neutrons can be increased by incorporating a hydrogenous material into the dosimeter. The accuracy of these methods is not sufficient to allow their use as clinical dosimeters but they have been widely used in radiation protection, particularly for personnel monitoring. Photographic film is also useful for quickly determining the position and size of a neutron beam.

Attempts have been made to use ferrous sulphate dosimeters in neutron dosimetry. This requires the determination of the radiation chemical yield, G, for fast neutrons, which has been done by comparing the ferrous sulphate method with other dosimetric methods. The uncertainty in determining absorbed dose with a ferrous sulphate dosimeter is therefore greater than that of the method used for calibration. For this reason and because of the technical complexity of the method, it has been little used in neutron dosimetry.

1.3 AIMS OF THE PROJECT

It has already been stated that the uncertainty in determining absorbed dose to tissue with a TE ionisation chamber, in a d(15)+Be neutron beam, is 6.5%. This is due to uncertainties in the factors required to calculate absorbed dose to tissue from ionisation chamber measurements. These factors depend on measurements of quantitities such as kerma factors for hydrogen, carbon and oxygen, and the average energy required to produce an ion pair in TE gas irradiated by neutrons. Although the basic data are always improving it is unlikely that the uncertainty in the ionometric determination of absorbed dose will be significantly decreased in the near future. The most promising alternative to ionisation dosimetry is absorbed dose calorimetry. Several neutron absorbed dose calorimeters employing absorbers made of TE plastic have been reported (Bewley et al 1974, McDonald et al 1976, Caumes et al 1984), as well as one employing a polyethylene absorber (Greene et al 1975). However, TE plastic calorimeters, like TE ionisation chambers, measure absorbed dose to the plastic. This has to be converted to absorbed dose to standard tissue (ICRU muscle) using the ratio of kerma factors for the two materials. The uncertainty in this kerma ratio is a major contributor to the overall uncertainty in measuring absorbed dose to tissue with a TE plastic dosimeter. Moreover, the uncertainty in this kerma ratio increases rapidly with increasing neutron energy. For instance one assessment (Bewley 1980) puts the uncertainty in the kerma ratio at 2.6% for a d(16)+Be spectrum and 10.6% for a p(66)+Be spectrum. At the higher energy the uncertainty in the kerma ratio of ICRU muscle to water is only 1.8%. This is because the matching of oxygen content between water and tissue is far better than for TE plastic, and the mismatch of hydrogen content

is less important due to the accuracy to which the hydrogen cross-section data are known. A direct measurement of neutron absorbed dose to water would avoid the large uncertainty in the ICRU muscle to TE plastic kerma ratio. A water calorimeter could therefore provide a more accurate method of measuring neutron absorbed dose, particularly for high energy neutron beams.

Water calorimeters have been used successfully to measure absorbed dose in photon and electron beams (de Marles 1981, Domen 1982, Kubo 1983, Schulz and Rothman 1983, Mattsson 1984). They are ideally suited for this purpose since water is the standard reference material for these radiations. The heat defect in water is a major obstacle in using a water calorimeter to measure absorbed dose absolutely. The heat defect is due to chemical reactions being induced in the water by the radiation. Such reactions, which will affect the temperature rise measured by the calorimeter, can be either exo- or endothermic and will cause the calorimeter to respectively over or underestimate the absorbed dose. The problem of the heat defect is discussed in more detail in subsequent chapters. The development of the water calorimeter can therefore be considered as consisting of two distinct stages. Firstly, the method must be proved as a reliable way of measuring the temperature rise, induced by a radiation beam, at a point in a mass of water. Secondly, the heat defect must be accurately determined in order that water calorimeters can be used to measure absorbed dose absolutely. The heat defect is not necessarily the same for different conditions of irradiation. It must therefore be determined for radiation beams of different energy and different LET.

The aim of the work reported here is to develop a water calorimeter to measure neutron absorbed dose. The calorimeter is to be irradiated in the d(15)+Be neutron beam generated by the cyclotron at the Western General Hospital, Edinburgh. Calorimetric measurements will then be directly compared with measurements made with a TE ionisation chamber, which is the method used for the clinical dosimetry of the neutron beam.

CHAPTER 2

PRINCIPLES OF RADIATION CALORIMETRY

2.1 ABSORBED DOSE CALORIMETERS

Apart from absorbed dose, calorimeters have also been used to measure the energy fluence of radiation beams and the activity of radioactive sources. Only calorimeters employed to measure absorbed dose will be considered here. Although calorimetry is a very direct way of measuring absorbed dose, calorimeters do suffer some limitations. Their sensitivity is adequate for the doserates encountered in therapeutic and diagnostic applications but is insufficient for radiation protection purposes. Certain radiation processes can lead to the loss of some of the energy which should be detected by the calorimeter, or to the gain of energy from sources other than the radiation beam. This can occur if exo- or endothermic chemical reactions are induced by the radiation or if energy is stored in or liberated from a crystal lattice in the calorimetric material. However, many calorimeters have been used successfully for the measurement of absorbed dose. This chapter discusses the theory behind absorbed dose measurement using a water calorimeter, and the last section reviews neutron absorbed dose measurement by calorimetry and the use of water calorimeters for absorbed dose determination.

2.1.1 Structure of Calorimeters

Since its development in the 1950s virtually all radiation calorimeters have employed the thermistor as a temperature transducer. Its

high temperature sensitivity and its small size make it ideally suited for the purpose. Platinum resistance thermometers, which were the standard method of resistance thermometry before the advent of the thermistor, have a temperature coefficient which is approximately a factor of ten lower than that of a thermistor. Hence the thermistor has revolutionised radiation calorimetry, enabling more precise measurements to be made and lower doserates to be measured.

In the last 30 years most calorimeters for beam dosimetry have been of the "isolated absorber" type. Such a calorimeter consists of a thermally isolated core - or absorber - surrounded by a jacket, which is itself often surrounded by a mantle. The temperature of the jacket is either held constant or constrained to rise at the same rate as that of the absorber. The size of the absorber is generally small enough that the absorbed dose is uniform throughout its volume, and the temperature rise of the absorber is measured by a thermistor. The calorimeter is normally evacuated in order to reduce conductive and convective heat transfer and the dominant mode of heat transfer is by radiation. Some calorimeters have been operated at low temperatures to reduce radiative heat transfer. However there are heat conduction paths in the structures used to suspend the absorber inside the jacket and in the wires connecting the thermistor to the measuring device. Such calorimeters have had absorbers made of various different substances including tissue equivalent plastic, aluminium, magnesium, graphite and water filled containers. Such calorimeters were not normally designed to measure the absolute temperature rise of the absorber, but were calibrated by comparing the calorimeter's response during irradiation with its response to a known amount of electrical heating introduced into the absorber.

Domen (1980) described the first water calorimeter which was a radically different approach to absorbed dose calorimetry. The water calorimeter has no isolated absorber and the absorbed dose at a point is inferred from a measurement of the temperature rise at a point in the extended water medium. The calorimeter consists of a tiny thermistor suspended at a fixed height in a large tank of water (see figure 3.1 in chapter 3). To hold the thermistor at a fixed depth and to electrically insulate it from the water the thermistor is sandwiched between two polyethylene sheets. The sheets are held clamped between two perspex rings which sit on three perspex rods fixed to the bottom of the tank. The temperature rise produced by a vertical radiation beam is measured by the thermistor. The absorbed dose can be calculated from the equation

$$D = c \Delta T \qquad (2.1)$$

where c is the specific heat of water and ΔT the temperature rise. Since convection does not occur and heat conduction in the water is negligible (see sections 2.1.3 and 2.1.4), absorbed dose is obtained from a measurement of ΔT and the value of c, which is well known.

The design of the water calorimeter has certain advantages over the isolated absorber type of calorimeter. Ideally a measurement of absorbed dose would be made at a point and the water calorimeter comes closer to this ideal than those calorimeters with an isolated absorber. The measured temperature rise in an isolated absorber is necessarily representative of the average temperature rise in the whole absorber. In turn the absorbed dose measurement represents the average absorbed dose within the absorber. Although the dimensions of the absorber are

generally small, particularly along the axis of the beam (typically a few millimetres), the absorbed dose measurement is not as localised as it is with the water calorimeter. Solid calorimeters consist of several nested bodies separated by vacuum gaps. Vacuum gaps change the absorption and scattering of radiation in a complex fashion which is difficult to evaluate. The water calorimeter has no such gaps; an absorbed dose measurement being very similar to a standard measurement with an ionisation chamber in a water phantom. The standard method of obtaining absorbed dose in a solid calorimeter is to compare the heating produced by irradiation with the electrical energy required to heat the absorber by a similar amount. This involves incorporating some kind of electrical heater into the absorber, usually a resistive wire, which has the undesirable effect of introducing further foreign material into the absorber. Absorbed dose is determined in the water calorimeter by an absolute measurement of the temperature rise, therefore no form of electrical heating is required.

One of the main advantages of the water calorimeter is its simplicity, which is in direct contrast to the complex construction of solid calorimeters. The absorber must be held suspended within, and completely surrounded by, the jacket. In turn the jacket is similarly contained within the mantle. If there is some temperature regulation of the jacket and mantle, electrical connections for temperature sensors and heaters are required for all three parts of the calorimeter. Finally the whole calorimeter is inside a vacuum tight container. Clearly the initial construction and any subsequent repair of such a calorimeter is not an easy task. The water calorimeter, which is described in detail in Chapter 3 is a much simpler device. One

advantage of solid calorimeters is that it is possible to operate them adiabatically or quasi-adiabatically. If the jacket and mantle contain temperature sensors and heaters their temperature can be controlled, either through a feedback mechanism or through a predetermined heating cycle, to follow that of the absorber. If adiabatic conditions are achieved no corrections need be applied for heat transfer, to or from the absorber, during a measurement. However, in practice it is difficult to achieve truly adiabatic conditions and the small remaining heat losses can be difficult to correct for.

2.1.2 Choice of Absorbing Material

The absorbing material in a water calorimeter is obviously water. However, any other liquid could equally well be used, for example a tissue equivalent liquid, as long as its specific heat was known and its thermal properties were similar to those of water. The absorbing material in a solid calorimeter is that from which the absorber is constructed. Normally the jacket is constructed from the same material to provide a homogeneous absorbing medium. There are many different factors affecting the choice of absorbing material and many different materials have been used in solid calorimeters, as was indicated at the beginning of this chapter.

A material having a low heat capacity is desirable since the temperature rise for a given heat input is inversely proportional to the heat capacity of the material. A material exhibiting a negligible, or well known, heat defect is necessary to enable an accurate calorimetric measurement to be made (see section 2.1.7). On both these counts water is a poor choice of absorbing material, but there are other reasons why a direct measurement in water has been carried out. The way in which

radiation deposits energy in water is very similar to the way it is deposited in tissue. Water is therefore the standard reference material, recommended by the ICRU (1969), in which absorbed doses should be quoted for photon and electron beams. Depth dose measurements and standard calibrations of dosemeters are normally carried out in a water phantom or one made of a material whose radiation absorbing properties are similar to those of water.

For dose measurements in a neutron beam absorbed dose in a standard tissue composition, known as ICRU muscle, is recommended (ICRU 1977). This is because the exact elemental composition of a material has a large effect on the absorbed dose; in particular the hydrogen content of a material is very important in determining the absorbed dose which will be observed in a material. It is impractical to measure neutron absorbed dose in standard tissue and dosemeters constructed of tissue-equivalent plastic have been routinely used. The absorbed dose to the plastic must then be converted to absorbed dose in ICRU muscle using the ratio of kerma factors for the two materials. The uncertainty in the kerma ratio of water to ICRU muscle is considerably smaller than that of tissue-equivalent plastic to ICRU muscle, making a direct measurement in water attractive. It has been recommended that depth dose measurements in a neutron beam be carried out in a water phantom (Broerse et al 1981, Awschalom et al 1983). One reason for recommending water is that scaling absorbed dose measurements from water to standard tissue can be done more accurately than scaling from a tissue-equivalent liquid to standard tissue. For all of these reasons a method of directly measuring absorbed dose in water, such as the water calorimeter, is a valuable development in the field of radiation dosimetry.

2.1.3 Convection

Probably the main reason that water calorimeters were not investigated until recently was the assumption that convection currents would immediately disturb any temperature gradients that were set up in the water by a radiation beam. In fact this is not true, and the temperature gradients produced by a medical therapy beam are small enough that no convection occurs.

Conditions required for the onset of convection have been discussed theoretically by McLaughlin (1964) and recently Verlarde and Normand (1980) have discussed the phenomenon in general. Even though buoyant forces may exist in a liquid (because of a vertical temperature gradient) convection does not occur until the dimensionless Rayleigh number (R) exceeds a certain critical value. For simple geometries such as two parallel planes or concentric cylinders the critical value of R is approximately 1000. The Rayleigh number is the product of two independent quantities; the Prandtl number (P_r) and the Grashof number (G_r) given by

$$\left.\begin{aligned} G_r &= g\ \phi\ \rho^2\ \Delta T\ d^3 / \eta^2 \\ \text{and}\quad P_r &= \eta\, C / k \end{aligned}\right\} \quad R = G_r P_r \qquad (2.2)$$

where

g is the gravitational force per unit mass

ϕ is the volumetric expansion coefficient

ρ is the density

ΔT is the temperature difference between two horizontal planes

d is the distance between the planes

η is the viscosity

C is the specific heat

k is the thermal conductivity

The Grashof number is a measure of the relative importance of the buoyancy and viscous forces in the liquid, and the Prandtl number is a measure of the ratio of the molecular diffusivity of momentum to the molecular diffusivity of energy.

During a calorimetry measurement the maximum temperature rise in the water would be approximately 1 mK (equivalent to 420 cGy), and would occur at the build-up depth. Inserting this figure into equation 2.2 gives a Rayleigh number of 1000 when the separation (d) is 4 cm. This indicates that for two horizontal planes, where the temperature of the lower plane is 1 mK above that of the upper plane, convection would be expected if the separation of the planes was greater than 4 cm. This calculation gives the first indication that the temperature rises involved may be smaller than those required to produce convection. Below the build-up depth in an irradiated water tank the water temperature decreases with depth and there should not therefore be any buoyant forces in the water if the radiation beam is vertical.

However, the temperature rises discussed so far are small compared to the temperature rise caused by power dissipation in the thermistor. The problem of power dissipation in the thermistor is fully discussed in section 4.5.2 and the temperature rise has been measured to be 4.0 mK per microwatt of power dissipation. Typically the thermistor was 50 mK above the temperature of the bulk of the water, with an equilibrium temperature gradient surrounding the thermistor. These sharp temperature gradients around the thermistor provide a sensitive arrangement for detecting movement in the water. Any movement would

disturb the equilibrium temperature gradient around the thermistor, resulting in a cooling of the thermistor. Such a rapid cooling of the thermistor was observed if the side of the calorimeter was gently tapped: the temperature of the thermistor would instantly drop and then return to its equilibrium value within approximately one minute. Temperature changes of 10 μK were easily detectable and much larger changes than that would be expected if convection currents were to disturb the temperature gradient around the thermistor. The fact that long periods of stable drift were observed, such as in figure 2.2, was the most convincing evidence that convection did not occur in the calorimeter. Equally stable drifts were obtained with power dissipations of up to 30 μW in the thermistor. Domen (1982) carried out water calorimetry measurements with convection barriers close to the thermistor. These were compared with measurements in the absence of the convection barriers but the results, with or without the barriers, were identical.

Schulz and Weinhous (1985) have investigated this problem experimentally using a water calorimeter which had two temperature sensors, 3.8 cm apart. To ease calorimetry measurements they used a high doserate of 16 Gy min^{-1}. At this doserate convection would be more likely to occur than at the doserates of 200-300 cGy min^{-1} which are typical of linear accelerators. They concluded that no convection occurred if the calorimeter was irradiated vertically, by a broad beam irradiating the whole of the calorimeter. Convection was detected when the calorimeter was irradiated horizontally, and this disappeared if the calorimeter was operated at $4^{o}C$. Had lower doses been delivered to the calorimeter this convection might not have been present.

Hence it was concluded that for broad beam vertical irradiation the temperature gradients produced by the radiation beams employed in this work were well below the level required for the onset of convection.

2.1.4 Conduction

Even in the absence of any convection the natural fate of a temperature gradient in a water tank would be for it to be dissipated by conduction of heat from the hotter areas to the cooler areas. This is why, in a solid calorimeter, the absorber is thermally isolated from its surrounding jacket, generally by suspending it within the jacket and evacuating the gap between the two. Calorimetry measurements are possible in an extended water medium, without recourse to such complications, because the rate of heat conduction in water is slow.

Since the temperature rise is proportional to the absorbed dose, a broad radiation beam directed vertically downward on a tank of water produces an axial temperature profile similar in shape to the depth dose curve for that particular radiation. As soon as irradiation begins and a small temperature gradient appears, heat conduction will also begin. If the beam is broad and flat there will be no temperature gradient in planes perpendicular to the axis of the beam and heat conduction will only occur in the direction parallel to the beam axis. Domen (1982) has calculated the change in profile of such a temperature gradient. He used a numerical method described by Schmidt (1924) to determine the temperature change. His calculations showed that for an instantaneous pulse of a broad beam of cobalt-60 radiation, the temperature rise at a depth of 5 cm in water would decrease by only 0.02% of the initial rise in 4 minutes. There are two reasons for this. Firstly, the fact that water has a low thermal diffusivity means that temperature changes are

intrinsically slow to occur in water. Secondly, the temperature rise produced by the radiation beam decreases, to a first approximation, linearly with depth resulting in essentially the same amount of heat entering as leaving the point of measurement. Although this simplified calculation of the change in temperature caused by conduction may not be an accurate representation of what would occur in practice, it gives an idea of the magnitude of the changes that would be expected. Rothman and Nath (1983) developed an equation describing the heat diffusion in a water calorimeter. The equation was solved analytically to predict the temporal variation of the temperature distribution for different initial conditions. In general they concluded that temperature changes caused by heat conduction were small; several hours being required for the re-establishment of thermal equilibrium after irradiation. In view of the very small effects which would be expected it was concluded that, for calorimeter runs lasting a few minutes, corrections for heat condution would be negligible.

For narrower radiation beams heat conduction in the radial direction (perpendicular to the beam axis) might become important and significant corrections might be required. For this reason all the experiments in this thesis were carried out with broad beams covering most, if not all, of the water tank. The low thermal diffusivity of water can be illustrated by comparing it to the thermal diffusivities of metallic elements. The thermal diffusivity of water is 1.44×10^{-7} $m^2\ s^{-1}$. The thermal diffusivities of aluminium and graphite, two materials from which solid calorimeters have been constructed, are 2.19×10^{-4} $m^2\ s^{-1}$ and 1.65×10^{-4} $m^2\ s^{-1}$ respectively. The thermal diffusivity of water is three orders of magnitude lower than that of

these materials, giving one indication that heat conduction in water is slow.

2.1.5 Calibration

There are three methods of calibrating a radiation calorimeter: (a) by irradiation in a known radiation field, (b) by calibration of the thermistor in terms of temperature and (c) by comparing the temperature rise produced by irradiation with that produced by a known amount of electrical heating. Calibration in a known radiation field defeats the purpose of using the calorimeter as an absolute instrument and will not be considered further. The comparative method of calibration is commonly employed in solid calorimeters where there is an isolated absorber. A heater wire is embedded in, or wrapped around, the absorber to simulate the heating produced by irradiation. A knowledge of the resistance of the heater wire and a measurement of current through, or the voltage across, the wire gives an accurate measure of the heat input to the absorber. The electrical energy input to the absorber divided by its mass is exactly analogous to the absorbed dose when the calorimeter is irradiated. By comparing the response of the thermistor during electrical calibration to its response when irradiated, the absorbed dose can be determined. Although attractive because the measurements are easy to carry out this method does have some drawbacks. During calibration all of the heat is dissipated within the wire resulting in steep temperature gradients within the absorber, whereas during irradiation the heat is deposited virtually uniformly throughout the absorber. The temperature rise measured by the thermistor, for equal heat inputs, may be different in the two cases since the thermistor measures temperature at a point. This can, to some

extent, be overcome by using an absorber constructed of a resistive material, such as conducting plastic, so that the electrical heating within the absorber is uniform. Another disadvantage of the comparative method is that foreign material (the heater wire and connections) is incorporated into the absorber. Any foreign material in the absorber is undesirable since the absorbed dose and the resultant temperature rise will differ in the two materials.

It is impractical in a water calorimeter to employ the comparative method of calibration because there is no isolated absorber. The other method was therefore used; that is to calculate the absorbed dose from an absolute measurement of the temperature rise of the thermistor. The absorbed dose is calculated from equation 2.1 by multiplying the temperature rise by the specific heat of water. The specific heat of water is accurately known and the values given by Kaye and Laby (1973) were used. To determine the temperature rise with a thermistor it is necessary to calibrate the thermistor against a standardised thermometer. A conventional mercury in glass thermometer, which was calibrated at the National Physical Laboratory, was used to calibrate the thermistor and details of this calibration are given in section 4.5.

2.1.6 Foreign Materials

Any foreign material near the point of measurement (including the thermistor) will affect the temperature rise observed in a water calorimeter. The aim of the water calorimeter is to measure absorbed dose to water at a point in a large homogeneous mass of water. Materials other than water will have different heat capacities and receive different absorbed doses, and will consequently exhibit

different temperature rises during irradiation. The amount of such materials must therefore be small enough for their effects to be negligible, or the effect must be calculated and corrected for. The detector (briefly described in section 2.1.1) consists of a thermistor sandwiched between two layers of polyethylene. In a sphere of diameter 10 mm around the thermistor, the thermistor, its leads and the polyethylene take up 0.8% of the volume of the sphere; the other 99.2% being water. As the thermistor is small it is the polyethylene sheets that produce the most significant thermal effect.

The absorbed dose in polyethylene and water differs by a few percent in the photon and electron beams and approximately 25% in the neutron beam but the specific heat of polyethylene is approximately half that of water. This difference in heat capacity is the dominant factor and causes the temperature rise in the polyethylene sheets to be almost double the temperature rise of the surrounding water. There will be a sharp thermal gradient between the polyethylene and the water which will cause heat to be conducted from the polyethylene to the surrounding water, until they reach the same temperature. As the thermistor is sandwiched between the polyethylene sheets any residual excess in the temperature of the polyethylene will cause the thermistor to overestimate the temperature rise in the water. Details of the evaluation of this excess temperature in the polyethylene are given in chapter 7. It is shown that only very small corrections are required.

2.1.7 Heat Defect

The heat, or thermal, defect is a major problem in all radiation calorimeters. The absorbed dose (D) in a small mass Δm is defined as

$$D = \frac{\Delta E_D}{\Delta m} = \frac{\Delta E_h}{\Delta m} + \frac{\Delta E_s}{\Delta m}$$

where ΔE_D is the energy imparted to the mass by ionising radiation and ΔE_h is the energy which appears as heat. ΔE_s is the difference between the two and is known as the heat defect. The heat defect arises because of exo- or endothermic chemical reactions induced in the material by the radiation. To determine the absorbed dose by measuring the heat produced requires a knowledge of the heat defect in the irradiated material. This point was succinctly put by Laughlin and Genna (1966): "Exothermic reactions do not contribute to the dose, and endothermic reactions cannot deplete it, because these reactions involve energy only in a nonionising degraded form." Several solid calorimeters have had absorbers constructed of pure elements (for example, carbon) because they exhibit a negligible heat defect since no chemical reactions occur. However, even in a pure element energy can be taken up by, or liberated from a crystal lattice, resulting in a non-zero heat defect. Small amounts of dissolved oxygen, which often occur in plastics, can also result in a significant heat defect.

In a water calorimeter irradiation can induce chemical reactions between the constituents of the water. The radiation chemistry of water is complex and has been discussed by Fletcher (1982), specifically because of the interest in water calorimetry. Fletcher lists thirty-nine different reactions that are possible in pure water. These include reactions between hydrogen ions, hydroxyl ions, molecular hydrogen, hydrogen peroxide, free electrons and other more exotic species. The overall energy balance was calculated by a computer and the results depended on the initial concentrations of H_2, O_2 and H_2O_2, the pH and

the doserate. The predicted chemical effects could be either exo- or endothermic depending on the initial conditions. Fletcher's calculations do not point to a constant, easily determined value for the heat defect in water. However, several water calorimeters have been compared with other standard methods of dosimetry (de Marles 1981, Domen 1982, Kubo 1983, Schulz and Rothman 1983, Mattsson 1984) and consistent results suggesting an exothermic heat defect of 3-5% have been reported. However these results were all obtained with low LET radiation. The heat defect in water irradiated by high LET radiation (e.g. neutrons) may be quite different. The heat defect is the largest uncertainty in determining absorbed dose with the water calorimeter and this is discussed further in chapter 9.

2.2 CALORIMETRIC METHODS

Three methods of carrying out a calorimetric measurement can be distinguished; these are (a) isothermal calorimetry, (b) adiabatic calorimetry and (c) constant-temperature-environment calorimetry. In an isothermal calorimeter the whole system is constrained to remain at a fixed temperature and the heat deposited in the core of the calorimeter is measured by the change in state in one of the constituents of the core. The only noted use of this method for radiation calorimetry is in calorimeters consisting of an equilibrium mixture of ice and water (e.g. Holm et al 1961). Such calorimeters suffer difficulties in maintaining thermodynamic equilibrium but have been used successfully at high doserates (> 1000 cGy min^{-1}). However the isothermal method is clearly inappropriate in the case of the water calorimeter. The adiabatic (or quasi-adiabatic) method has been used with solid calorimeters. In a

truly adiabatic calorimeter the temperature of the jacket and mantle surrounding the absorber must be made to follow exactly the temperature of the absorber. This ensures that there is no heat transfer to or from the absorber during a measurement, and that no corrections for heat transfer are required. In the quasi-adiabatic mode a small and constant thermal head is maintained between the absorber and the jacket throughout the measurement. Both the adiabatic and quasi-adiabatic methods often employ heating wires to raise the temperature of the jacket at the same rate as the radiation beam increases the temperature of the absorber. Alternatively, if the jacket is also irradiated, and is made of the same material as the absorber, their temperatures will rise at the same rate. It is not practical to operate a water calorimeter adiabatically and the method known as constant-temperature-environment calorimetry must be employed.

As its name suggests constant-temperature-environment calorimetry involves surrounding the calorimeter with a jacket which is held at constant temperature. Considerable heat transfer to or from the calorimeter core is acceptable as any energy transfer can be evaluated, and corrected for, by the laws governing heat flow. For the water calorimeter described fully in chapter 3, the constant temperature jacket is that provided by the layer of air around the calorimeter (figure 3.1), which is maintained at a fixed temperature (T_J) by a thermostatic control. This situation is shown schematically in figure 2.1, where T_s represents the temperature of the thermistor. The heat flow between the water (at temperature T_W) and the jacket (T_J) is proportional to the difference in their temperatures and can be expressed by Newton's law of cooling

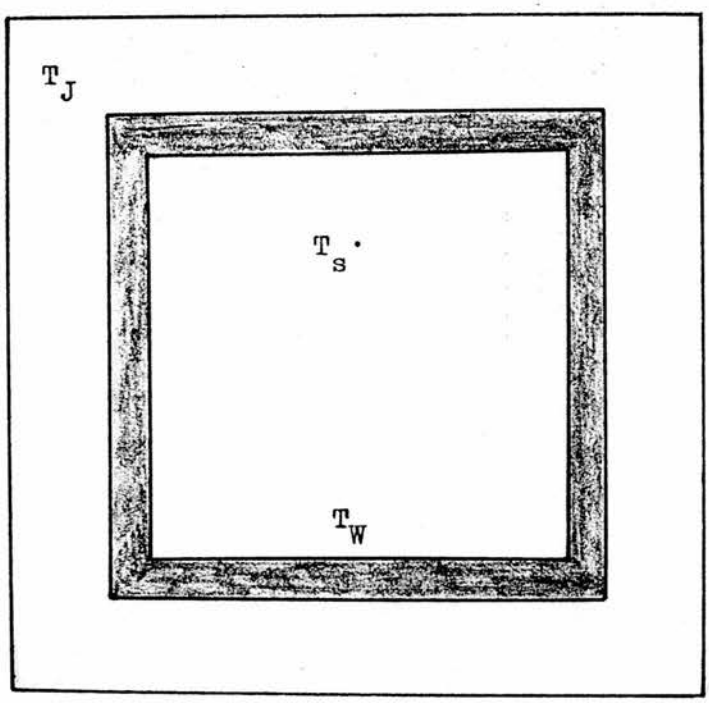

Figure 2.1 Temperature gradients within the calorimeter.

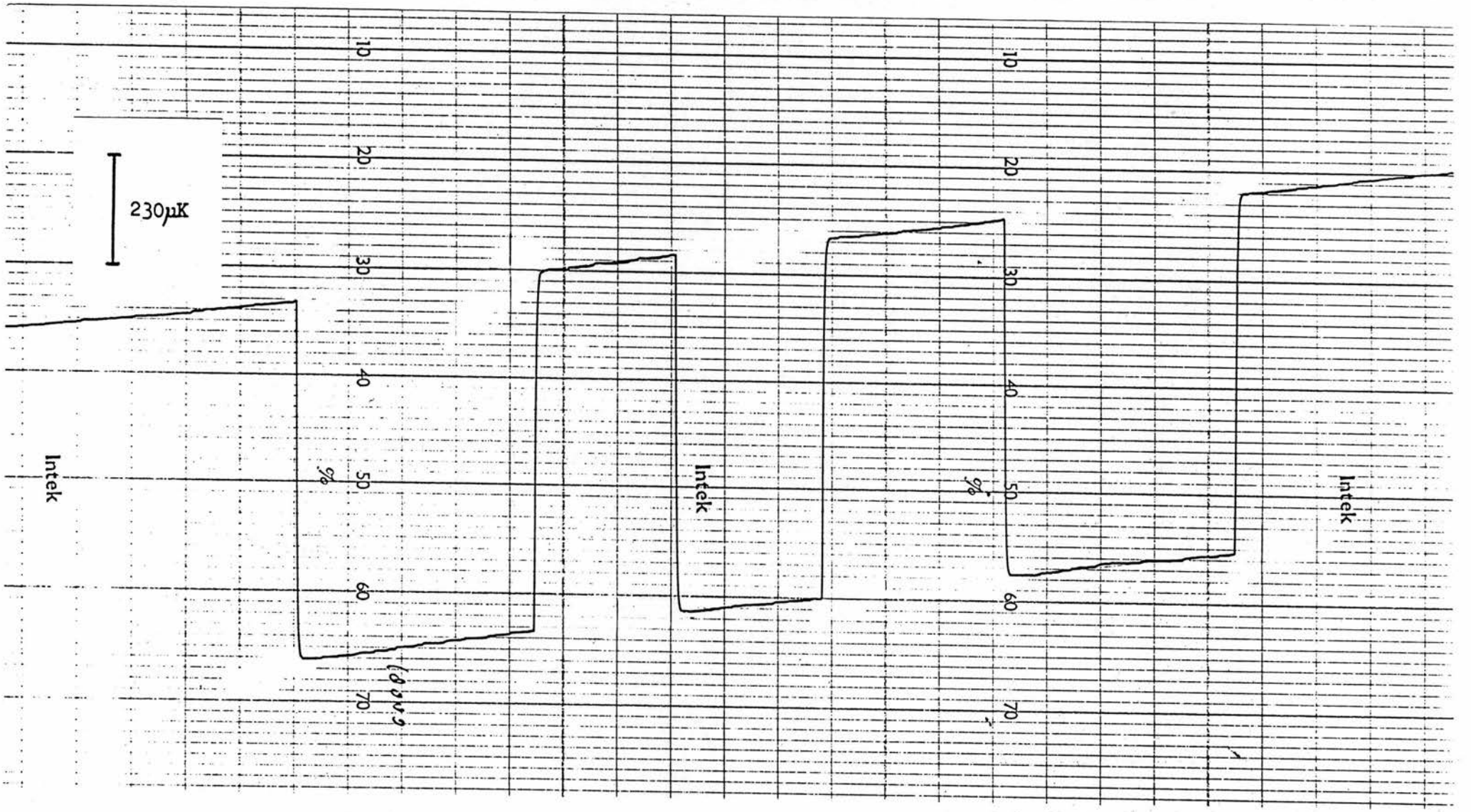

Figure 2.2 A stable heating drift with resistance calibrations superposed

$$\frac{dE}{dt} = -A\sum_i h_i \, (T_W - T_J) \qquad (2.3)$$

where $\sum_i h_i$ is the summation of the heat transfer coefficients for radiation, conduction and convection, and A is a constant. Since dE = mcdT, where m is the mass of the water and c is the specific heat of water, substituting $K = (A/mc)\sum_i h_i$ into equation 2.3 gives

$$\frac{dT_W}{dt} = -K \, (T_W - T_J) \qquad (2.4)$$

The coefficient K, known as the leakage modulus, is equal to the rate of change of temperature of the water per unit temperature difference with respect to the jacket. Although to be strictly accurate T_W should be the temperature of the water at its surface, assuming that the temperature of the water is uniform means that the water temperature in equation 2.4 can be replaced by the temperature of the thermistor, giving

$$\frac{dT_s}{dt} = -K \, (T_s - T_J) \qquad (2.5)$$

Figure 2.3 illustrates an idealised record of time against temperature for a calorimetry measurement where the jacket temperature is lower than that of the water. This analysis is similar to that of Laughlin and Genna (1966) where the periods t_1 to t_i and t_f to t_2, before and after the introduction of thermal energy, were known as the initial and final "rating" periods. During the rating periods the temperature of the thermistor drifts towards the jacket temperature. In figure 2.3 this drift is shown as a straight line. This represents the short term

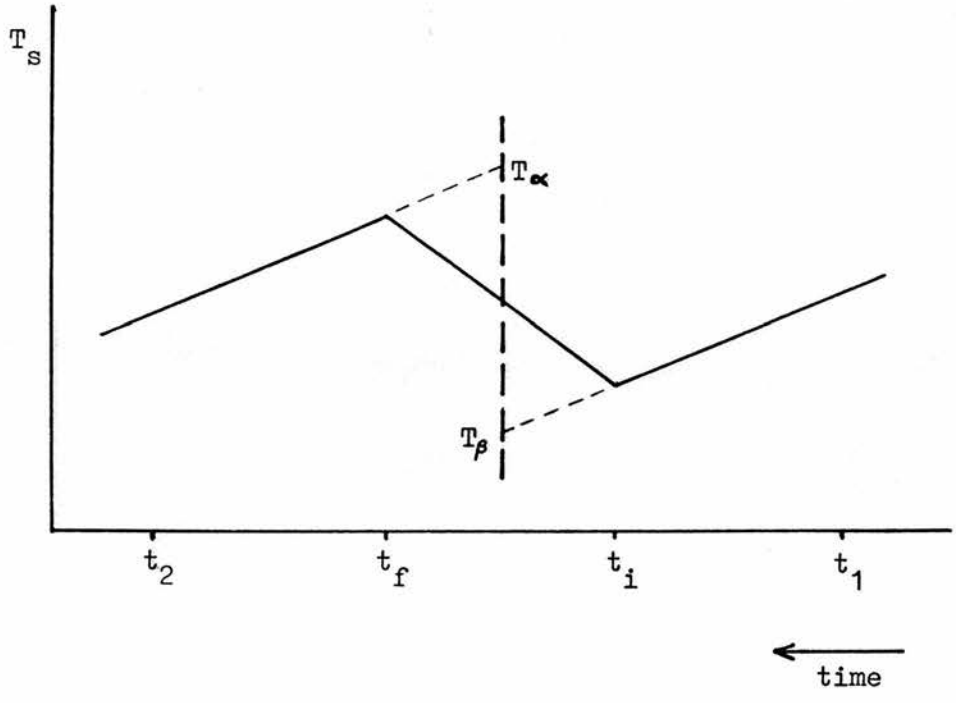

Figure 2.3 Schematic calorimeter heating curve

approximation of the exponential approach to the equilibrium temperature (T_J) according to the solution of equation 2.5. The leakage modulus can be evaluated from the drift rates during the two rating periods. If the rates of temperature change during these periods at temperatures T_i and T_f are measured, then from equation 2.5

$$K = \frac{(dT_{si} / dt) - (dT_{sf} / dt)}{T_f - T_i} \qquad (2.6)$$

An easier way to obtain the value of K is to plot the equilibrium temperature drift of the thermistor against the difference in temperature between the thermistor and the jacket. This was measured and has been plotted in figure 5.4 in chapter 5. Their relationship is linear and the value of K is calculated from the slope of the graph. The value obtained for K, for the calorimeter described in this thesis, was $4 \times 10^{-6}\ s^{-1}$.

If the radiation beam is of constant intensity the rate of the temperature rise measured by the thermistor will be constant. Letting $\dot{\theta}_s$ be this constant rate of temperature rise, equation 2.5 can be modified to give

$$\frac{dT_s}{dt} = \dot{\theta}_s - K (T_s - T_J) \qquad (2.7)$$

Since $\dot{\theta}_s$ and T_J are constant the solution is

$$T_{sf} - T_{si} = \left[\frac{\dot{\theta}_s}{K} - (T_{si} - T_J)\right] (1 - e^{-K \Delta t}) \qquad (2.8)$$

where the boundary conditions are that at t_i, $T_s = T_{si}$ and at t_f, $T_s = T_{sf}$; $\Delta t = t_f - t_i$ and the subscripts si and sf indicate the initial and final thermistor temperatures. Expanding the exponential and

solving for $\dot{\theta}_s$ gives

$$\dot{\theta}_s = \frac{T_{sf} - T_{si}}{\Delta t} + K\left(\frac{T_{sf} + T_{si}}{2} - T_J\right) - \frac{K^2 \Delta t}{6} (T_{sf} - T_{si}) \quad (2.9)$$

plus higher order terms. Using equation 2.5 to substitute for K and T_J we obtain

$$\dot{\theta}_s \approx \frac{T_{sf} - T_{si}}{\Delta t} - \frac{(dT_{si}/dt) + (dT_{sf}/dt)}{2} - \frac{K\Delta t}{6}\left(\frac{dT_{si}}{dt} - \frac{dT_{sf}}{dt}\right) \quad (2.10)$$

If the quadratic term is neglected, equation 2.10 represents the linear approximation of the thermal process. It essentially states that the average rate of heat loss from the thermistor is equal to the average of the rates of heat loss before and after the "X" period. The net temperature rise induced by irradiation is, in practice, obtained from the graphical construction illustrated in figure 2.3. The linear drifts during the rating periods are extrapolated to mid-run and the corrected temperature rise is equal to $T_\alpha - T_\beta$ (see figure 2.3).

In order that the simple graphical construction is sufficiently accurate, the quadratic term in equation 2.9 should be small, so that ignoring it will not introduce significant error. Comparing the quadratic term with the first term in equation 2.9

$$\frac{T_{sf} - T_{si}}{\Delta t} \quad : \quad \frac{K^2 \Delta t}{6} (T_{sf} - T_{si}) \quad (2.11)$$

which reduces to

$$1 \quad : \quad \frac{K^2 (\Delta t)^2}{6}$$

Inserting the longest time which was used for Δt (5 minutes), and the

value of 4×10^{-6} s^{-1} for the leakage modulus, gives a ratio of 1 : 2.4×10^{-7}. Clearly, ignoring the quadratic term will not significantly affect the accuracy of the measurement of the temperature rise. The reason for this is primarily that the leakage modulus for the calorimeter is small, due to the large amount of thermal insulation surrounding the water tank. The analysis of calorimetry measurements was therefore carried out using the graphical method illustrated in figure 2.3. Details of how this graphical analysis was applied to the calorimetry runs in practice are given in chapter 5.

2.3 REVIEW OF RADIATION CALORIMETRY

The full scope of radiation calorimetry is vast and a complete review of the subject would be inappropriate here. Gunn (1964) reviews the subject and gives details of the many and varied applications of calorimeters to radiation dosimetry. This section will be restricted to considering calorimeters employed to measure absorbed dose in a neutron beam and to the recently developed field of water calorimetry.

2.3.1 Neutron Absorbed Dose Calorimeters

One disadvantage of using a calorimeter to measure absorbed dose is its low sensitivity (see chapter 1). This problem becomes more significant when measuring absorbed dose in a neutron beam because of the low doserate. Neutron beams used for radiotherapy rarely produce doserates greater than 50 cGy min^{-1}, a typical value being 20 cGy min^{-1}. However, several calorimeters have been used in neutron beams for absorbed dose measurement. They have all been of the "solid" or "isolated absorber" type of calorimeter as described in section 2.1.1

and they have all employed thermistors in conjunction with Wheatstone bridges as temperature detectors.

The first such calorimeter was built by Bewley et al (1974), based on an earlier design which was used with megavoltage X-rays (Bewley 1963). The calorimeter consisted of a disc-shaped tissue equivalent plastic (A-150) absorber contained within a thin jacket of tissue equivalent plastic. Another identical jacket and absorber were contained within the aluminium vacuum enclosure but only one of the absorbers was irradiated, the other serving as a control. Thermistors sensed the temperature in the absorbers and were connected in adjacent arms of a Wheatstone bridge. The bridge therefore measured the differential temperature rise in the two absorbers. Any temperature drift in the calorimeter, which was presumably similar in both absorbers, should not produce a signal from the bridge. Calibration was carried out by dissipating electrical energy in the absorber. By using the resistivity of the tissue equivalent plastic, a current passed through the absorber produced in it a uniform heating, simulating the heating effect of the radiation beam. An identical temperature rise was produced in the jacket also by electrical heating. The calorimeter was irradiated in a d(16)+Be neutron beam producing a relatively high doserate of 60 cGy min^{-1} at the absorber. Resistance changes in the thermistor were detected by an equal arm a.c. Wheatstone bridge excited at 20 Hz. The calorimeter measured absorbed dose to tissue, in absolute terms, with an uncertainty of $\pm$6% (95% confidence level), which was similar to the accuracy attainable with an ionisation chamber. This value of 6% assumed an uncertainty of $\pm$1% in the size of the heat defect in A-150 plastic.

Inada et al (1974) described a calorimeter which had dimensions similar to those of an ionisation chamber. A small tissue equivalent plastic absorber was contained within a tissue equivalent plastic jacket with overall dimensions 2 cm x 4 cm. A feedback mechanism was employed to supply heat to the jacket, as required to keep it at the same temperature as the absorber, in an attempt to maintain adiabatic conditions. As with Bewley's calorimeter an identical dummy calorimeter, which was not irradiated was constructed so that any temperature changes not caused by irradiation would not be detected. A thermistor in the irradiated absorber and one in the unirradiated absorber were connected in adjacent arms of a d.c. Wheatstone bridge. The calorimeter was calibrated in a cobalt-60 beam against a ferrous sulphate dosemeter. The heat defect in tissue equivalent plastic was assumed to be the same for cobalt-60 gamma rays and neutrons produced by the d(2.8)+Be reaction. This assumption may be in error considering the work of Fleming and Glass (1969) who measured a value of 4% with 1.7 MeV protons and Bewley et al (1974) who noted large and variable heat defects when dissolved oxygen was present in the plastic. Green et al (1975) who also calibrated their neutron calorimeter in a cobalt-60 beam concluded that there was a 2% ($\pm$3%) difference between the heat defect for low LET radiation and that for high LET radiation. However, Inada et al (1974) found good agreement between their calorimeter and other dosimetric methods.

Another system employing twin absorbers was described by Greene et al (1975). The structure of the calorimeter was similar to that of Bewley et al (1974) except that the absorbers (and jackets) were made of polyethylene. There were two thermistors in each absorber and they were connected in an a.c. Wheatstone bridge excited at 1 kHz, the output of

which was detected by a lock-in amplifier. The calorimeter was calibrated against a Farmer ionisation chamber in a cobalt-60 beam. The calorimeter measured absorbed dose to polyethylene in a 14 MeV neutron beam and was compared with a polyethylene ionisation chamber filled with ethylene gas. As the calorimeter was calibrated in a cobalt-60 beam the measurement was essentially a check on the value of W_N/W_c for ethylene i.e. the ratio of the mean energy per ion pair for the secondary charged particles produced by neutrons, to the mean energy per ion pair for electrons. Both the calorimeter and the ionisation chamber measured absorbed dose in polyethylene with an uncertainty of $\pm 4\%$.

A sophisticated calorimeter designed as a primary standard for neutron dosimetry was described by McDonald et al (1976). All the major components of the calorimeter were constructed from tissue equivalent plastic. It consisted of six separate structures, all nested within one another, then enclosed in a vacuum tight container. The central absorber was surrounded by a jacket, in turn surrounded by the thermal buffers, and finally a temperature regulated control shield. The massive control shield, which was regulated by an automatic feedback mechanism supplying heat when necessary, meant operation was close to being adiabatic. During electrical calibration heat was supplied to the jacket as well as the absorber to keep as near as possible to adiabatic conditions. The d.c. Wheatstone bridge was adjacent to the calorimeter and was therefore controlled remotely, avoiding any problems with long signal leads. The calorimeter was irradiated in a d(7.5)+Be neutron beam at a maximum doserate of 25 cGy min^{-1} and the uncertainty in the measurement of absorbed dose to tissue was quoted as $\pm 5\%$.

Recently another calorimeter fabricated entirely of tissue equivalent plastic was described by Caumes et al (1984). It consisted of four nested bodies; a core surrounded by a jacket, surrounded by a shield, surrounded by a larger block of tissue equivalent plastic. The whole calorimeter was evacuated and temperature measurement was by a thermistor and a d.c. Wheatstone bridge whose output was measured by a nanovoltmeter. The operation of this calorimeter is best described as quasi-adiabatic since the temperature of the shield is kept constant. During irradiation both the jacket and the absorber rise in temperature by similar amounts. This also happens during electrical calibration as both the absorber and jacket are heated. The heating is produced by resistive heaters embedded in the absorber instead of using the resistivity of the plastic itself. Using the resistivity of the plastic has the advantage that the energy is deposited uniformly, which simulates the situation occurring during irradiation. The calorimeter was irradiated in a p(34)+Be neutron beam at a doserate of 20 cGy min^{-1}. Absorbed dose to A-150 plastic was measured with an uncertainty of less than 2%. The bulk of this uncertainty in the heat defect in A-150 plastic, which was taken as 1.5%. The calorimeter was therefore capable of very precise measurement of the temperature rise produced by irradiation; better than $\pm$1% (95% confidence level).

2.3.2 Water Calorimeters

Since the first water calorimeter was described by Domen (1980) several similar calorimeters have been constructed. The reasons for building a water calorimeter have already been discussed and this section will simply review the literature on water calorimetry.

The report by Domen (1982) describes in detail his water calorimeter and the theoretical background to its operation. The water tank was similar to the one described in this thesis; the main difference being that polystyrene rings (rather than perspex) were used to clamp the polyethylene sheets together. The water tank was surrounded by a layer of expanded polystyrene and housed in a duraluminium container. The temperature rise was measured by two thermistors positioned 2.5 mm apart in the centre of the rings. The two 3 kΩ thermistors were connected in opposite arms of an equal arm d.c. Wheaststone bridge, to give twice the sensitivity of a bridge containing only one thermistor. A novel method of controlling background temperature drifts was employed. Two stainless steel plates, one on either side of the water tank, were used to apply a potential across the water. A 67 volt battery and a rheostat provided a variable current through the water. By varying the applied voltage, background cooling drifts in the water could be compensated for. A perforated plastic tube, positioned around the bottom edge of the water tank, allowed gas to be bubbled through the water. This was used to agitate the water (for stirring) or to saturate the water with a gas other than air (nitrogen or oxygen).

Dose measurements were made with the calorimeter in a cobalt-60 gamma ray beam in which the doserate at the position of the thermistors was 110 cGy min^{-1}. Exposure times were three minutes and the standard deviation on a daily set of measurements was typically 0.6%. A graphite calorimeter was irradiated under exactly the same conditions as the water calorimeter in order to make a direct comparison. Measurements with the graphite calorimeter were converted to absorbed dose to water. Ignoring any radiochemical effects, the dose measured by the water

calorimeter was consistently 3.5% higher than that determined from the graphite calorimeter measurements.

Water that had been once distilled was used in the calorimeter, but water to which impurities had been added was also investigated. Tap water, and distilled water to which cadmium sulphate, iso-propyl alcohol or sodium formate had been added was used. Considerable exo- or endothermic chemical effects were noted especially at accumulated doses of less than 100 Gy. However, results with distilled water were reproducible from day to day despite the fact that the distilled water contained significant impurities and that its electrical conductivity varied over a wide range. Measurements were made with water that had been saturated with oxygen or nitrogen. This was achieved by blowing gas through the perforated tube in the water tank for up to 70 minutes at a flow rate of approximately 1.5 l min^{-1}. Under the conditions Domen described no difference in the absorbed dose rate was found between oxygen saturated and nitrogen saturated water.

With a copy of Domen's calorimeter, de Marles (1981) carried out water calorimetry measurements in both photon and electron beams. A two thermistor, equal arm, d.c. Wheatstone bridge was again employed, containing thermistors of nominal resistance 5 kΩ. Drift control electrodes were incorporated into the calorimeter, but were not needed to control background temperature drifts. This may have been because of the additional fibreglass insulation which surrounded the calorimeter or because the ambient temperature in the air-conditioned rooms was fairly stable. The calorimeter was irradiated in 1.25, 6, 18 and 25 MV photon beams and electron beams with nominal energies of 13, 17 and 20 MeV. Doubly distilled water was used although some measurements were carried

out with deionised water, and no difference was found. Dose measurements with the calorimeter were compared with six different ionisation chambers. The ionisation chamber measurements were not done in the water calorimeter, but in a water phantom having the same dimensions as the calorimeter. The duplication of ionisation measurements seems to be unnecessary since they were presumably all calibrated against the same exposure standard. In the photon beams measurements of absorbed dose to water with the calorimeter were 3.8% higher than measurements with the ionisation chambers. A quite different result was found with the electron beams. Doses measured with the calorimeter were 1% lower than those derived from the ionisation chamber measurements.

Kubo (1983) made measurements with a calorimeter slightly larger than those previously described but of essentially the same design. The water surface was 40 cm x 40 cm and deionised water was used for all measurements. The polystyrene rings could either hold two insulated thermistors or a Farmer type ionisation chamber, against which the calorimetry measurements were compared. The temperature detector was an equal arm d.c. Wheatstone bridge containing two 6 kΩ thermistors. The calorimeter was irradiated in cobalt-60, 10 MV and 25 MV X-ray beams, and 16.6 MeV and 23.3 MeV electron beams. Doserates ranged from 200 to 900 cGy min^{-1} and no doserate dependence was observed. Two methods were used to calculate absorbed dose to water from the ionisation chamber measurements. Firstly the method employing C_λ and C_E in conjunction with the values for C_λ and C_E given in ICRU (1969) and ICRU (1972) respectively. Secondly the method described in the recent AAPM protocol (AAPM 1983) which, at the higher energies, yields slightly higher doses than the first method. The effect of using the AAPM

protocol is similar to that of using the recently revised values of C_λ and C_E (HPA 1983, HPA 1985). It is therefore more appropriate to consider the results obtained by the second method. In the photon beams absorbed dose to water measured by the calorimeter was 2 to 4% higher than that measured by the ionisation chamber. A similar result was obtained in the electron beams, where the calorimeter results were 3.5% higher.

Schulz and Rothman (1983) described a water calorimeter which was cylindrical in shape. The central core was 10 cm high and 15 cm in diameter, and was nested within a cylindrical jacket. The core was watertight and water, at a constant temperature was circulated inside the jacket. This arrangement allowed the calorimeter to be operated at any desired temperature and eliminated problems with background temperature drifts. Two pairs of 1000Ω thermistors were suspended at different depths in the core. Each pair of thermistors was connected in a Wheatstone bridge whose output was amplified and displayed on a chart recorder. The thermistors were not sandwiched between polyethylene sheets but were uninsulated and in intimate contact with the water. The calorimeter was designed to be irradiated either horizontally or vertically. For comparison ionisation chamber measurements were performed in a dummy calorimeter which was essentially identical to the water calorimeter. Irradiation was carried out in a 25 MV X-ray beam at very high doserates (up to 1570 cGy min^{-1}). Calorimetric dosimetry was found consistently to be 3-5% higher than ionisation chamber dosimetry.

Mattsson (1984) used a water calorimeter in an intercomparison of three dosimetric methods; water calorimetry, Fricke dosimetry and

ionisation chamber dosimetry. The water calorimeter was an identical replica of that described by Domen (1982) operated in exactly the same way. In order to use the calorimeter as an absolute instrument for the determination of absorbed dose to water, the heat defect had to be determined. This was done by comparing the calorimeter with two calibrated ionisation chambers in a cobalt-60 beam. The ionisation chambers were sent for calibration to the National Bureau of Standards in Washington, which is where Domen's calorimeter was constructed. The chambers were calibrated against the same graphite calorimeter which was used by Domen. Mattsson's measurements were therefore essentially a repeat of those made by Domen, although the calorimetry measurements were completely independent. Indeed the results of the measurements were virtually identical: absorbed dose to water, determined with the water calorimeter, was a factor of 1.033 higher than that determined with the ionisation chamber. Considering all the available water calorimetry results, Mattsson concluded that the heat defect in water was 3.5% $\pm$0.3% (an exothermic effect). The heat defect was assumed to be constant for all low LET radiation and the same value was used for all of the beams used in the study (up to 20 MV X-rays).

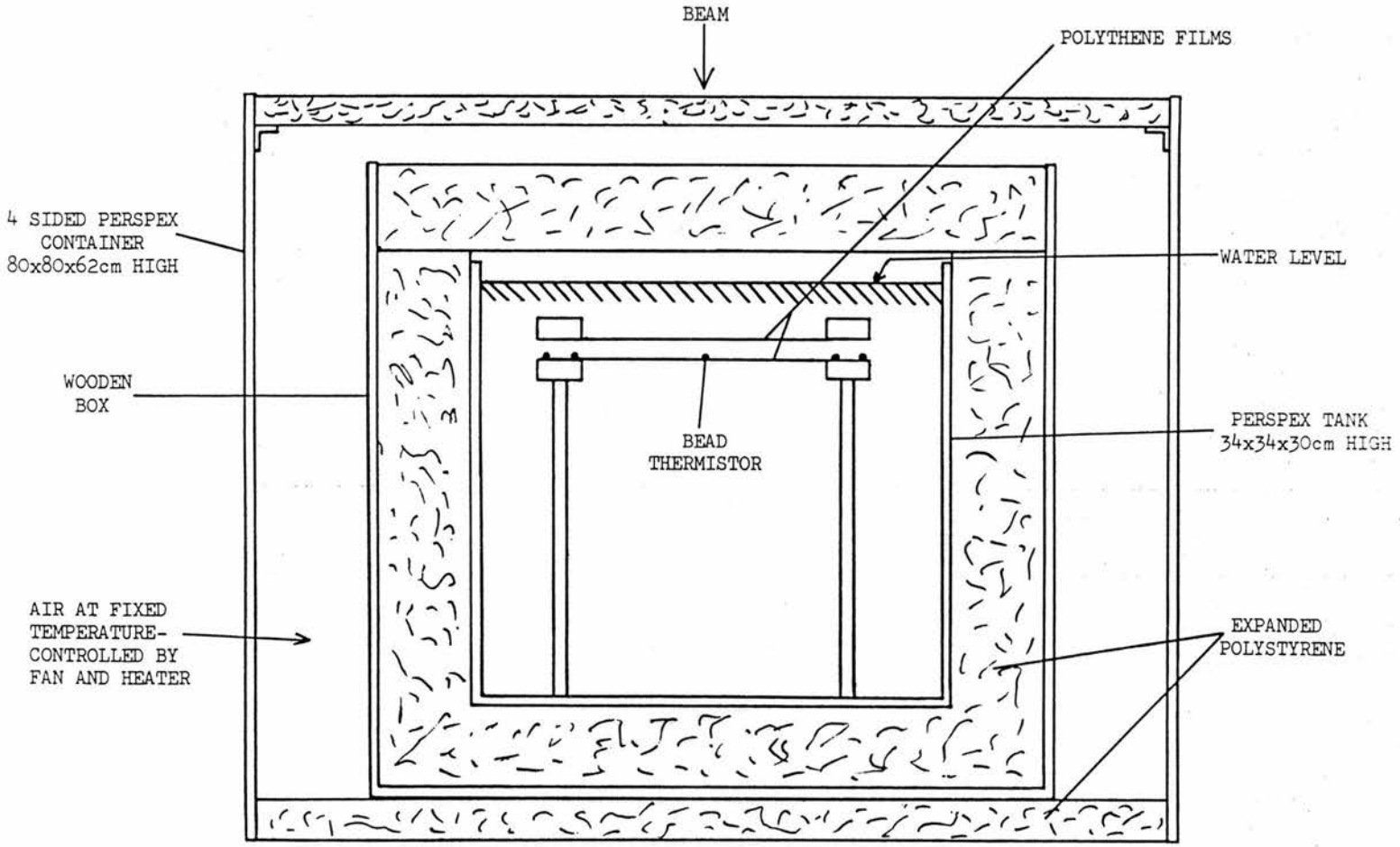

Figure 3.1 The water calorimeter

CHAPTER 3

THE WATER CALORIMETER

3.1 THE CALORIMETER

The water calorimeter was based on a design by Domen (1980), who showed that the concept of a water calorimeter was feasible. Figure 3.1 is a cross-sectional diagram of the calorimeter. It consisted of a 0.5 mm diameter bead thermistor (figure 3.2) which was sandwiched between two 25 μm layers of polyethylene sheeting. The two sheets of polyethylene were stretched taut and held in place by two perspex (polymethylmethacrylate) rings, shown in figure 3.3, which were clamped together by three stainless steel screws. The rings were attached to three perspex rods, again with stainless steel screws, which suspended the rings at a fixed height in a perspex tank, 34 cm x 34 cm x 30 cm deep.

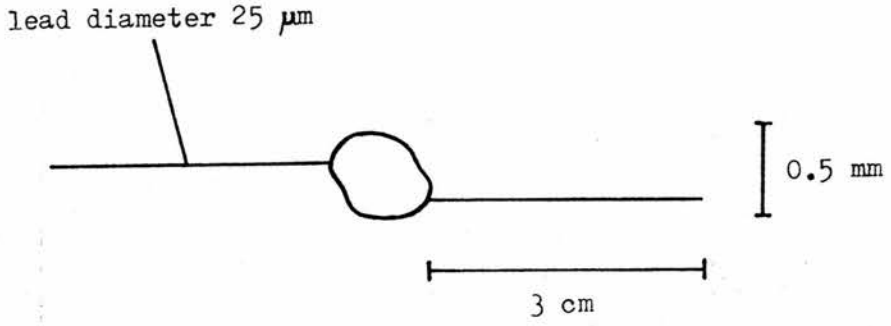

Figure 3.2 The bead thermistor

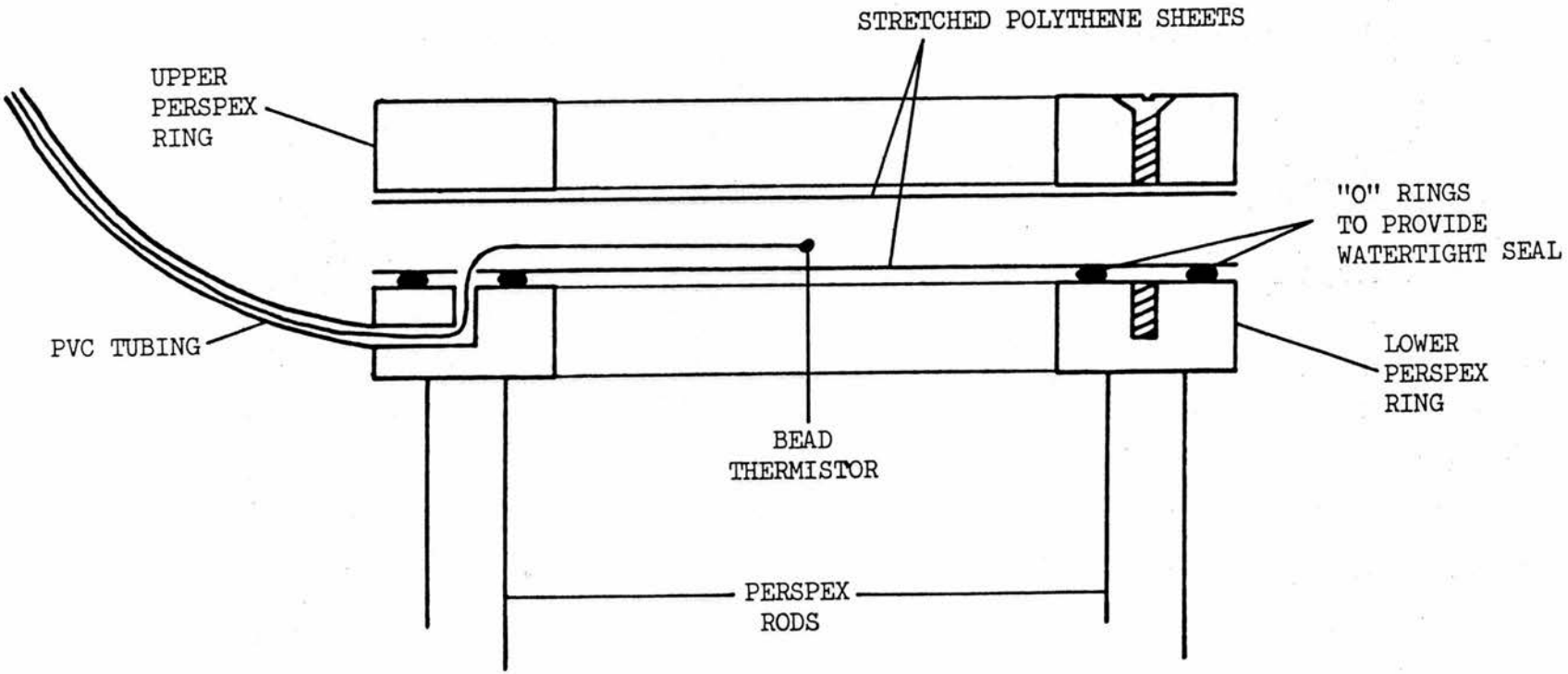

Figure 3.3 Perspex rings

The thermistor wires were soldered to 80 μm lacquered copper wires which were led to the edge of the polyethylene sheets through a hole in the bottom ring, and out of the water through a length of PVC tubing. The depth at which the thermistor was suspended was altered by adding water to, or removing water from the perspex tank. The external surface of the perspex tank was covered with a layer of aluminium foil to reduce radiative heat losses. The perspex tank was contained within a larger wooden box which was lined with a 7 cm thick layer of thermally insulating expanded polystyrene. Another layer of expanded polystyrene fitted snugly into the top of the wooden box and formed the lid of the calorimeter. The inner side of the wooden box and the lower side of the calorimeter lid were covered with a layer of aluminium foil which was electrically grounded, and formed an electrostatic shield. The overall dimensions were 52 cm x 52 cm x 47 cm high.

Inside the perspex tank were two stainless steel plates situated on opposite sides of the tank; these can be seen in figure 3.4 on the upper and lower sides of the tank. Domen (1982) described a method of controlling temperature drifts by applying a d.c. voltage across such plates. The size of the resultant electrical heating of the water could be altered to balance a natural cooling drift in the water and give a small overall temperature drift. Drift control electrodes were therefore installed during the construction of the calorimeter but were not used because of an alternative method of controlling background temperature drifts described in section 3.2. One of the electrodes was connected to earth to ground the water.

Also shown in figure 3.4, attached to the right hand wall of the tank, is a 500 Watt immersion heater which was built into the side of the perspex tank. The heater was 5 cm above the bottom of the tank, and

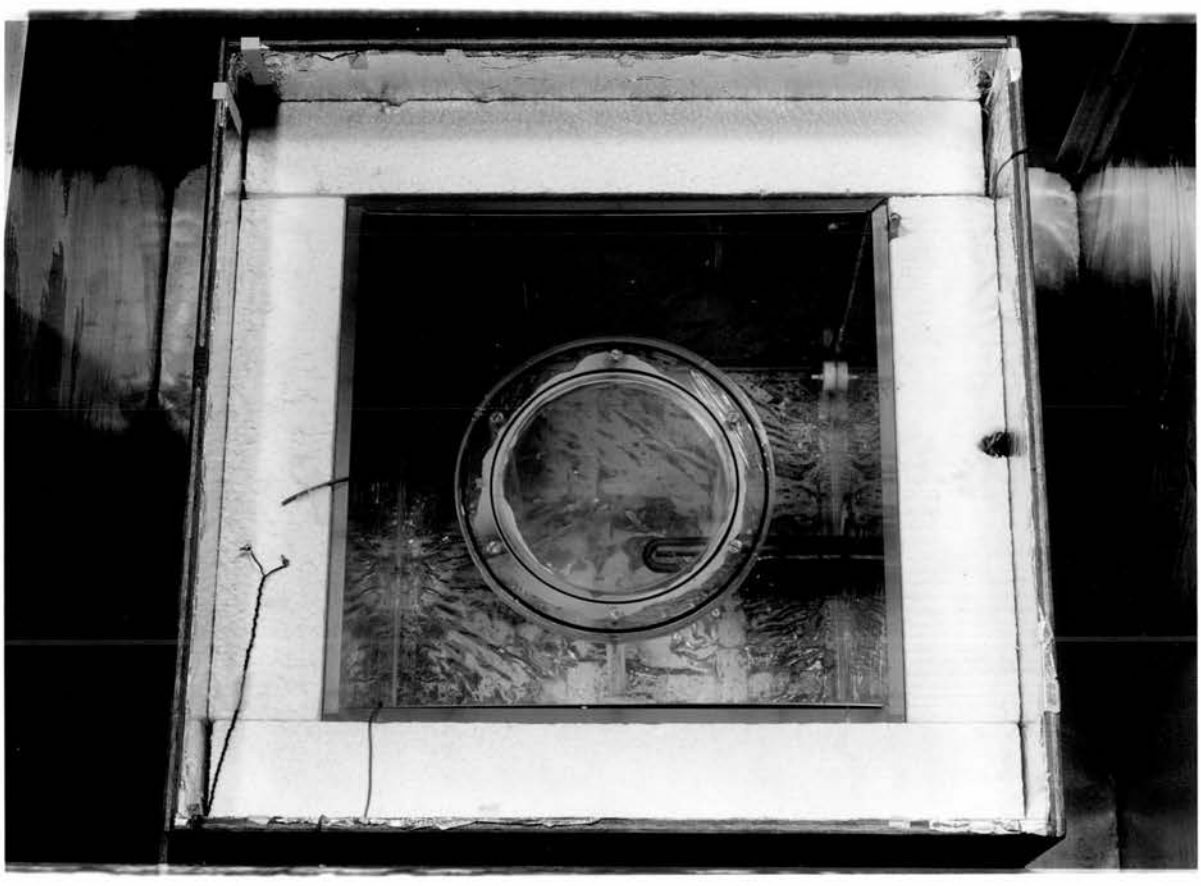

Figure 3.4 The Water Calorimeter

was used to bring the water to the appropriate temperature when setting up the calorimeter. The water used for all of the calorimetry measurements was triply deionised and also had dissolved organic compounds removed. It first passed through an Elgastat deioniser and then through a Millpore unit which contained two deionising columns and a carbon filter. The carbon filter removed any large organic molecules such as proteins. The resistivity of the water was greater than 15 MΩ-cm. Normally two or three measurements were made with the calorimeter over the course of a weekend. The same water was re-used during the weekend and was then discarded. The water was collected and stored in a large 25 litre plastic container and two similar 5 litre containers. Before setting up the calorimeter the water was heated to around 50°C, by the immersion heater, then allowed to cool back to room temperature. This drove out any dissolved oxygen and prevented bubble formation on the legs, rings and polyethylene sheets, which was a problem if the water was not de-oxygenated.

3.2 AIR TEMPERATURE CONTROLLER

To measure the small temperature rises produced by irradiation it is necessary that the background temperature drifts in the water be reduced to very low levels. Control of these background drifts was one of the major problems in developing the calorimeter, and is discussed further in chapter 5.

The air temperature controller consisted of a large perspex structure, which completely enclosed the calorimeter, inside of which the air temperature was kept constant. Figure 3.5 shows the calorimeter enclosed in the perspex box.

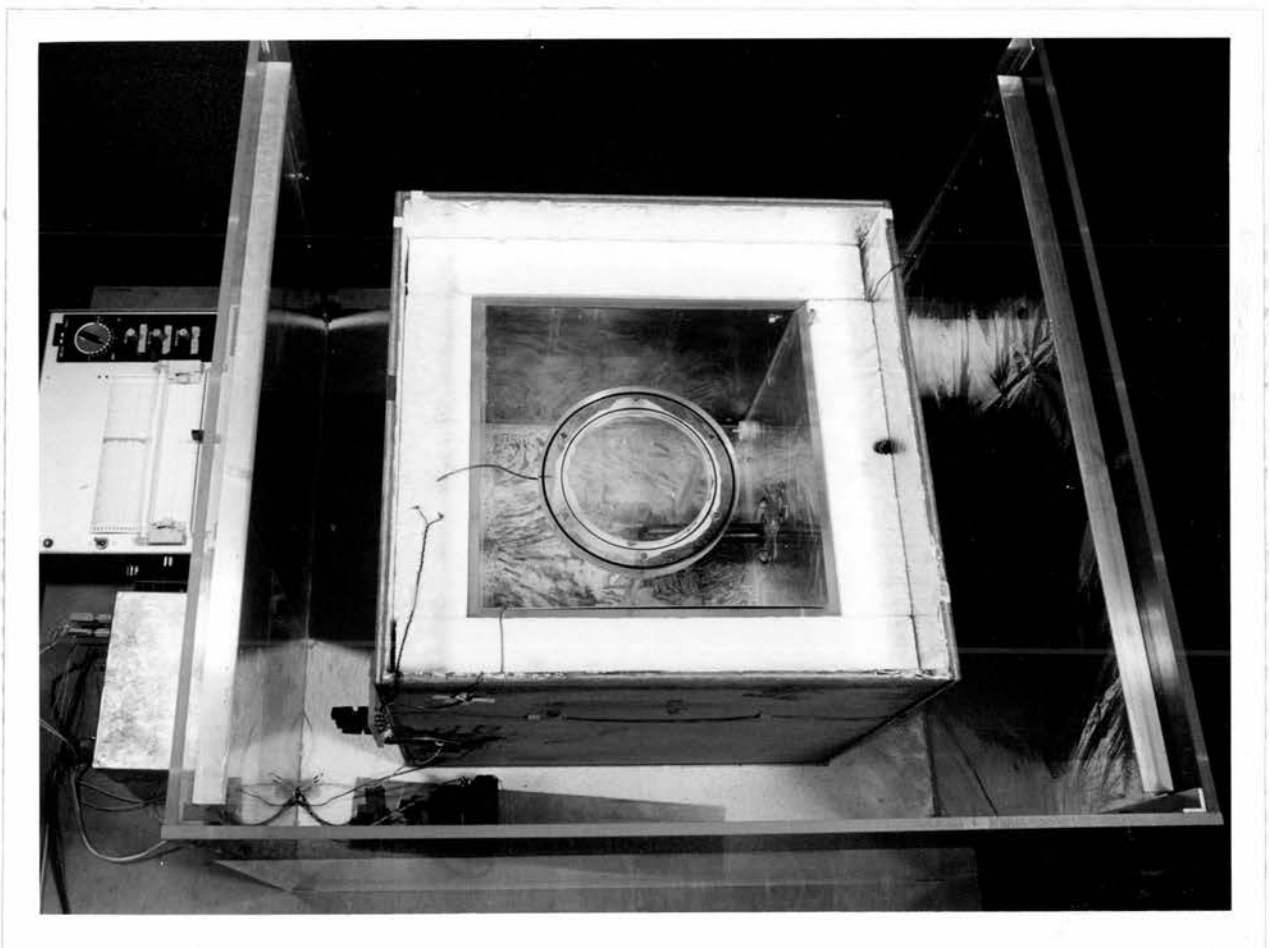

Figure 3.5 The water calorimeter and air temperature controller

The air temperature within the structure was controlled with a pair of heating coils and a small fan. The fan dissipated 15 watts, so the air temperature was necessarily a few degrees above ambient room temperature even with no power to the heating coils. The calorimeter was placed on a slab of expanded polystyrene 78 cm x 78 cm x 3.7 cm thick. A four-sided structure, made of 10 mm thick perspex, was built around the calorimeter and an identical slab of expanded polystyrene formed the lid of the structure. The lid sat on two ledges at the top of the perspex walls and both the lid and one side of the perspex structure were easily removed for access to the calorimeter.

The small fan (8 cm x 8 cm) had a flow-rate of 50 l/minute and remained permanently on while the air temperature controller was being used. Two 9Ω heating coils were attached to the front of the fan to supply the necessary heating to keep the air temperature constant. The power supplied to the heating coils was controlled by a circuit contained in the control box, seen on the left of figure 3.5. A detailed description of the circuit is given in Appendix A. The air temperature was measured by a thermistor and the voltage supplied to the heating coils was proportional to the difference between the temperature at which the control box had been set, and the temperature of this thermistor. The thermistor made up one arm of a Wheatstone bridge, the other arm being a fixed reference resistor. The reference resistor was situated within the perspex structure rather than in the control box so that large room temperature variations did not change the value of the reference resistor, and thus change the setting of the temperature control circuit.

The temperature of the air at one point within the perspex enclosure was monitored using another thermistor. The temperature indicated by this thermistor was displayed on a chart recorder (figure 3.5), so that the air temperature could be accurately set to match the water temperature. The temperature control circuit was powered by a 50 Watt transformer and the maximum power supplied to the heating coils was 45 Watts, which enabled the enclosure to be up to 8°C above room temperature. The power dissipated in the fan meant that the enclosure was always at least 2.4°C above room temperature. The calorimeter was operated at 3°C above the maximum ambient room temperature, which meant that the room temperature had to drop by 5°C before the air temperature control became ineffective. This was not a problem in the treatment rooms where the temperatures were fairly predictable and daily variations were small due to the large masses of concrete surrounding the rooms, and the air conditioning.

The temperature of the air within the enclosure oscillated rapidly about a mean value as the voltage to the heating coils was switched on and off by the control circuit. Since there was a large amount of thermal damping in the calorimeter it was the average temperature of the surrounding air which was important in determining the temperature drifts in the water. This temperature was stable to within $\pm$ 0.05°C over periods up to 24 hours. The calorimeter was made airtight so that the circulation of the air around the enclosure did not induce evaporation, which could have resulted in undesirable cooling of the water.

3.3 PREPARATION OF THE TEMPERATURE SENSOR

The temperature transducer was a small ITT bead thermistor, type U23UD, whose resistance was 2 kΩ at 20°C. Figure 3.2 shows the 0.5 mm diameter bead thermistor with its 25 μm diameter platinum-iridium leads. These leads, which were soldered to 80 μm lacquered copper wires, were long enough to be led out to above the surface of the water. The two films sandwiching the thermistor were 25 μm thick polyethylene, and were stretched taut between the two perspex clamping rings of outside diameter 214 mm, and inside diameter 152 mm (figure 3.3). The rings were made from 12.5 mm thick perspex.

It is desirable in an absorbed dose calorimeter that the "absorber" contains as little foreign material as possible. In the water calorimeter there is no isolated "absorber", but instead a continuous water medium, in which the absorbed dose at a point in the water is inferred from a measurement of the temperature rise at that point. Materials other than water around the thermistor will have different specific heats and absorbed doserates to those of water and so must be kept to a minimum, if the absorbed dose to water is to be measured accurately. In a sphere of diameter 10 mm centred on the thermistor, the amount of material other than water (i.e. thermistor, leads and polyethylene sheets) was 0.8% of the volume of the sphere. In a larger sphere of diameter 100 mm they amount of 0.08% of the volume of the sphere.

The thermistor was sealed into the rings before each set of measurements. The polyethylene sheets and rings were required to electrically insulate the thermistor from the water and to hold the thermistor at a fixed and known position in the water tank. Firstly the lower ring was placed directly on top of a drawing of a circle which

had its centre marked, to enable the thermistor to be positioned in the centre of the rings. Two O-rings sat in grooves in the lower ring and ensured good contact between the two polyethylene sheets. The lower polyethylene film was then placed on the perspex ring and the copper wires connected to the thermistor were passed through a hole in the polyethylene, and through the hole in the lower perspex ring (figure 3.3). Lead blocks were used to lightly stretch the polyethylene sheet over the perspex ring while silicone grease was placed on the sheet. Silicone grease was smeared sparingly onto the sheet in radial lines as shown in figure 3.6. Once the thermistor was sealed between the sheets the silicone grease slowly spread out over the inner surfaces of the polyethylene, making the two sheets adhere together, giving good thermal contact between the thermistor and the water. Inevitably a certain amount of air was trapped between the sheets; it collected in pockets as the silicone grease spread out, but because of the radial distribution of the grease the air bubbles were forced away from the centre and collected around the inner edge of the perspex rings.

Once the silicone grease had been applied to the lower sheet, a layer of silicone sealant was applied above the inner of the two O-rings. Silicone sealant is a silicone, water repellant, rubber based adhesive and it was used to seal the polyethylene sheets together, to prevent water reaching the thermistor. The top polyethylene sheet was then carefully lowered into place, followed by the top perspex ring. The sheets were held tightly clamped between the two perspex rings which were secured together by three stainless steel screws. A PVC tube, through which the copper wire had been fed, was sealed into the hole in the lower perspex ring with a small amount of silicone sealant. This

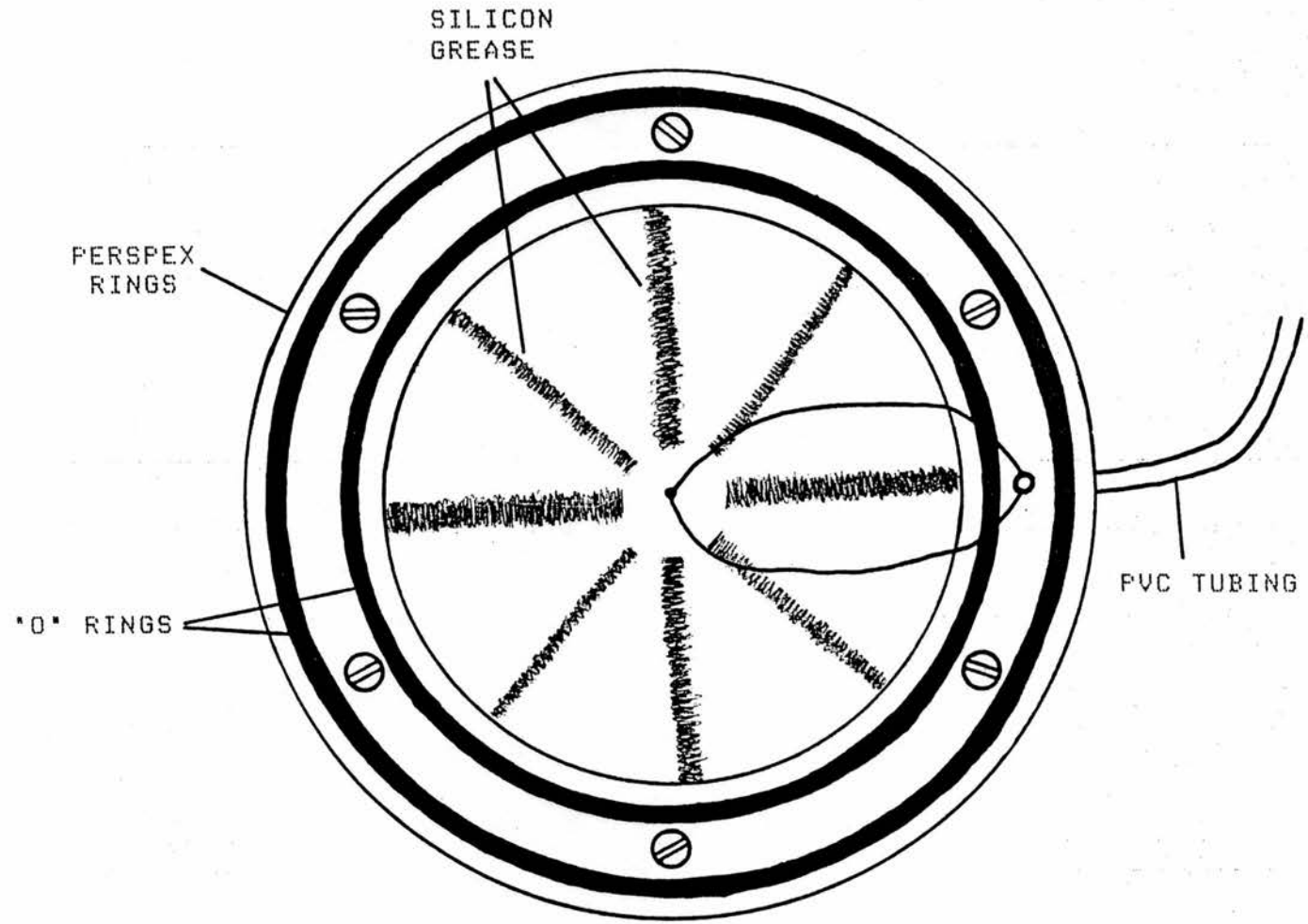

Figure 3.6 Position of silicone grease

tube was secured at one side of the water tank, where the copper wires were connected to the screened cables leading to the Wheatstone bridge. Each of the fine copper wires was connected by crimping it between two washers with a very small brass nut and bolt (see figure 3.4).

3.4 IONISATION CHAMBER JIG

The calorimeter was used to make an absolute measurement of absorbed dose to water at the point of the thermistor. It was desirable to compare this measurement with an absorbed dose measurement using an ionisation chamber. The easiest way to do this was to remove the thermistor and position an ionisation chamber such that its centre coincided with the position previously occupied by the thermistor. In order to do this reliably a jig was constructed into which the ionisation chamber could be inserted; a cross section of this jig is shown in figure 3.7. The jig was similar in construction to the perspex rings used to sandwich the thermistor between the polyethylene sheets. It was made from identical sheets of perspex, cut into rings of the same dimensions. The rings were cemented together and a perspex sheath was cemented between them as shown in figure 3.7. The TE ionisation chamber fitted into the sheath in such a way that the centre of the chamber was at the centre of the rings and at the same height as the thermistor. The sheath fitted snugly over the chamber, with no air gaps, at the end with the gas cavity. The perspex wall of the sheath was also thinner at this end, being 1 mm thick. A flexible PVC tube was connected to the end of the perspex sheath so that water would not come into contact with the ionisation chamber when the jig was immersed. The jig was secured to the perspex rods in the water tank by three stainless steel screws, in the same way as the thermistor and rings

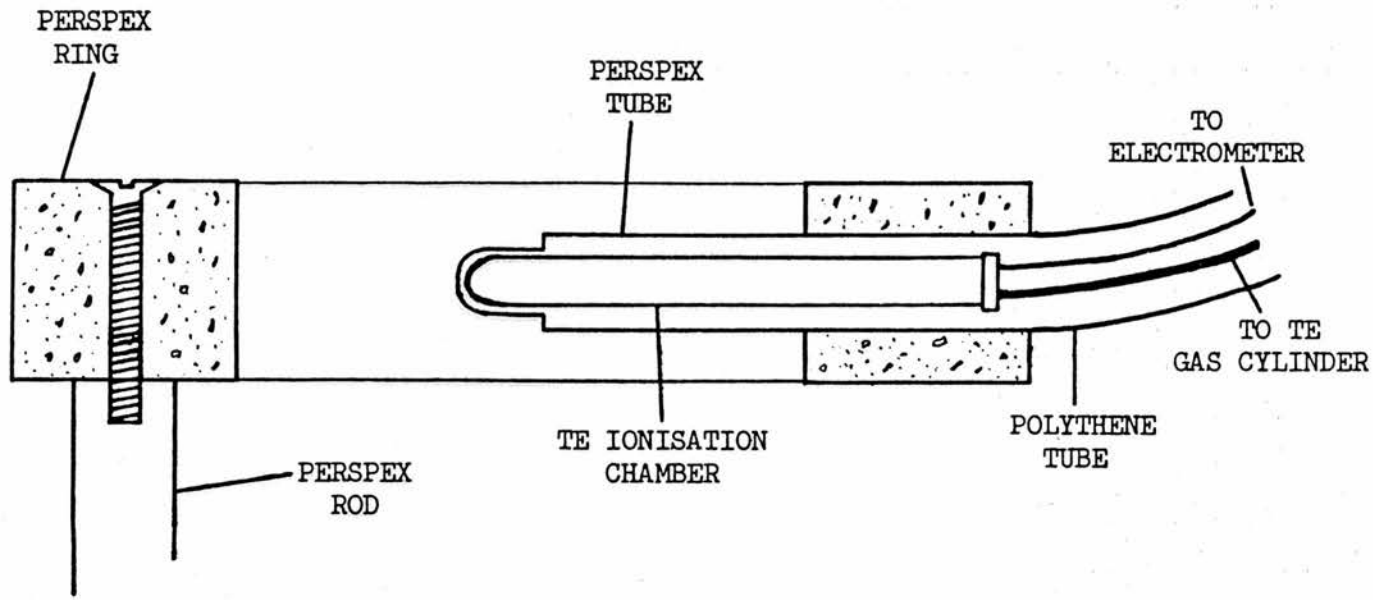

Figure 3.7 Ionisation chamber jig

assembly. This meant that after a series of calorimetry measurements the thermistor could be quickly removed and replaced by the ionisation chamber, without any depth measurements being required. As the ionisation chamber jig displaced more water than the thermistor assembly, water had to be removed from the tank in order to ensure that the centre of the ionisation chamber was at the same depth as the thermistor. The difference in volume amounted to 50 cm^3 and 50 ml of water was therefore removed from the tank each time the ionisation chamber was inserted.

The jig was constructed in such a way that when the ionisation chamber was pushed fully into the perspex sheath, the centre of the chamber was at the geometrical centre of the rings. Due to the difficulty in positioning the thermistor when sandwiching it between the polyethylene sheets, its lateral position could deviate slightly from the centre of the rings. Normally it was 1 to 2 mm away from the centre and the maximum noted distance was 4 mm. The lateral positioning was not critical since the radiation beams were broad and flat in profile. The vertical positioning, or depth, was much more important. At the depth of measurement the depth dose is changing by approximately 5% per centimetre, depending on the particular radiation beam. An error of 1 mm in the depth of the ionisation chamber would therefore effectively cause an error of 0.5% in the dose measurement. On several occasions the distance between the lower surface of the rings and the thermistor, and the distance between the lower surface of the rings and the centre of the ionisation chamber sheath, were measured using a height gauge. The difference between these two distances was consistently found to be less than 0.2 mm.

CHAPTER 4

THE TEMPERATURE DETECTOR

4.1 INTRODUCTION

The accuracy to which absorbed doses can be measured with the water calorimeter depends on the accuracy to which the temperature rises in the water can be measured. A typical daily dose given in radiotherapy of 2 Gy produces a temperature rise in water of 4.8×10^{-4} °C. To measure such a temperature rise with sufficient precision for absorbed dose determination requires a temperature measuring system capable of resolving temperature changes of a few microdegrees. A modern linear accelerator has an output of 2-3 Gy min^{-1} at the normal treatment distance. In the neutron beam the doserate is 25 cGy min^{-1}, a factor of ten lower than that in the photon beams from the linear accelerators, and the difficulty in measuring the temperature rise is even more acute.

This chapter discusses in detail the factors which must be taken into account in constructing a temperature measuring system for radiation calorimetry. The merits of different configurations of Wheatstone bridge and temperature sensor are considered. Previously reported temperature measuring arrangements for radiation dosimetry, in particular those for neutron absorbed dose calorimetry, are reviewed. The low power a.c. Wheatstone bridge which was used is described including its calibration and its performance in terms of its temperature resolution and signal-to-noise ratio.

4.2 CHOICE OF TEMPERATURE SENSOR

The ideal temperature transducer for radiation calorimetry would be of small size, with a high temperature sensitivity, and would have a response that was linear with temperature. It is necessary that the sensor be small so that there is negligible foreign material in the calorimeter around the point at which absorbed dose is to be measured. The sensor should not introduce heat conduction paths to the external environment because of required connections for the signal to be extracted. The sensor should not remove heat from or add heat to the calorimeter in its operation. Finally, the sensor should not be susceptible to radiation damage which would change its characteristics, up to a cumulative dose of a few kGy. All of these factors are not attainable in practice and a compromise between what is possible and which of the above criteria is most important, must be found.

Many different methods have been used in the past to measure the small temperature rises encountered in radiation calorimetry. Rump (1927) used mercury to completely absorb kilovoltage X-rays and measured the temperature rise by observing the expansion of the mercury absorber into a long capillary tube. Callendar (1911) and more recently, Mann (1954), used the Peltier effect in a microcalorimetric balance, although this was used for source strength measurement rather than beam calorimetry. Several calorimeters employing thermocouples or multi-junction thermocouples (thermopiles) have been reported. Pruitt and Domen (1962) employed a thermopile in order to obtain a higher sensitivity than is possible with a single thermocouple. The large number of connections to the calorimeter absorber, in this case, results in undesirable heat conduction paths. Pettersson (1967) used water as the absorbing material and calculated the temperature rise from the

measured expansion of the water absorber along a thin capillary. Also using a fluid absorber Schmidt and Buck (1969) calculated the temperature rise from the variation in electrical conductivity of a phosphate buffer solution.

Since the advent of the thermistor in the 1950's virtually all radiation calorimeters have used thermistors as temperature sensors. Thermistors combine the advantages of very small size and a high temperature sensitivity. They are commercially available with beads of diameter 0.05 mm and lead wires of diameter 0.01 mm. A very small thermistor will have a small thermal capacity and will therefore respond rapidly to changes in temperature. In addition, it will contribute a negligible amount of foreign material to the calorimeter. Such thermistors have electrical connections made of very fine wire which minimises any leakage of heat, by conduction through the wires, during irradiation.

The variation of the resistance of a thermistor with temperature is given by equation 4.1

$$R_t = R_o e^{B(1/T-1/To)} \qquad (4.1)$$

where R_t is the resistance of the thermistor at temperature T, and R_o is its resistance at temperature T_o. The temperature coefficient of a thermistor is about 4% per degree centigrade, which is a factor of ten greater than the temperature coefficient of a platinum resistance thermometer. Equation 4.1 is inherently non-linear but, it will be shown that, over the very small temperature rises encountered in calorimetry negligible error is introduced by assuming that the response is linear. One significant disadvantage of using a thermistor,

compared for example to a thermocouple, is that a thermistor necessarily dissipates power in the calorimeter. The power dissipation in the thermistor can be kept small and the fact that the thermistor is at a slightly higher temperature than its surroundings can be allowed for. The self-heating of the thermistor is discussed further in section 4.5. Another point that must be considered before employing a thermistor in a radiation calorimeter is whether the thermistor will be susceptible to radiation damage. Thermistors are made of metallic oxides and, in general, ionising radiation has an adverse effect on the electrical properties of semiconductors. Many radiation calorimeters have been constructed with thermistors as the temperature sensor and no problems with radiation damage have been reported. Regular calibration of a thermistor keeps a check on whether its characteristics are being affected by irradiation.

The overriding factor in choosing the thermistor as a temperature sensor is its high sensitivity. Another important reason is that a thermistor can be easily incorporated into a Wheatstone bridge circuit which can accurately measure very small changes in the resistance of the thermistor. Thus, at present, thermistors are universally employed as the temperature sensors in radiation calorimeters for use in medical therapy beams. The thermistor has revolutionised the use of calorimeters in beam dosimetry, making the calorimeter a practical instrument for use in therapy beams, even at low doserates. The technique has been developed to such an extent that, in the United States, a graphite calorimeter has been constructed as a primary standard of absorbed dose.

4.3 RESISTANCE MEASUREMENT

4.3.1 Use of Wheatstone Bridges for Resistance Measurement

Before thermistors became available platinum resistance thermometers were used with d.c. Wheatstone bridges for the measurement of temperature. The temperature sensitivity of platinum is only 0.4% per degree, making the measurement of the temperature rises involved in absorbed dose calorimetry very difficult. Thus, thermocouples or thermopiles were generally preferred for absorbed dose calorimetry. Thermistors have a temperature sensitivity ten times greater than that of platinum and many calorimeters using a thermistor and a Wheatstone bridge for temperature measurement have been described.

The first calorimeter using such a temperature measuring system was that of Laughlin and Beattie (1951), which was used for the measurement of energy fluence rather than absorbed dose. Two thermistors, one in each of two lead cylinders were connected in opposite arms of a conventional Wheatstone bridge. Only one of the cylinders was irradiated and the out of balance voltage from the bridge was amplified by a d.c. chopper amplifier. With an essentially similar calorimeter Genna and Laughlin (1956) made absorbed dose measurements in a polystyrene absorber irradiated by ^{60}Co gamma rays. Operating at low temperatures reduces the problem of radiative heat loss from the absorber and Schleiger and Goldstein (1964) described a calorimeter working at the temperature of liquid nitrogen, again with a d.c. Wheatstone bridge and chopper amplifier. There have been several other calorimeters with discrete absorbers in which a thermistor, d.c. Wheatstone bridge and chopper amplifier have been used for temperature detection in gamma or X-ray beams (e.g. Bradshaw (1965), Mitacek and Frigerio (1965), Pinkerton (1969), Inada et al (1974)).

Calorimeters of this type have also been constructed for the measurement of absorbed dose in fast neutron beams (McDonald et al (1976), Greene et al (1975), Caumes et al (1984)). These three calorimeters all used conventional d.c. bridges with chopper amplifiers. McDonald's calorimeter consisted of an isolated tissue equivalent plastic absorber in which a 30000Ω thermistor was embedded. One side of the Wheatstone bridge contained two fixed resistances, the other a thermistor and a variable balancing resistor. Both the Wheatstone bridge and the chopper amplifier were close to the calorimeter inside the treatment room to reduce the noise levels, by having short signal cables. The balancing resistor of the bridge was controlled remotely by a stepping motor outside the treatment room. The bridge was electrically shielded and also thermally insulated. The calorimeter was used successfully to measure temperature rises of 60 μK min^{-1}; ten measurements giving a standard deviation about the mean of $\pm$ 2%.

Wheatstone bridges excited by a.c. voltages have also been used in absorbed dose calorimetry. Bewley (1963) described a calorimeter constructed of carbon which employed an a.c. Wheatstone bridge to measure the rise in temperature. Two 100 kΩ thermistors were employed, one in the absorber and the other serving as a control. The other half of the bridge consisted of two 100 kΩ wire wound resistors and a decade resistance box for balancing. The bridge was excited at 20 Hz and the out-of-balance voltage was amplified and synchronously rectified. The lowest doserate measured corresponded to a temperature rise of 800 μ K min^{-1} which was measured with an experimental uncertainty of $\pm$ 2% standard deviation about the mean. Redpath (1967) used a conventional resistance bridge excited at 1 kHz in conjunction

with a phase sensitive detector for the calorimetry of low energy X-rays of 30 kV and below. Tedman (1975) described a similar system which was used for absorbed dose determination in megavoltage X-ray and electron beams. The system had an ultimate resolution of 2×10^{-5}°C, but problems of instability in the oscillator, which both excited the bridge at 285 Hz and provided the reference signal to the phase sensitive detector, were encountered. Hohlfeld (1975) constructed a carbon calorimeter intended for use as a national standard of absorbed dose. Two thermistors, in opposite arms of a Wheatstone bridge, were embedded in a carbon absorber. The bridge voltage was amplified by a lock-in amplifier and recorded, and the whole measurement and calibration sequence was automatically controlled.

The heat capacity of water is approximately six times larger than that of carbon. The temperature rises in water are therefore lower by the same factor, for equivalent absorbed doses. The water calorimeter was constructed to be used in a neutron beam which produced a doserate of 25 cGy min^{-1} at a depth of 5 cm in water. This doserate corresponds to a temperature rise of 60 μK min^{-1} and the measuring system had to be able to measure such a temperature rise accurately.

4.3.2 Choice of Wheatstone Bridge

As is clear from the previous section both a.c. and d.c. systems have been widely used in absorbed dose calorimetry. More recently a.c. systems have been favoured because of the introduction of phase sensitive detectors. Although this is generally true many modern calorimeters have employed d.c. systems; notably McDonald et al (1976) and Caumes et al (1984). There has been considerable recent interest in water calorimetry and all of the water calorimeters reported to date

have employed d.c. systems; Domen (1982), de Marles (1981), Kubo (1983) and Mattsson (1984).

Thermoelectric EMFs are a major problem in d.c. bridge circuits. Any contacts between dissimilar metals result in small EMFs which change if the ambient temperature of the junction changes. If such EMFs are injected into the amplifier input they will be indistinguishable from genuine temperature variations of the thermistor. This problem can be partially overcome by thermally insulating the connections in the Wheatstone bridge or by using special low thermal EMF connectors. Bridges excited by alternating currents are not affected by thermoelectric potentials. The out-of-balance voltage from a d.c. bridge is normally amplified using a chopper amplifier. Alternating current amplifiers are generally more stable than direct current amplifiers and the d.c. signal is therefore "chopped" to produce an a.c. voltage, whose amplitude is proportional to the magnitude of the initial d.c. signal. This a.c. signal can then be amplified to give sufficient sensitivity for calorimetric measurements.

A bridge excited by an a.c. voltage does not require a chopper amplifier and in addition a phase sensitive detector can be employed to extract a small a.c. signal which is submerged in a much larger noise component. The use of a phase sensitive detector means that a.c. systems can employ much lower sensor power dissipations than d.c. systems to achieve the same sensitivity. Furthermore inductive ratio arms mean that only one reference resistor is required in the bridge (Thompson and Small, 1971). The size of the resistance changes that very sensitive bridges measure can be comparable to the Johnson noise in the resistors of the bridge. Good inductors have a very low d.c. resistance and consequently the Johnson noise contribution is very

small. As the voltage ratio is determined by the turns ratio of the transformer winding, it is inherently stable with respect to temperature changes.

In conclusion, it was decided that an a.c. Wheatstone bridge employing a phase sensitive detector would be the most suitable system. Inductive ratio arms instead of conventional d.c. resistances were used in order to reduce the noise and improve the stability of the bridge. The next section describes the Wheatstone bridge which was constructed and used in all of the calorimetry measurements.

4.4 LOW POWER A.C. WHEATSTONE BRIDGE

The type of Wheatstone bridge used in conjunction with the water calorimeter was described by Calverd (1982). It was an a.c. bridge employing asymmetric inductive ratio arms and a lock-in amplifier. The bridge was designed at the National Physical Laboratory specifically for use with an X-ray calorimeter.

The noise voltage, V_N, generated by a resistance (R) is given by the classical Johnson formula:

$$V_N = 2\sqrt{kTBR} \qquad (4.2)$$

where T is its temperature, B the bandwidth and k is Boltzman's constant. For a 2 kΩ resistor and 1 Hz bandwidth the noise voltage, at room temperature (300 K), is therefore approximately 6×10^{-9} V. At a sensor power dissipation of 2 μW there is approximately 60 mV RMS across the thermistor and assuming a constant current through the thermistor, and a temperature coefficient of 4% per degree, the voltage change across the thermistor is 2.5×10^{-9} V per microdegree. Considering only

this source of noise, a time constant of about 0.2 s would permit resolution to $\pm$ 180 $\mu\Omega$ in 2000 Ω corresponding to $\pm$ 2 μK at room temperature. Allowing the rest of the bridge to contribute up to ten times the Johnson noise amplitude of the thermistor, the time constant need only be increased to 2 s to retain this resolution.

Many reported Wheatstone bridges have had equal impedance arms but it is possible to increase the sensitivity of the bridge by using unequal arms. Figure 4.1 shows a simple bridge with inductive ratio arms. At balance the output voltage, V, is given by

$$V = V_o \left(\frac{R_t}{R_s + R_t} - \frac{n_2}{n_1 + n_2} \right) \qquad (4.3)$$

where n represents the number of turns and R_t is the resistance of the thermistor. The voltage sensitivity is given by:

$$\frac{\partial V}{\partial R_t} = \frac{\partial}{\partial R_t} \left(\frac{V_o R_t}{R_s + R_t} \right) = \frac{V_o R_s}{(R_s + R_t)^2} = \frac{i R_s}{R_s + R_t} \qquad (4.4)$$

where i is as shown in figure 4.1. This approaches a maximum value (i) when $R_s >> R_t$, giving twice the sensitivity of an equal arms circuit, provided that the detector impedance is very large compared with R_t. A convenient choice is $R_s = 10\ R_t$ as 0.1 Ω increments are practicable and equivalent to 10 mΩ changes in R_t, and this ratio was used.

A further increase in sensitivity can be obtained in the output transformer of the bridge which couples the out-of-balance signal to the detector (R_d). If the primary to secondary turns ratio is X and the detector resistance R_d, then the detector is "seen" by the bridge as a

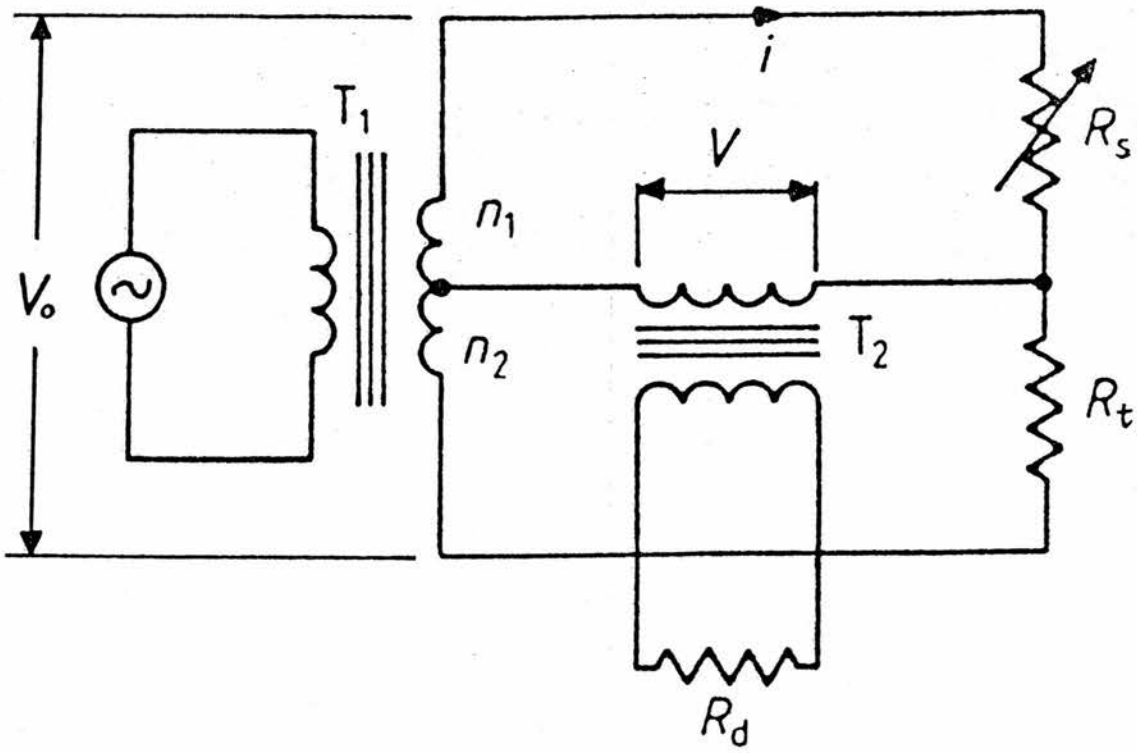

Figure 4.1 Simple bridge circuit with inductive ratio arms

reflected impedance of $R_d X^2$ in parallel with R_s. The voltage gain of the transformer is 1/X and equation 4.4 becomes:

$$\frac{\partial V}{\partial R_t} = \frac{i}{X} \frac{1}{(1 + R_t/R_X)} \qquad (4.5)$$

where R_x is the combination of R_s and $R_d X^2$ in parallel. The detector has a large input impedance (100 MΩ) and $R_d X^2$ is therefore very large compared to R_s. This means that the linearity of the bridge when off balance is not seriously affected but there is a substantial gain in sensitivity from the 1/X term in equation 4.5. Increasing the transformer ratio indefinitely is limited by the d.c. resistance of the secondary winding of the transformer and a value of X = 1/6 was used. The presence of this transformer also serves to isolate the bridge from the detector.

The leads from the thermistor to the Wheatstone bridge had to be over ten metres long in order to stretch from the calorimeter, inside the treatment room, to the control area, outside the treatment room. Temperature changes in leads of this length can change their resistance by a significant amount. Since the bridge is asymmetric such a resistance change would be indistinguishable from a change in the resistance of the thermistor. To eliminate this the configuration shown in figure 4.2 is used, where the resistances, r, represent the lead resistances. A tertiary winding on T_2, closely matched to the primary, carries a current roughly proportional to the lead resistance r, in antiphase to the current in the primary. When $R_c \simeq R_t(R_t+R_s)/R_s$ the resulting secondary voltage is independent of r for symmetrical changes in r, although the overall gain is reduced since the out-of-balance

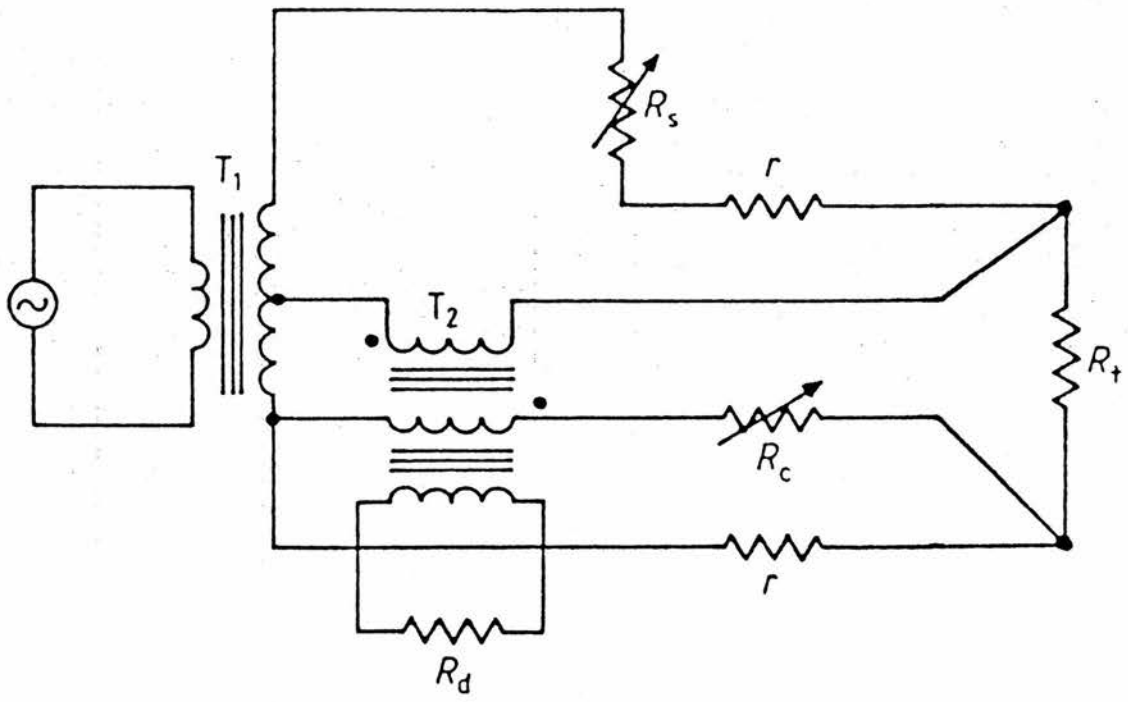

Figure 4.2 Bridge circuit including lead resistance compensation

signal now has to drive R_c. In practice an artificial change in r was introduced by switching 1Ω into both leads simultaneously and R_c was adjusted until this action produced no change in output voltage. This circuit reduces the lead resistance effect to approximately 1% of its nominal value in a simple two-lead configuration and leads 12.5 metres long were used successfully.

The most likely source of interference is "mains hum" at 50 Hz or harmonics thereof and a frequency of 375 Hz, lying between adjacent harmonics was therefore chosen to excite the bridge. It is clearly essential that the input voltage to the bridge is of constant amplitude and also that its frequency does not vary with time. A triangular waveform generated by a circuit employing CMOS logic excited the bridge and a square wave of the same frequency was buffered to provide a reference signal for the phase sensitive detector. Even operating at such low frequencies the reactive component of the d.c. resistances can be important. In order to keep the reactive component of the variable resistor R_s small, switched decades of bulk metal resistors with temperature coefficients of 10^{-6} K^{-1} were employed. A detailed description of the bridge, including the drive voltage is given in Appendix B.

The detector was a Brookdeal 9503 lock-in amplifier, having the ability to detect <0.01 μV RMS at the signal frequency in >0.5V peak-to-peak white noise. Figure 4.3 shows diagrammatically the complete path of the signal. The output of the lock-in amplifier was $\pm$10V full scale and was fed directly to a chart recorder.

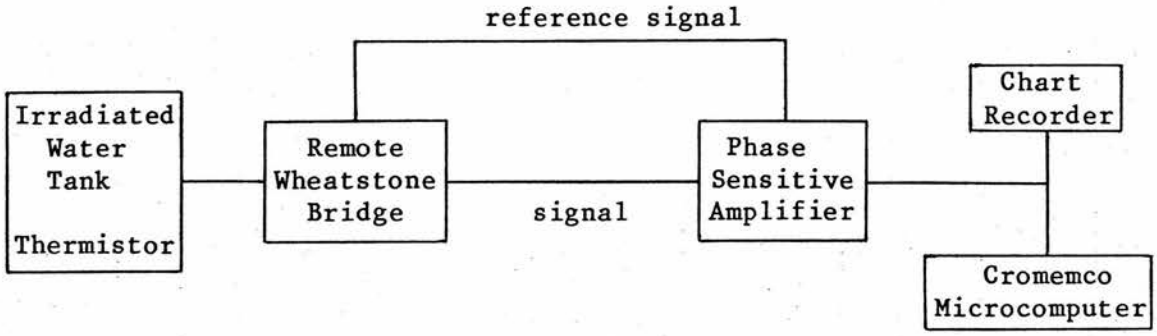

Figure 4.3

As described in section 2.2 the temperature change induced by irradiation was measured by extrapolating the initial and final drifts. If the only record of a calorimeter run is the chart recorder trace, this measurement must be carried out by a manual inspection of the trace. This sets a limit on the precision of the measurement, because of the limited accuracy of the chart recorder, and also due to the finite thickness of the trace on the recorder. In order to get round this and achieve a more objective method of determining the best straight line through the initial and final drifts, the output of the amplifier was fed directly to a microcomputer. The chart recorder remained connected to the amplifier, in parallel with the computer, so that a visual record of each calorimetry measurement was available. Details of the operation of the computer and its use are given in the next chapter.

4.5 ABSOLUTE CALIBRATION OF THERMISTORS

4.5.1 Introduction

As absorbed dose is to be derived from a measurement of the temperature rise produced by a radiation beam, the thermistor, which detects this temperature rise, must be calibrated in terms of

temperature. The resistance of a thermistor in terms of its temperature is given in equation 4.1. Differentiating this equation gives:

$$\Delta T = \frac{-T^2}{B} \frac{\Delta R}{R} = \frac{1}{S} \frac{\Delta R}{R} \qquad (4.6)$$

where S is the sensitivity of the thermistors. In general negative temperature coefficient thermistors have a nominal sensitivity of 4% per degree. The sensitivity of a thermistor is obtained by calibration against a standard thermometer. Equation 4.1 can be rewritten as:

$$\log R = \frac{B}{T} + (\log R_o - B/T_o) \qquad (4.7)$$

and the value of B for a particular thermistor is obtained from the slope of a graph of log R against I/T. B is known as the "material constant" and has a fixed value for any given thermistor.

As can be seen from equation 4.6 the sensitivity varies with temperature. The thermistor as a temperature detector is therefore inherently non-linear. The thermistors used had material constants of approximately 3000 K, and a change of 1^oC in the temperature results in a change in sensitivity (B/T^2) of approximately 0.7%. A typical dose of 3 Gy at the thermistor produces a temperature rise of less than 0.001^oC corresponding to a negligible change of 0.0007% in the sensitivity of the thermistor. Over the course of a number of calorimetry runs the temperature of the thermistor may change by up to 0.02^oC, corresponding to a 0.01% change in sensitivity, which again is negligible. Once the value of B is known for a thermistor its sensitivity is determined as a function of temperature. Over the small

temperature changes encountered in calorimetry, assuming that the sensitivity is constant does not lead to significant error since the sensitivity varies so little with temperature.

4.5.2 Self-heating of the Thermistor

As the operation of the Wheatstone bridge necessarily requires that a current flows through the thermistor there is a small power dissipation in the thermistor. The power dissipated in the thermistor raises its temperature above that of the surrounding water until an equilibrium is reached, when there is a constant temperature gradient around the thermistor.

$$\text{i.e.} \quad T = T_w + \delta T \tag{4.8}$$

where T is the temperature of the thermistor, T_w that of the water and δT the increase in the thermistor's temperature caused by self-heating.

In order to calibrate the thermistor, to determine the value of B, its temperature must be measured as a function of its resistance. Since the thermometer used in calibration measures the water temperature, the difference between this temperature and that of the thermistor is required. The self-heating factor is also needed when interpreting the results of a calorimetry measurement. As irradiation increases the temperature of the thermistor, its resistance decreases, increasing the power dissipated in the thermistor. Thus the temperature change of the thermistor is not completely due to the heating produced by irradiation but partly due to the change in δT.

The equilibrium resistance of the thermistor was plotted against power dissipation, at a fixed water temperature, in order to obtain the

self-heating factor. An example of this, for one particular thermistor is shown in fig. 4.4. The relationship between the two is clearly linear and the self-heating factor for the thermistor is obtained as follows. The best straight line through the points is of the form

$$R = mP + R_w \tag{4.9}$$

where m is the slope of the graph and R_w is the resistance of the thermistor when P = 0, i.e. its resistance at temperature T_w, the water temperature.

The sensitivity of the thermistor, at temperature T_w, is given by equation 4.6 as:

$$|\Delta T| = \frac{T_w^2}{B} \frac{\Delta R}{R_w} \tag{4.10}$$

and from equation 4.9 $\Delta R/\Delta P = m$. The resistance change produced by a power dissipation P is therefore $\Delta R = mP$, and the corresponding temperature change δT is given by:

$$\delta T = \frac{T_w^2}{B} \frac{mP}{R_w} = \frac{mP}{(B/T_w^2)\, R_w} = kP \tag{4.11}$$

The value of m was obtained from the plot of R against P, and the value of k from the above equation. The power dissipated in the thermistor was varied by "tuning" the primary of the bridge exciting transformer, as described in section 5.2. For the particular thermistor illustrated in figure 4.4 the value of k was 4.0 mK μW^{-1}. At a power dissipation of 10 μW, for example, the temperature of the thermistor would be 40 mK above the water temperature. During calibration of the thermistors this small temperature difference must be added to the measured water

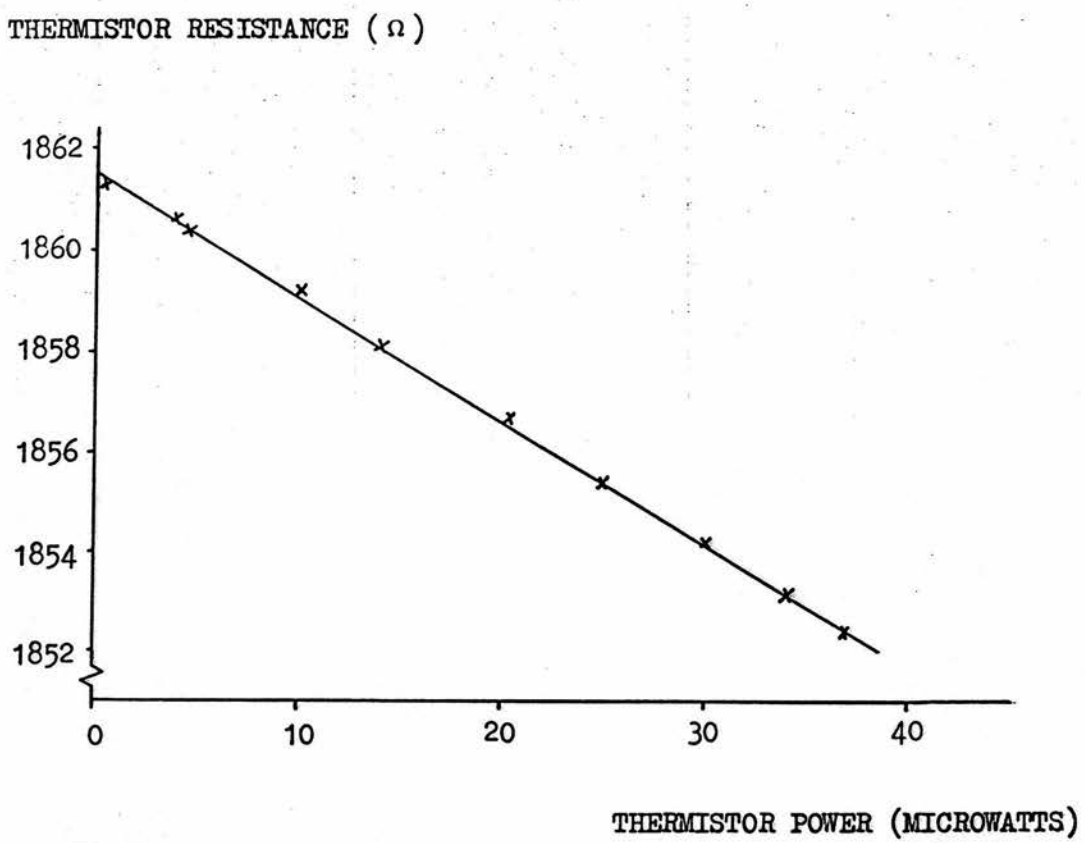

Figure 4.4 Thermistor resistance as a function of power dissipation

temperature so that the resistance of the thermistor can be plotted against its true temperature. More importantly the self-heating factor is used to calculate the change in the size of δT during a calorimetry run so that any necessary corrections to the observed temperature change can be made (see section 7.1.1).

4.5.3 Calibration

Two types of thermistor were obtained for use in the calorimeter. Both were miniature beads with platinum iridium alloy leads. ITT, types U23UD, had 0.5 mm diameter beads and Thermometrics B series, had 0.1 mm and 0.05 mm diameter beads and were consequently smaller and more fragile. They all had a nominal resistance of 2 kΩ at a temperature of 20°C. Several different thermistors were incorporated into the calorimeter and calibrated and some, under identical conditions, were found to be inherently noisier than others. All of the results reported here were obtained with an ITT type U23UD thermistor.

The thermometer used to calibrate the thermistors was a conventional, partial immersion, mercury in glass thermometer, constructed specially for this purpose. It read from 21°C to 27°C and was graduated in divisions of 0.01°C. After construction the thermometer was calibrated absolutely at the National Physical Laboratory. The calorimeter was set up with the lid removed and the thermometer clamped at the appropriate depth in the water. The water was heated, by the immersion heater in the tank, in steps of 0.5°C or 1° and allowed to settle at each new temperature. The water was stirred constantly during calibrations and when the heating was switched off the temperature reading on the thermometer reached equilibrium within

approximately 30 seconds. A polythene sheet covered the top of the water tank, with only the thermometer protruding, to reduce any evaporation as the water was heated above room temperature. This was done in case a temperature gradient was produced by a cooling of the surface of the water. The resistance of the thermistor was monitored by the Wheatstone bridge and when the drift in temperature was less than $0.001^{o}C$ per minute both the resistance of the thermistor and the water temperature were noted.

Figure 4.5 shows a plot of resistance against temperature for one thermistor and also a plot of log R against 1/T. At least squares method was used to fit the best straight line to the graph of log R against 1/T in order to obtain the value of B (see equation 4.7). The temperature on these graphs is the temperature of the thermistor i.e. the water temperature, plus δT, the temperature increase due to self-heating. A simple calculation shows that a systematic error of $0.1^{o}C$ throughout the range of the thermometer would result in an error in the value of B of only 0.07%. With this method it was possible to precisely determine the value of B. The values obtained for the thermistor used to make calorimetry measurements are given in table 4.1.

Date	B	Error on slope
26.1.83	2922	4
1.3.83	2914	5
26.5.83	2922	8
26.8.83	2923	1
17.5.84	2917	6

Table 4.1

The values for the error on the slope of the graph correspond to one standard deviation of the value of B. The first value of 2922 was used

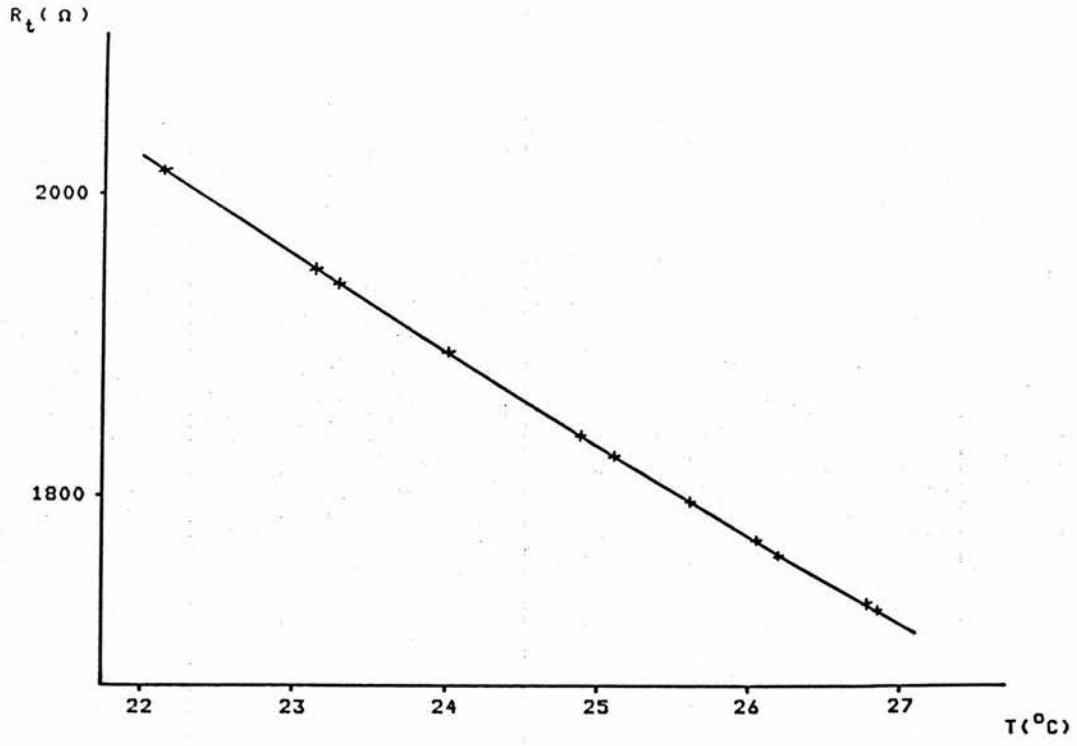

RESISTANCE AGAINST TEMPERATURE

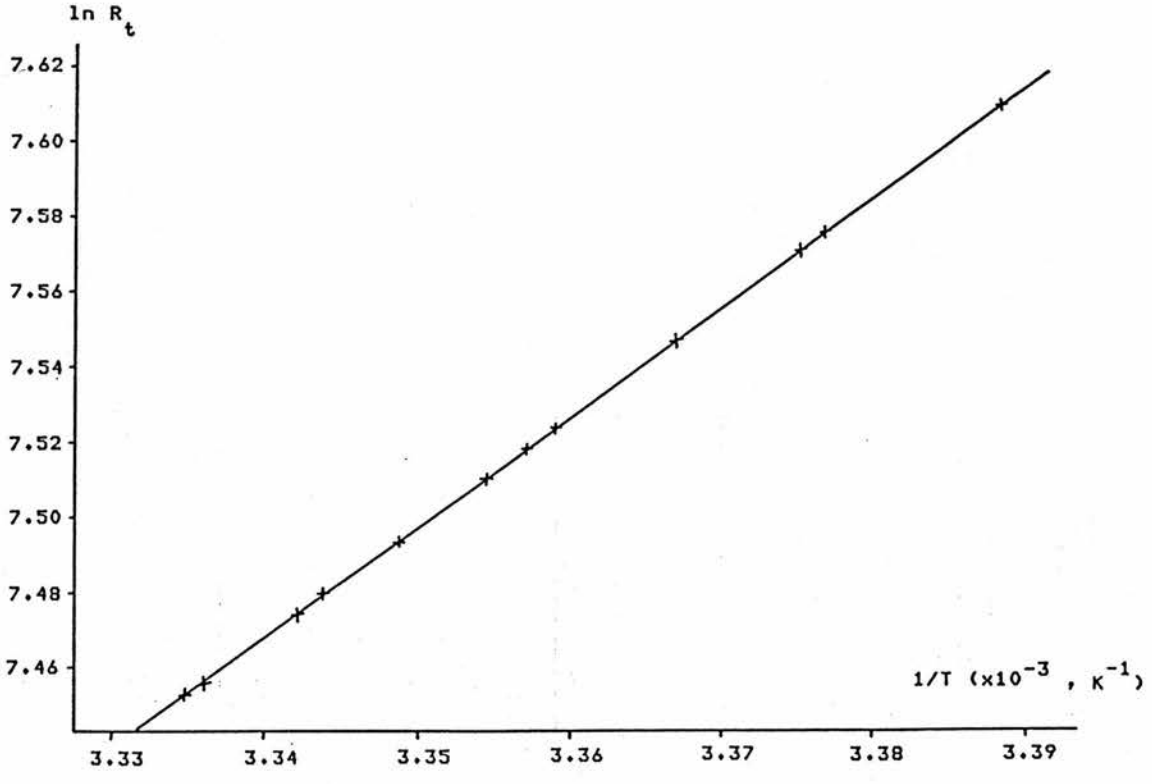

ln R_t AGAINST 1/T

Figure 4.5 Thermistor calibration

throughout as subsequent measurements did not disagree with this figure. The associated uncertainty was taken as 0.2%. Although the error on a single determination of B approached this value, repeated calibrations were necessary to check that irradiation did not alter the properties of the thermistor. It is well known that semiconductor materials are susceptible to radiation damage, but as is clear from table 4.1 the calibration was not changed by a dose of approximately 2 kGy, which was the cumulative dose delivered to the thermistor.

4.6 PERFORMANCE OF THE DETECTOR

The sensitivity of the temperature measuring system is not the only factor affecting the final precision of a calorimetric measurement. Many other factors concerned with the basic design of the calorimeter play a part in limiting the precision. Ideally the temperature detector should not itself place the limit on the precision of such a measurement. To fulfil this requirement a system capable of resolving temperature changes of a few microdegrees is necessary, as was stated in the first section of this chapter.

The performance of the Wheatstone bridge was investigated by replacing the thermistor with a decade resistance box and observing the resultant trace on the chart recorder. This was done with a resistance box consisting of wire-bound resistances, set to 2000Ω , the nominal resistance of the thermistor. Figure 4.6 is a trace showing the variation in resistance of the resistance box and the associated noise level. As the resistance box was not in a temperature controlled environment its resistance drifted, as can be seen from figure 4.6. If the resistance box was replaced by the thermistor the noise level would

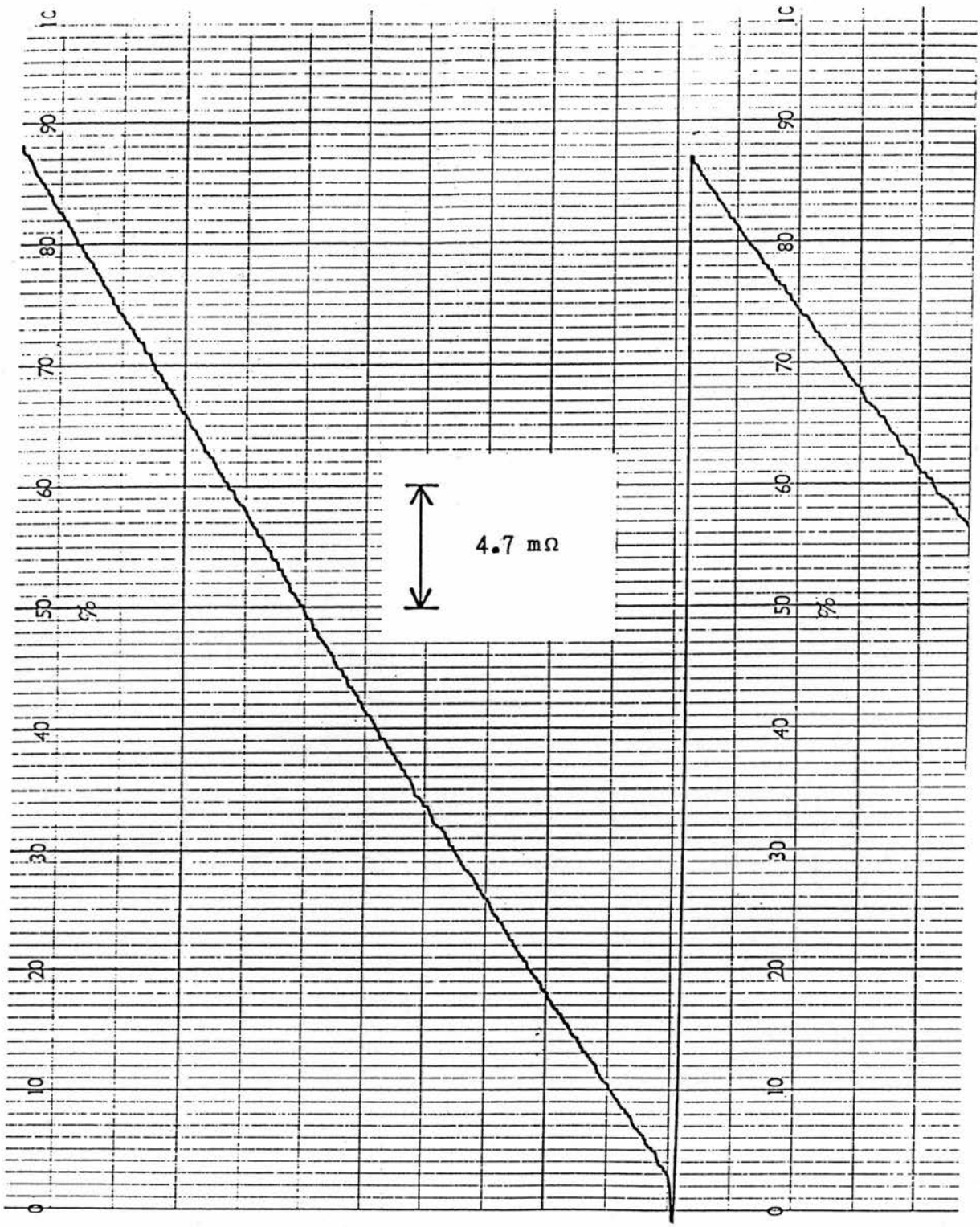

Figure 4.6 Record of bridge output with thermistor replaced by a decade resistance box set to 2000 Ω

be expected to be at least as great as that shown on this trace. This noise level therefore represents the ultimate resolution attainable with the Wheatstone bridge arrangement described in section 4.4. The peak-to-peak noise level is equivalent to approximately 200 $\mu\Omega$, depending to a certain extent on the thickness of the line from the chart recorder pen. A change of 200 $\mu\Omega$ in a 2000Ω thermistor corresponds to a temperature change of approximately 3 μK. This approaches the notional limit on the resolution, mentioned in section 4.4, set by the Johnson noise voltages produced in any resistor.

Figure 8.2 is a selection of three calorimetric runs in the neutron beam. The peak-to-peak noise level, in terms of temperature, on these traces is around 5 μK. On occasion the calorimeter was set up and the noise level was inexplicably much larger than normal. If the thermistor and rings were left in the water tank over a period of two or three days the noise level increased noticeably. This was attributed to water leaking into the space between the polythene sheets. This was prevented by dismantling and refabricating the rings after each set of calorimetric measurements. Another factor influencing the level of noise was the quality of the solder joints used to connect the thermistor to the copper wires leading to the bridge. Solder is specifically not recommended for the connection of the platinum-iridium alloy thermistor leads. In view of this other methods were tried. Very fine spot welding proved impossible due to the small dimensions of the thermistor leads. Connections were successfully made with a conductive silver doped epoxy, but they were unreliable and excessively bulky, causing pockets of air to be trapped between the polythene sheets. Conventional solder, which did provide a good connection, was therefore used and the thermistors were regularly re-soldered in order to maintain

a good contact between the fine copper wires and the thermistor leads.

Another measure of the performance of the thermistor bridge temperature detector is its sensitivity in terms of output voltage per unit temperature change. The sensitivity of the bridge, $\frac{\partial V}{\partial R_t}$, is given by equation 4.5. The sensitivity of the thermistors used was approximately 3.3% per degree, corresponding to a change of 65Ω/^{o}C under typical operating conditions. At a thermistor power dissipation of 9 μW and a typical value of R_t, the temperature sensitivity $\frac{\partial V}{\partial T}$, is 23 mV/^{o}C. This compares favourably with other workers who have employed d.c. bridges for water calorimetry. For example Domen (1982) describes a d.c. bridge having a temperature sensitivity of 15 mV/^{o}C, at the same power dissipation. Even at the lowest power dissipation employed (0.5 μW) the output of the Wheatstone bridge is still 5.5 mV/^{o}C.

In conclusion it can be said that the resolution of the Wheatstone bridge was more than adequate for measuring the temperature rises involved. Other factors such as large temperature drifts in the water, limited the usable sensitivity of the system; this is discussed further in the next chapter. Any practical difficulties with the detector were confined to the thermistor; its connection to the Wheatstone bridge or its sealing between the polythene sheets. No problems were encountered with the integrity of the solder connections between the thermistor leads and the copper wires, but the very thin thermistor leads were prone to break if not handled very carefully. The method of sealing the thermistor between the polythene sheets was not entirely sastisfactory as water did leak through if the rings were left submerged for long periods of time (~7 days). This necessitated the frequent disassembly and refabrication of the rings which, as well as

being a difficult operation, meant that the thermistor received a lot of undesirable handling. A method whereby the thermistor could be suspended in the water, but completely sealed from it would be advantageous. This would have to be done while keeping any materials other than the water away from the thermistor and without interfering with the connections to the Wheatstone bridge.

CHAPTER 5

OPERATION OF THE CALORIMETER

5.1 INTRODUCTION

The previous two chapters have described the water calorimeter and the associated Wheatstone bridge. This chapter describes the use of the calorimeter in practice and the difficulties encountered in putting it into operation. The method of controlling background temperature drifts in the water and the interpretation of calorimetry measurements are discussed in detail.

5.2 OPERATION OF THE WHEATSTONE BRIDGE AND AMPLIFIER

As was mentioned in section 4.4 the Wheatstone bridge incorporates a method of compensating for changes in the resistance of the leads running from the calorimeter to the bridge. These leads were 12.5 metres long and changes in ambient temperature could alter their resistance significantly. When the value of the compensation resistor $R_c \simeq R_t(R_t + R_s)/R_s$ (figure 5.1) the output voltage is independent of r for symmetrical changes in r. An artificial change of 1Ω was either inserted or removed from the current carrying leads, by means of a double pole single throw switch, as shown in figure 5.1. The resistance R_c was then adjusted until there was no change in the output voltage, monitored by the amplifier, when the switch was thrown. This was done for values of R_s and R_t which were typical of those during calorimetry measurements.

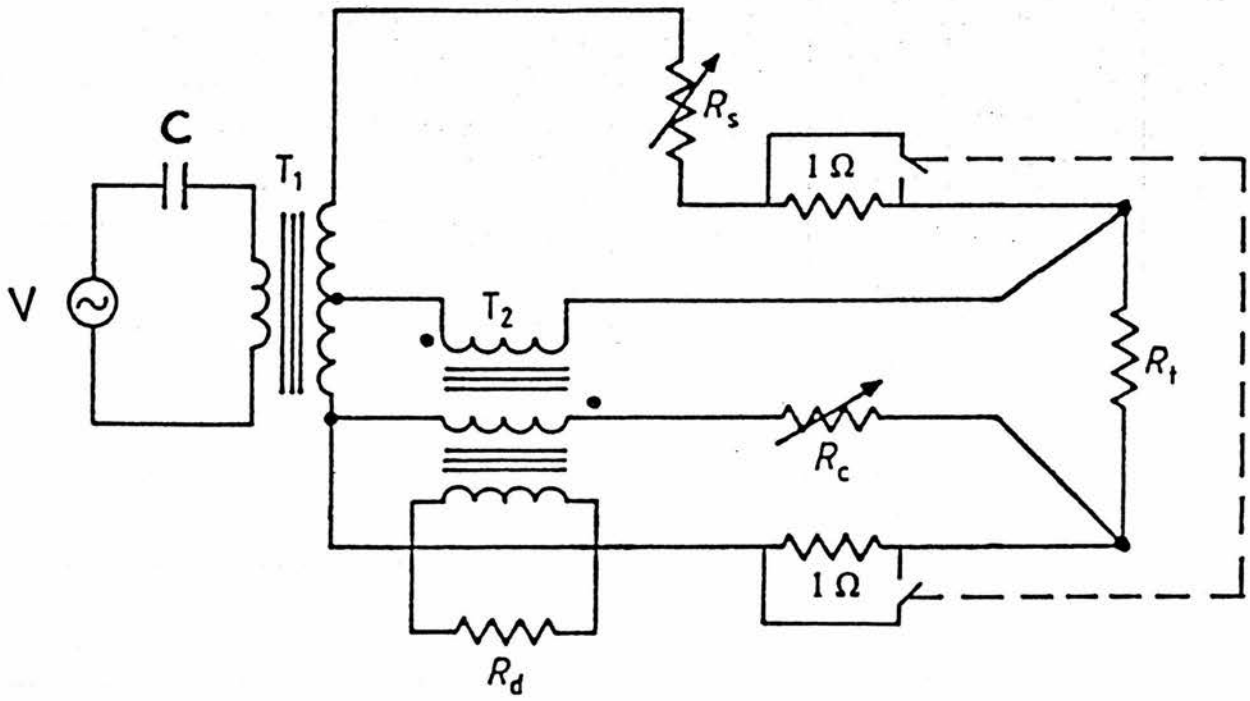

Figure 5.1 Lead resistance compensation

The power dissipated in the thermistor depends on the amplitude of the voltage V exciting the bridge. When it was necessary to change the power dissipation in the thermistor, either to alter the sensitivity of the bridge or to determine the self-heating factor for a thermistor, the amplitude of the voltage V had to be changed. The power supply was designed to produce a very stable voltage and therefore had no provision for varying this voltage. This was achieved by changing the value of the capacitor C (figure 5.1), effectively "tuning" the primary circuit of the bridge-exciting transformer. By varying the value of C between 10 nF and 10 μF the RMS value of V ranged between 2.9 and 24.2 volts, and the power dissipated in the thermistor between 0.5 and 35 microwatts. To select a particular thermistor power dissipation the appropriate value of capacitance was inserted into the bridge circuit. The full details of the bridge circuit and its power supply are given in Appendix B.

The principle behind the lock-in amplifier is that only signals of the same frequency as the reference signal are admitted and that components of the signal at different frequencies, i.e. noise voltages, are rejected. As the bandwidth of the amplifier is inversely proportional to the time constant employed, a longer time constant reduces the bandwidth and consequently improves the noise rejection. A time constant of 1 second was set on the amplifier. Typical calorimetry runs lasted 5 to 10 minutes and a shorter time constant was not necessary. To eliminate any frequencies significantly different to that of the signal the amplifier contained high and low pass filters. These were set to admit frequencies between 30 Hz and 1 kHz. The maximum sensitivity to which the amplifier could be set before noise overload occurred at the amplifier input corresponded to full scale deflection

for an input of 1 μV. The maximum sensitivity used for measurements was 5 μV giving full scale deflection, so noise overload was not a problem.

There was a facility on the amplifier which allowed the phase of the reference signal to be continuously altered i.e. the relative phase of the signal and reference voltages could be changed. The following procedure was adopted to set the phase of the reference signal so that it was exactly in phase with the signal to ensure maximum sensitivity to changes in R_t. The phase control was altered until changing R_s had no effect on the output of the amplifier. This was done with increasing amplifier gain and meant that the signal and reference were in quadrature. The phase was then changed by exactly 90^o, by means of a push-button, ensuring that the signal and reference were precisely in phase.

5.3 TEMPERATURE DRIFT CONTROL

Control of the temperature of the water in the calorimeter was the main difficulty encountered in developing the calorimeter to a stage where dose measurements could be made. Temperature rises induced by irradiation were approximately 60 $\mu K\ min^{-1}$ and 600 $\mu K\ min^{-1}$ in the neutron and photon beams respectively. In carrying out a calorimetry run it was necessary to observe the background temperature drifts for a few minutes before and after the "X" period (see Section 2.2). In order to extrapolate these drifts to the mid point of the run they had to be considerably less than the temperature rises produced by irradiation. The lower the background drifts were, the better, but measurements were practical when the drifts were approximately a factor of ten lower than

those during irradiation. Thus measurements were possible in the photon beams with background drifts of 60 $\mu K\ min^{-1}$, but measurements in the neutron beam required the drifts to be reduced to less than 10 $\mu K\ min^{-1}$.

Initially it was hoped that the thermal insulation surrounding the water tank would be sufficient to keep background drifts low, as long as the water temperature was reasonably close to the ambient air temperature. However, room temperature variations were unpredictable resulting in significant differences between the water and ambient air temperatures. Figure 5.2 shows the variation of the room temperature and the water temperature, as measured by the thermistor, over a two week period. Although the calorimeter was in an air conditioned room the ambient temperature spanned almost 5°C which meant that the difference between room temperature and the temperature of the water was at times greater than 2°C. This resulted in temperature drifts of up to 600 $\mu K\ min^{-1}$ in the water. To restrict the drift to 10 $\mu K\ min^{-1}$ clearly required a more sophisticated method of controlling the drift.

Domen (1982) described a method of controlling background cooling drifts by applying a d.c. potential across the water tank. Two stainless steel plates at opposite sides of his water tank were connected to a variable 0-67 volt supply. The potential across the water tank produced temperature gradients around the thermistor which tended to oppose any cooling of the thermistor. The potential could be altered to keep the background drifts small. This procedure required the initial drift to be cooling, and in the event of an initial heating drift this was achieved by heating the water to 0.1°C above ambient temperature and allowing it to settle down to a cooling drift.

Following Domen's design, drift control electrodes were built into the calorimeter as shown in figure 3.4. Control of cooling drifts up

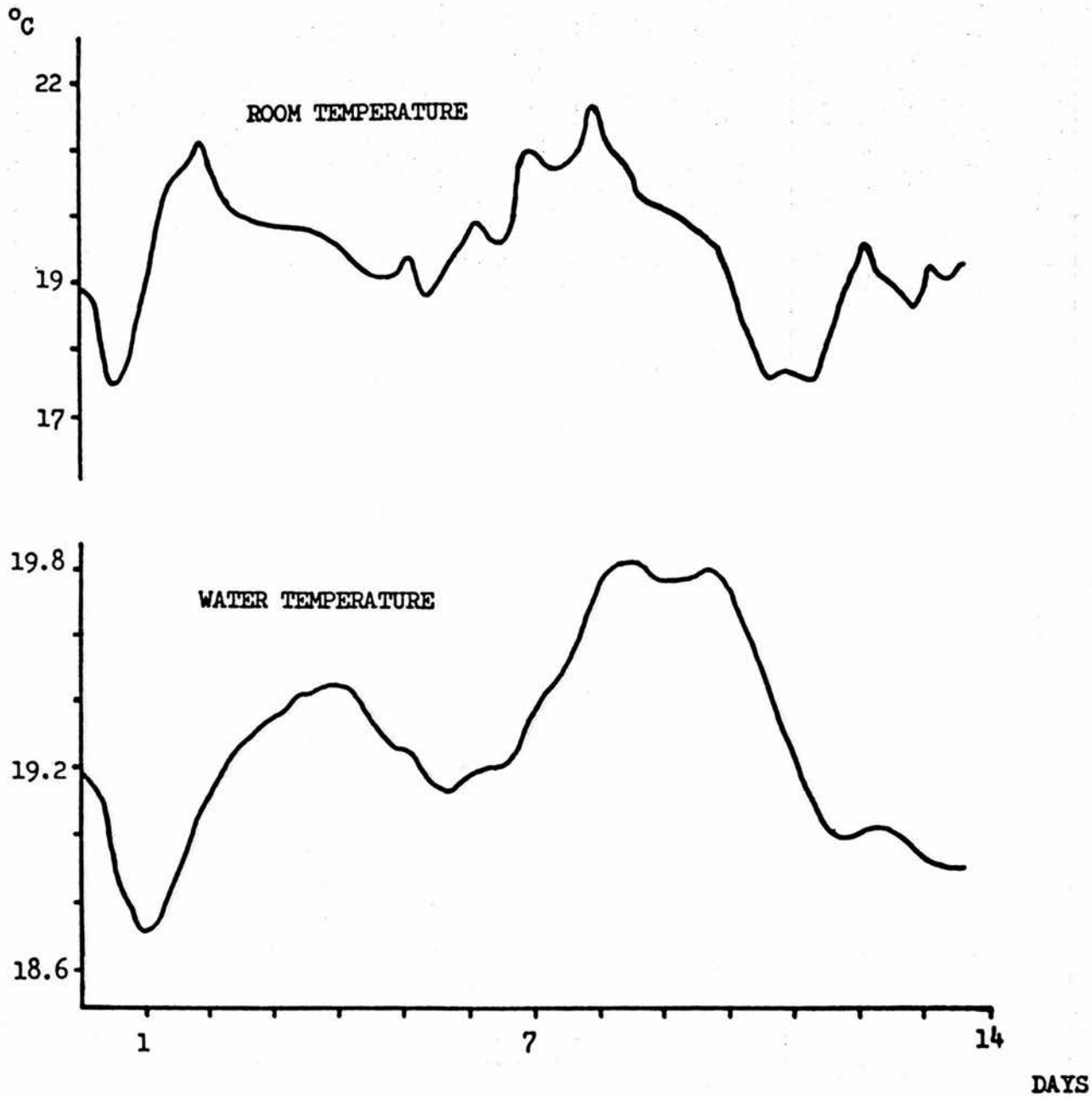

Figure 5.2 Variation of room temperature and corresponding water temperature

to 100 $\mu K\ min^{-1}$ was achieved by applying a potential across the plates and dissipating up to 400 mW in the water. Although it was possible to control drifts of up to 100 $\mu K\ min^{-1}$ and reduce them to virtually zero drift, this was only achieved on a few occasions. Before drift control could be attempted a reasonably small cooling drift had to be present and this in itself was not easy to achieve in a laboratory where the temperature was uncontrolled. Daily room temperature variations were often $5^{o}C$ and were generally unpredictable, which made it difficult to arrange for the water temperature to remain a few tenths of a degree above room temperature. Drift control was also considered unsuccessful since the drift could not be controlled for long periods of time, which was necessary to carry out a calorimetric measurement. The longest period of time that the drifts were kept under control was fifty minutes, after which the drifts became heating and were therefore uncontrollable. After short periods of successful drift control, the drift would return to its original cooling drift on switching off the potential across the plates. However, on removing the potential after longer periods of drift control the drift would often become large and variable (heating or cooling), and be completely uncontrollable. In view of the inconsistent performance of the drift control electrodes, they were abandoned in favour of the alternative method of drift control, already outlined in section 3.3. It is also worth noting that no other reported water calorimeters to date have employed drift control electrodes.

The method used to control the background temperature drifts was to enclose the calorimeter in a temperature controlled environment. Details of the electronics and the structure of the air temperature

controller have been given in section 3.2. In order to reduce the background drift the average temperature of the air surrounding the calorimeter was set so that it was very close to that of the water. The air temperature could be conveniently altered by a potentiometer on the control box. The air temperature was crudely but effectively monitored using a straightforward Wheatstone bridge consisting of three ceramic resistors, a 100 kΩ thermistor and a 1.5 V battery. The output from this bridge was fed directly into a chart recorder, giving a continuous display of the temperature of the air within the enclosure. Figure 5.3 is a typical trace of the temperature of this monitor showing the oscillations of the air temperature around a mean value. It is the long term stability of this mean value which is important in keeping the background drifts small and this temperature was stable to within 0.05°C over periods up to 24 hours.

The temperature of the air within the enclosure was altered and the resultant equilibrium temperature drift in the water was noted. This allowed a graph of temperature drift against the difference between the water temperature and the monitor temperature to be drawn (figure 5.4). It can be seen from this graph that, at the point where there is zero background drift, the two temperatures are not equal. This is presumably because the temperature of the air measured by the monitor thermistor does not represent the average temperature of the air within the enclosure. There was also an uncertainty of 0.2°C in the calibration of the monitor thermistor. However, this graph assisted rapid setting up of the calorimeter. If, once the calorimeter had come to equilibrium, there was a resultant background drift in the water, the graph showed the appropriate increase or decrease in the air temperature required to compensate for the drift. With this system background

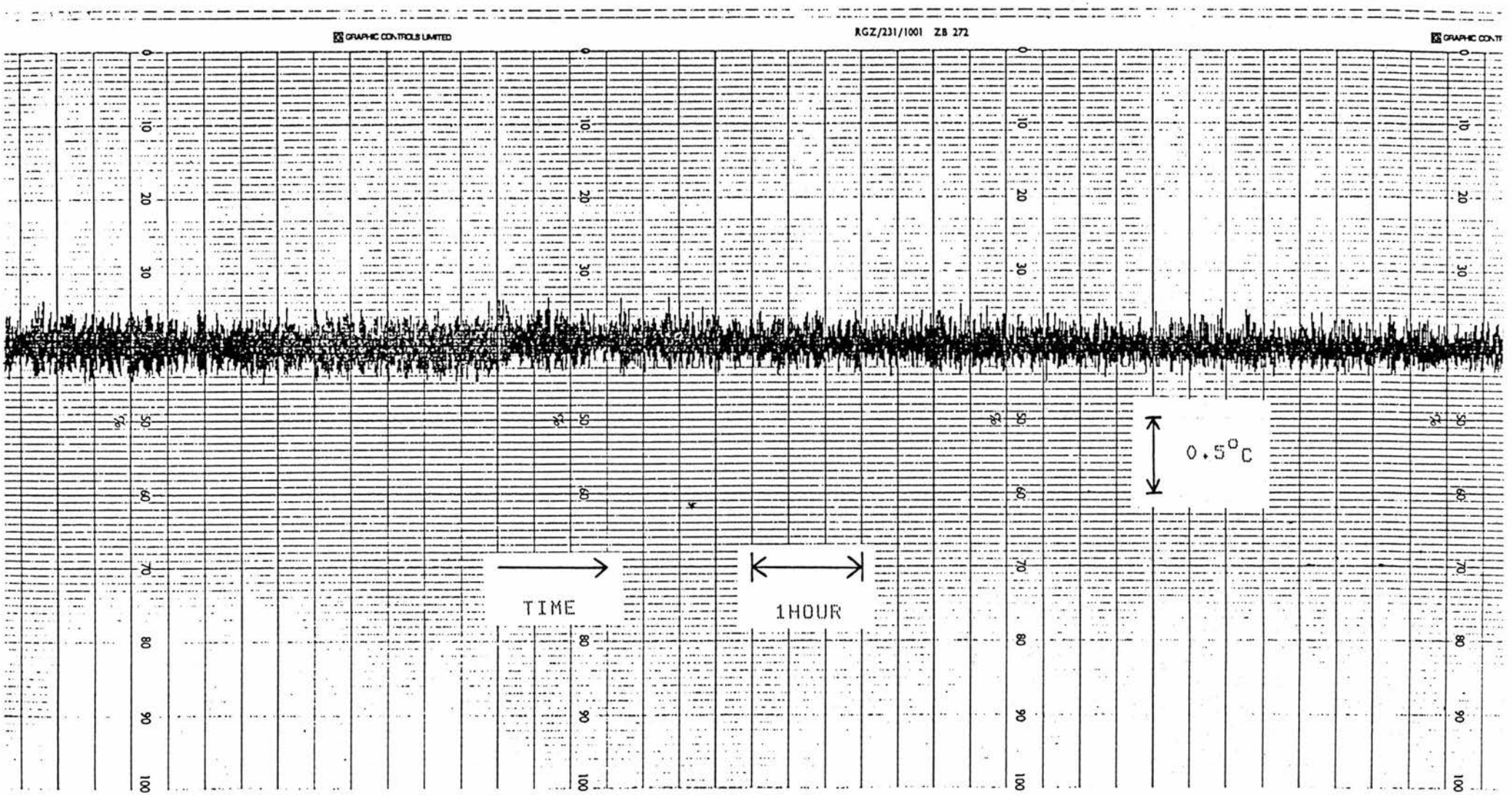

Figure 5.3 Sample of air temperature at one point within perspex enclosure

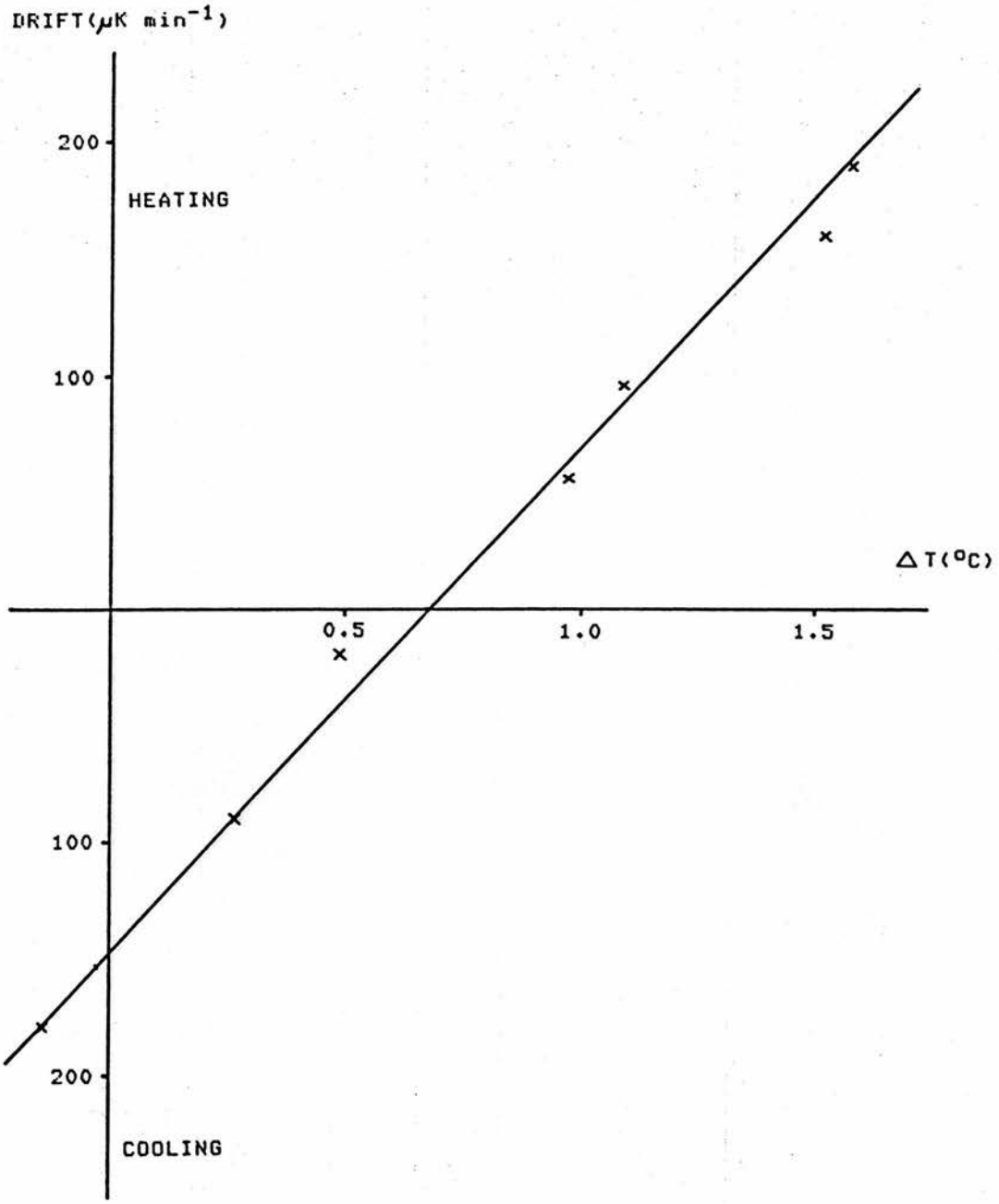

Figure 5.4 Temperature drift against temperature differential

drifts could be reduced to less than 50 $\mu K\ min^{-1}$ simply by setting the air temperature to the appropriate level. Further reduction of the drift was carried out by fine tuning of the air temperature and with care and appropriate re-adjustments of the air temperature, drifts could be reduced to less than 10 $\mu K\ min^{-1}$. If a drift had been established and the air temperature was altered, it took less than half an hour for the drift to respond and usually less than one hour to settle down to a new equilibrium value. A rapid change in the ambient temperature of the room containing the Wheatstone bridge was found to alter the drift significantly (e.g. when a window was opened), and was therefore avoided during measurements. This indicated that apparent temperature drifts in the water may not be entirely due to the changing water temperature, but also to drift in the electronics or the resistance of the balancing arm of the bridge. However, such changes would probably be slow and steady and the air temperature controller could equally well compensate for them as well as for true temperature drifts in the water.

5.4 CALORIMETRY MEASUREMENTS

A copy of a typical chart recorder trace from a run in the neutron beam is shown in figure 5.5. Time runs from right to left and the initial drift is cooling. The beam was switched on at point A and the trace immediately showed a heating of the thermistor. At point B there was a manual change in the value of the bridge balancing resistor R_s, causing the sharp deviation in the trace. At point C the beam was switched off and the drift returned to its initial value. The dotted lines which have been added to the trace are the extrapolations of the initial and final drifts. These are extrapolated to the mid-point of

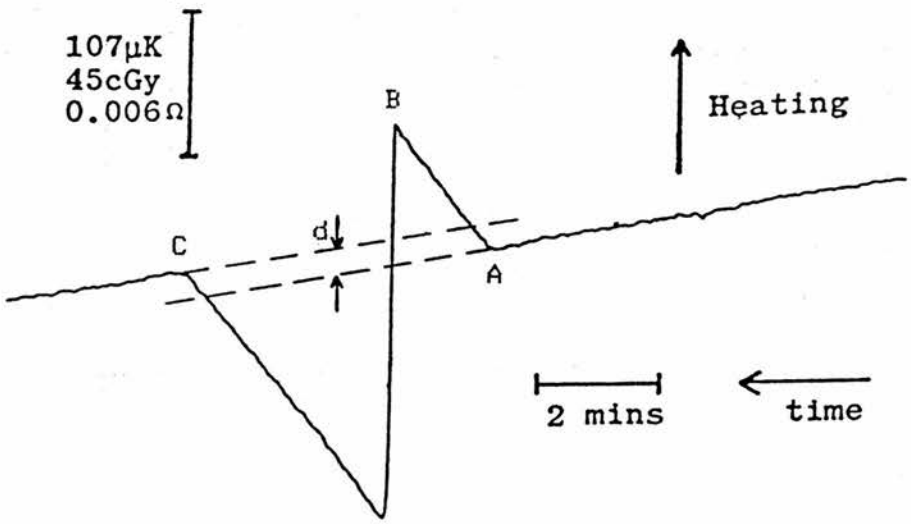

Figure 5.5 Typical calorimetry run in the neutron beam

the run in order to determine the value of the deviation, d. It is necessary to calibrate the chart recorder in terms of resistance so that the change in resistance corresponding to d can be calculated. This was done by changing the value of R_s by a known amount as shown in figure 5.6. From such a calibration the chart recorder is calibrated in $\Omega\,mm^{-1}$ and the value of d can be converted to a resistance change (δR_s). In the Wheatstone bridge the fractional resistance change of the thermistor is identical to the fractional change of R_s required to bring the bridge back to its original state, assuming that background drifts are allowed for. Thus the fractional resistance change in R_s ($\triangle R_s/R_s$) can be used in equation 7.1 in place of the fractional change in the thermistor's resistance ($\triangle R_t/R_t$). $\triangle R_s$ is made up of two parts: (a) δR_s, which is calculated from the deviation d, and (b) the manual change in R_s which was introduced at point B in figure 5.5. A typical value for this manual change in R_s was less than 0.2Ω . Changing the 0.1Ω decade of the resistance box was found unsatisfactory as the calibrations were inconsistent, probably due to the effects of contact resistance. The arrangement of figure 5.7 was therefore adopted to allow such small changes in R_s to be made accurately and reproducibly. The 50Ω resistor was wirewound, had a tolerance of 0.1% and a temperature coefficient of 3 ppm. The 0-10 $k\Omega$ decade box was altered by a few thousand ohms in order to obtain changes in R_s of a fraction of an ohm. Taking the manufacturer's uncertainty of 0.1% in the value of the 50Ω resistor, the calculated uncertainty in changes in R_s using this method was less than 0.3%.

In general eight to twelve calorimetry runs were done in a set of measurements. Calibrations were done either between calorimetry runs or immediately before and immediately after them. At least as many

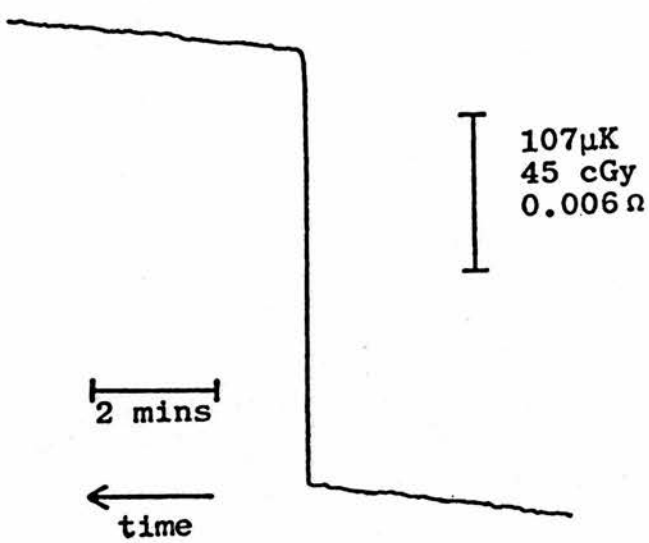

Figure 5.6 Resistance calibration

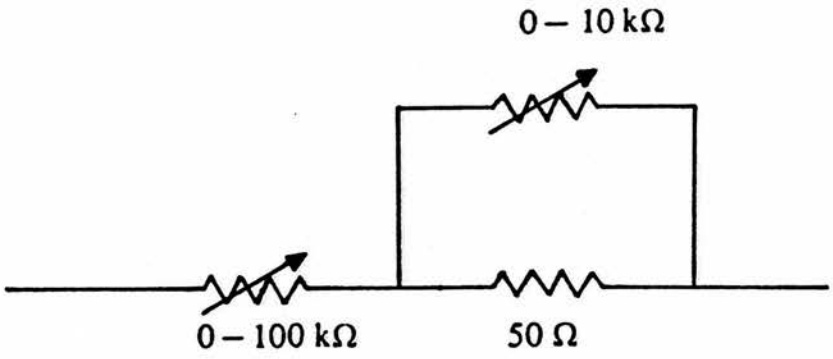

Figure 5.7 Parallel combination of resistors in R_s

calibrations were done as calorimetry runs to reduce the experimental uncertainty. R_s was altered during runs to keep the trace within the limits of the amplifier and the chart recorder paper. This aided interpretation of the runs since it was then easier to see if the initial and final drifts were parallel. It also meant that δR_s was only a small part of the total change in R_s. The experimental uncertainty in the chart calibration was approximately 1%, implying a 1% uncertainty in δR_s, whereas the manual change in R_s was known more accurately. The fact that δR_s was itself small therefore reduced the overall uncertainty in the fractional change of R_s.

So far only measurements in the neutron beam have been described. Measurements in the photon and electron beams were in principle identical to those in the neutron beam. Figure 5.8 illustrates runs with 4 MV and 9 MV photons and 10 MeV electrons. The principles behind analysing these runs is exactly as described above. The main difference in the photon and electron beams was that the doserate was much higher. It was approximately 250 cGy min^{-1} in the electron and 4 MV photon beams and 350 cGy min^{-1} in the 9 MV beam, and runs lasting one to two minutes were sufficient. The high doserate is illustrated in figure 5.8 by the rapid heating produced when the beam is switched on. The presence of several spikes on these traces is caused by more than one change in R_s during the course of a run. The sensitivity of the amplifier was a factor of two lower in both of the traces in the photon beams than it was in the neutron beam. This was because higher background drifts were acceptable and a large enough signal was obtained with the reduced amplifier gain. The interpretation of calorimetry runs has been described in terms of the chart recorder trace for ease of explanation.

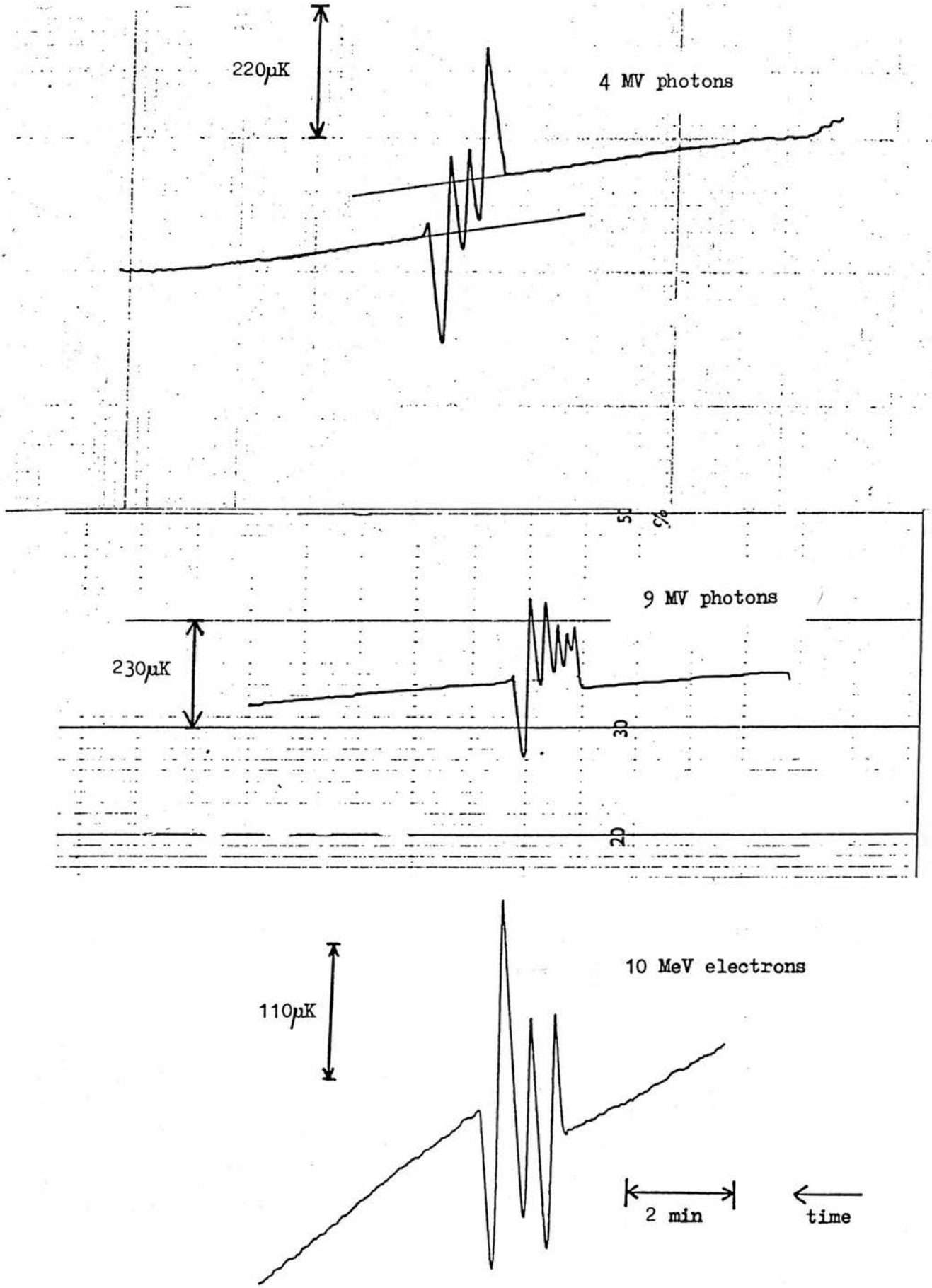

Figure 5.8 Calorimetry runs in the photon and electron beams

In fact the analysis of the runs was carried out by a computer and this is described in the following section.

5.5 DATA RECORDING AND ANALYSIS BY COMPUTER

At first the chart recorder traces were analysed by extrapolating the initial and final drifts by eye and measuring the deviations at mid-run with a ruler. A more objective method of obtaining δR_s was desired and the ouptut of the amplifier was therefore input to a Cromemco microcomputer. The $\pm$10 V output of the amplifier was directly connected to the analogue-to-digital convertor (ADC) of the computer. The chart recorder remained connected to the amplifier, in parallel with the computer, giving a visual record of each calorimetry run. The ADC had 12 bit resolution i.e. 4096 states, corresponding to the -10 V to +10 V range. The stability of the ADC was checked over a one week period; the zero (short circuit) value did not vary during the week and the number corresponding to +1.5 V was stable to $\pm$1 in 4096. The accuracy of the ADC was therefore $\pm$1 state corresponding to approximately $\pm$5 mV. The thickness of the line on the chart recorder trace was 0.5 mm and the deflection corresponding to the full 20 V was 250 mm. This meant that the resolution of the chart recorder was approximately $\pm$40 mV. Using the computer therefore improved the resolution of the signal coming from the amplifier.

The operation of the program used to analyse the calorimetry runs was as follows. The signal from the amplifier was read by the ADC at two second intervals. This value, in volts, was fed into an array which could store a maximum of 500 points (equivalent to a time of 17 minutes). Once sufficient points had been recorded to obtain an initial drift the beam was switched on. The computer was informed of this via

the keyboard and the points were then stored in a second array. When the beam went off the computer was again informed via the keyboard and the points for the final drift were recorded in a third array. When enough points had been accumulated for the final drift, data collection was terminated. The computer then carried out linear regression on the points in the first and third arrays to obtain two straight lines corresponding to the initial and final drifts. These lines were extrapolated to the mid point of the run, i.e. the point half-way through the number of entries in the second array, and the voltage difference at mid-run was calculated. At the end of each run several parameters were printed out: the run number and the voltage difference at mid-run along with the slope and intercept of both lines and the extrapolated values of the voltage at mid-run for each line. The run number, the number of points in each array and all of the values in the first and third arrays were then written onto floppy disc. Finally there was an option of carrying out another run or exiting from the program.

In the same way that the chart recorder had to be calibrated in Ω mm^{-1} the computer had to be calibrated in Ω V^{-1} in order that the voltage difference at mid-run could be related to a resistance change. This was done using the same program that was used for calorimetry runs. For a calibration the "beam on" period did not correspond to irradiation but to a manual change in R_s, and the initial and final drifts and the voltage difference at mid-run, were calculated in exactly the same way as in a calorimetry run.

The arrays were filled as indicated schematically in figure 5.9. If more than 500 points were collected, only those adjacent to the "beam

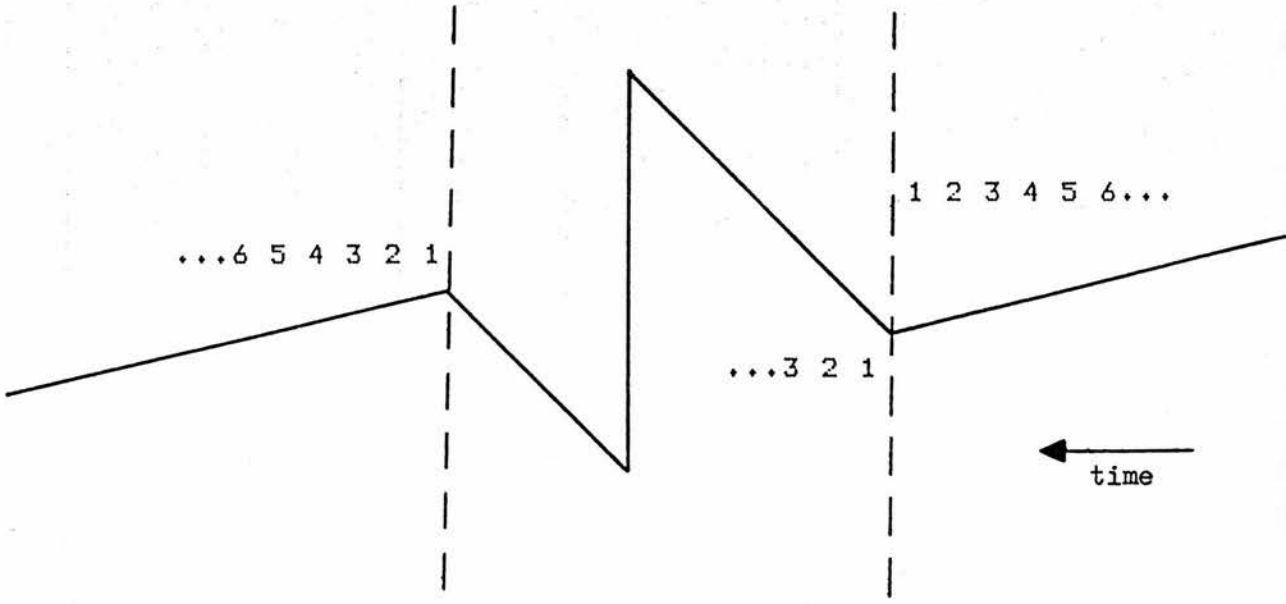

Figure 5.9 Allocation of data into arrays

on" period were stored. When there were periods of erratic drift it was sometimes desirable to eliminate certain points when calculating the straight lines. A program was written to re-analyse the calorimetry runs stored on disc. The program allowed the number of points used to calculate each straight line to be chosen independently. This allowed erratic periods of drift at the beginning of the initial drift or at the end of the final drift to be eliminated. In general a minimum of 30 points (one minute) was used to define a straight line. To check the operation of the program, several sets of calorimetry measurements were also analysed manually using the chart recorder traces, and the results were identical. The use of the computer gave an objective determination of $\triangle R_s$ and greatly speeded up the analysis of the calorimetry runs. It also gave a value for the deviation at mid-run immediately after the run, making any unexpected results immediately apparent.

CHAPTER 6

IONISATION CHAMBER DOSIMETRY

6.1 PHOTON AND ELECTRON DOSIMETRY

The use of ionisation chambers has long been accepted as the most practical method for the dosimetry of photon, electron and neutron beams. The precise methods for different radiations have, to some extent, been developed by different people and each radiation type is often considered separately. However, the underlying principles are common to all three radiations. Photon and electron dosimetry can be conveniently considered together and will be discussed first, followed by neutron dosimetry.

6.1.1 Cavity Theory

Consider the situation depicted in figure 6.1. A block of material (m) is irradiated by a beam of gamma rays. Within the material there is a radiation sensitive probe containing a gas (g) surrounded by a wall (w). The relationship between the absorbed dose in the vicinity of the point P and the signal from the radiation sensitive probe is the domain of cavity theory. Many authors have considered the problem in detail and only a brief discussion will be given here. The energy absorbed per unit mass of the gas (D_g) is given by

$$D_g = J_g \frac{W_g}{e} \qquad (6.1)$$

where J_g is the charge per unit mass produced in the gas, W_g is the average energy required to produce an ion pair in the gas and e is the

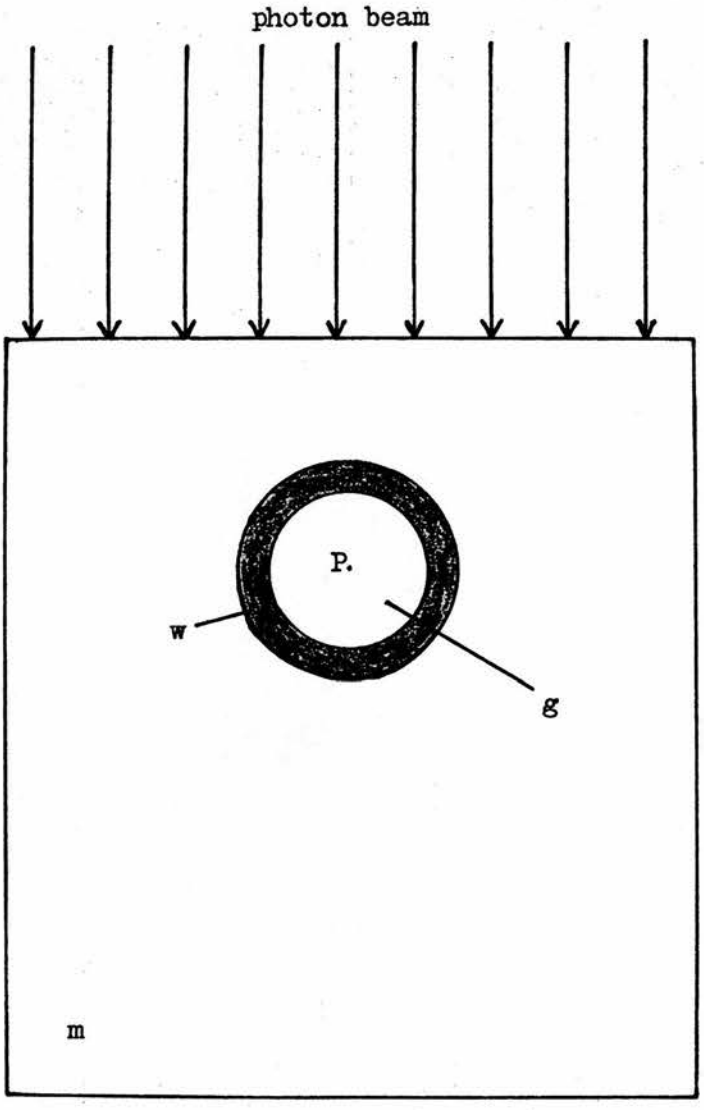

Figure 6.1

electronic charge. From this, and with the assumptions stated below, it follows that the absorbed dose in the medium (D_m) is given by

$$D_m = D_g \, s_{m,g} = J_g \frac{W_g}{e} \, s_{m,g} \qquad (6.2)$$

where $s_{m,g}$ is the ratio of mass stopping powers for the medium and the gas. Equation 6.2 is the familiar Bragg-Gray relationship, one obvious consequence of which is that the absorbed dose in the medium is proportional to the amount of ionisation produced within the probe.

There are several assumptions implicit in the derivation of equation 6.2. Charged particle equilibrium must exist in the region of P in the absence of the cavity. The presence of the cavity must not significantly affect the flux of charged particles produced by the incident radiation. As it stands equation 6.2 assumes that $s_{m,g}$ does not vary with energy and that the secondary charged particles, in slowing dose, lose their energy continuously. However, if the dimensions of the cavity are small, relative to the range of the secondary charged particles, the Bragg-Gray relationship is valid.

6.1.2 Exposure Calibration of Ionisation Chambers

Before the absolute calibration of ionisation chambers is discussed it is worth considering certain refinements to the simple cavity theory described in the previous section. Such refinements have mainly been concerned with the most appropriate quantity to use for the mass stopping power ratio in equation 6.2. Equation 6.2 assumes that the $s_{m,g}$ is constant for any two materials, whereas in reality it varies with energy. The most obvious modification to the ratio $s_{m,g}$ was to average the mass stopping powers over the spectrum of the secondary

electrons which traversed the probe. Spencer and Attix (1955) suggested that the mass stopping power ratio should be calculated using only collisions in which the energy loss was less than some cut-off value, Δ, where Δ was related to the dimensions of the cavity. These restricted mass stopping power ratios took into account the presence of delta rays, that is electrons, set in motion by the secondary electrons, but having enough energy themselves to cause further ionisation. The presence of delta rays contradicted the previous assumption that the secondary electrons slowed down essentially continuously, by a large number of collisions each involving the loss of a small amount of energy. Further theories also incorporated the density effect which causes a reduction in the stopping power due to the polarisation of the medium near the tracks of the charged particles. In photon dosimetry when the cavity becomes large relative to the range of the electrons produced in the surrounding material, the absorbed dose in the gas will be due to photon interactions in the cavity. In this case it is appropriate to use the ratio of mass absorption coefficients (μ_{en}/ρ) instead of $s_{m,g}$ in equation 6.2 (Nahum, 1978). In practice an expression containing both terms is used, where the relative proportions of the two ratios depends on the size of the cavity. Burlin (1966) has described a cavity theory encompassing all the above points.

The practical dosimetry of radiotherapy beams has generally been carried out using cavity ionisation chambers which have been calibrated in terms of exposure. It is not possible to use equation 6.2 directly because of the difficulty in determining the mass of gas within the cavity and ionisation chambers are therefore calibrated by irradiation in a known exposure of X-rays. If the ionisation chamber is irradiated

by a known exposure, X, of X-rays and gives a reading, R, then the exposure can be expressed as

$$X = R\ N_c \tag{6.3}$$

where N_c is the exposure calibration factor (X/R). The subscript c denotes the calibration conditions. If the chamber is subequently placed in a material, m, and irradiated by a different radiation beam, r, the absorbed dose to the material (D_m) can be determined from cavity theory, and is given by

$$D_m = R\ N_c \left(\frac{W_{air}}{e}\right)_c \left[\frac{(\mu_{en}/\rho)_w}{(\mu_{en}/\rho)_{air}}\right]_c \frac{(s_{m,g})_r}{(s_{w,g})_c} \frac{(W_g/e)_r}{(W_g/e)_c} \tag{6.4}$$

where the subscripts w and g refer to the chamber wall material and the gas respectively (Greening, 1981). D_m is the absorbed dose to the material at the position of the chamber, in the absence of the chamber. Several assumptions are made in the derivation of this equation. In particular it is assumed that in the calibration beam the ionising particles arise solely from the wall of the chamber whereas in the other radiation beam they arise solely from the surrounding medium. The effect of the displacement of the medium by the chamber must also be considered. There are therefore several small corrections to equation 6.4 which must be made.

Once the ionisation chamber has been calibrated against an exposure standard (for example, a free air chamber) it will indicate the exposure at the centre of the chamber in the absence of the chamber. In a water phantom the chamber will give the exposure at the centre of a "hole" in the water. It is necessary to correct this measured exposure to allow

for the absorption in, and scattering from, the water which would have been present had it not been displaced by the "hole". In a 2 MV photon beam with an ionisation chamber of diameter 6 mm this correction is a factor of 0.985 on the right hand side of equation 6.4 (Greene et al, 1962). A factor, known as the "perturbation correction" must also be included in equation 6.4 if the wall material is different to the medium in which the chamber is placed. The presence of the chamber wall will affect the photon and electron fluence since the mass energy absorption coefficient and the stopping power of the wall material will be different to those of the medium. Another factor must be included to account for the attenuation and scatter of the radiation in the walls of the chamber when it is being calibrated in air against an exposure standard.

A factor known as C_λ (where the parameter λ signifies the photon energy) was introduced by Greene (1962) such that equation 6.4 could be rewritten

$$D_w = R\ N_c\ C_\lambda \qquad (6.5)$$

C_λ contains the appropriate factors to convert the quantity RN_c to absorbed dose to water (D_w) when an air filled ionisation chamber is irradiated in a photon beam. Generally, published values of C_λ have also included the corrections described above. C_λ varies slowly with energy and provides a convenient method of calibrating megavoltage photon beams. The quantity C_λ is required because there is no primary standard available for the direct calibration of ionisation chambers at energies above 2 MV.

6.1.3 Photon Beams

The routine calibration of photon beams used in radiotherapy is performed with cavity ionisation chambers calibrated in terms of exposure according to the theory outlined in the previous section. The procedure is simplified by the use of the factor C_λ (equation 6.5). In both photon and electron beams it is absorbed dose to water which is usually determined from the ionisation chamber measurements. In order to measure absorbed dose to water absolutely it is necessary to have a chamber which has been calibrated absolutely in terms of exposure. In the United Kingdom this service is provided by the National Physical Laboratory and all radiotherapy departments have access to a "secondary standard" chamber which has an exposure calibration. Using such a chamber the absorbed dose to water is given by

$$D_w = R\, N_{2MV}\, C_\lambda \qquad (6.6)$$

where N_{2MV} is the exposure calibration factor for 2MV X-rays. This equation gives the absorbed dose to water at the centre of the chamber in the absence of the chamber. Values for C_λ have been obtained by calculation and from experiment, and several protocols have been published giving values of C_λ and conditions under which measurements should be performed (ICRU 1969, HPA 1969, HPA 1983). Using this method enables absorbed dose to be measured in photon beams of any energy, provided the appropriate C_λ value is known. Over the years modifications to the recommended values for C_λ have occurred due to theoretical considerations and to improvements in the basic data required to evaluate C_λ. To a certain extent C_λ is chamber dependent and this problem has been avoided in the HPA (1983) protocol which recommends a specific ionisation chamber for use as a secondary

standard. In the past it has been assumed that the chamber wall was water equivalent and that all the ionisation in the cavity arose from secondary electrons originating in the water. In fact a proportion of the ionisation arises from secondary electrons produced in the chamber wall. This proportion varies with energy and the HPA (1983) protocol takes this into account in evaluating C_λ. The values for C_λ given in the HPA (1983) protocol were used in this work.

In practice the secondary standard chamber is not used for routine measurements but another chamber, known as the field instrument, which is calibrated against the secondary standard, is used. All of the ionisation measurements in the photon beams (as well as the electron and neutron beams) carried out in this work employed a tissue equivalent ionisation chamber as the field instrument. This was an Exradin type T-2 chamber with a collecting volume of 0.5 cm^3 and constructed of tissue equivalent (A-150) plastic. This particular chamber, flushed with tissue equivalent gas, was the type used to calibrate the neutron beam for clinical use.

The main aim of this work was to measure absorbed dose in the neutron beam with the water calorimeter, and to compare the results with ionometric methods. In order to do this a jig was constructed which held the Exradin ionisation chamber at the appropriate depth in the water tank (see section 3.5). As this jig had already been constructed, it was convenient to use the Exradin chamber in the photon and electron beams, as well as in the neutron beam. One reason for making calorimetric measurements in the photon beam was that the doserate was a factor of ten greater than in the neutron beam. This made initial measurements with the calorimeter much easier to carry out, which aided

the development of the calorimeter. However, the measurements with photons and electrons were interesting in their own right.

If the HPA (1983) protocol is followed, a field instrument is calibrated in the beam in which it is to be used. In this beam the absorbed dose to water is obtained from the reading of the secondary standard chamber, using equation 6.6. Both chambers are given an identical exposure in a phantom; usually by interchanging the positions of the chambers and averaging the readings. This gives a value for the ratio between the reading of the field instrument (R_f) and the reading of the secondary standard chamber (R). Since the reading of each chamber is proportional to dose this ratio is constant whatever the magnitude of the given dose. Equation 6.6 can then be written

$$D_w = R_f \frac{R}{R_f} N_{2MV} C_\lambda$$

$$= R_f F_\lambda \qquad (6.7)$$

where F_λ can be considered as the calibration factor for the field instrument in the beam in which it has been calibrated. This calibration must be carried out for each energy at which the field instrument is to be used, because the C_λ factor is applied to the reading of the secondary standard chamber and not to the reading of the field instrument.

The above procedure was followed in calibrating the Exradin chamber in X-ray beams generated at 4 and 9 MV. The chamber was air-filled and calibrations were carried out in a perspex phantom at a depth of 5 cm in both beams. In general several correction factors should be applied to the reading of the chamber so that it corresponds to the charge produced

in an ideal cavity at a reference temperature and pressure. Good chamber design ensures that these corrections are small. The effect of reversing the polarising voltage on the Exradin chamber was investigated and was found to be negligible. The leakage current on the Exradin chamber and electrometer combination was also negligible. The ionisation measurements were corrected for the effect of ion recombination. Since the calibration and measurement depths were identical (5 cm) a recombination correction for the Exradin chamber was not necessary. The secondary standard readings were corrected for ion recombination, and the correction factors were 1.001 and 1.004 in the 4 and 9 MV beams respectively.

The uncertainties in determining absorbed dose to water using an exposure calibrated ionisation chamber have been analysed in detail by ICRU (1969). The uncertainty for megavoltage X-ray beams was estimated to be approximately $\pm$3%, and this value has also been quoted in more recent protocols. When using the Exradin chamber, with TE gas flowing through it, in the calorimeter an additional systematic uncertainty was introduced because the temperature of the gas within the chamber was not accurately known. After a calorimetry measurement the water into which the ionisation chamber was put was typically 3 to 4 degrees above the ambient air temperature and the TE gas cylinder was at the ambient temperature. It was therefore unclear which temperature should be used to correct the ionisation chamber measurements to standard temperature and pressure. An error of 4^{o}C in the gas temperature would result in an error of 1% in the dose measurement. The ionisation chamber was in the water tank at least 15 minutes before measurements were begun, and the temperature of the body of the chamber was probably close to that of the water. The temperature of the gas within the cavity was probably also

fairly close to the water temperature. In practice the gas temperature was assumed to be the same as the water temperature and consequently the dose measured by the ionisation chamber may have been slightly overestimated. Any error in the photon beams would be minimal since the chamber was air filled. In the electron and neutron beams, where TE gas flowed through the chamber, an upper limit of 0.5% for the error in the dose measurement is probably reasonable. This should be borne in mind when considering the calorimeter to ionisation chamber ratios.

6.1.4 Electron Beam

Essentially the same methods are used to calibrate electron beams as are used for photon beams. An ionisation chamber calibrated in terms of exposure is used to determine absorbed dose to water. Equation 6.4 is again the starting point and is rewritten as (HPA, 1971)

$$D_w = R \; N_c \; C_E \qquad (6.8)$$

where C_E is analogous to the factor C_λ used for photon beams. The same corrections to equation 6.4, described in section 6.1.2, are incorporated into C_E. C_λ included a correction to account for the fact that the exposure measured by a chamber in a phantom was not the same as it would have been in the absence of the chamber. In electron dosimetry this correction is more appropriately made by moving the effective point of measurement from the centre of the chamber towards the radiation source. For a cylindrical chamber the effective point of measurement is moved 2/3 to 3/4 of the chamber radius from the centre of the chamber. There is an additional consideration with electrons because the gas cavity scatters electrons less than the more dense

phantom material. Therefore another small correction is required since the electron fluence in the cavity is not the same as it would be in the absence of the chamber. From equation 6.4 it is clear that C_E depends on the mass stopping power ratio for the electrons crossing the cavity, which is a function of the energy spectrum of these electrons. In passing through a material the electron energy is reduced (by approximately 2 MeV cm^{-1} in water) and consequently the value of C_E changes significantly with depth. For the above reasons flat chambers are often used for the accurate dosimetry of electrons.

Several protocols have described appropriate methods for determining absorbed dose to water in an electron beam with an ionisation chamber calibrated in terms of exposure (HPA 1971, ICRU 1972, HPA 1985). The method used here was that described by HPA (1971) and ICRU (1972) but the more up to date data of HPA (1985) was used. The ionisation chamber used routinely to measure absorbed dose in the 10 MeV electron beam was a graphite walled Farmer chamber (type 2505-3A). This chamber had an exposure calibration factor (N_f) obtained by calibration against the secondary standard chamber, in a perspex phantom, in a 4MV beam. 4MV photons were used because neither a cobalt-60 nor a 2MV beam was available. When the Farmer chamber is placed in a phantom, in an electron beam, the absorbed dose to water is given by

$$D_w = R\, N_f\, C_E \qquad (6.9)$$

where the value of C_E depends on the average energy of the electrons (E_d) at the depth of the chamber (d). These are related to the initial energy of the electrons (E_o) by the equation

$$E_d = E_o\ (1 - d/R_p) \qquad (6.10)$$

(Harder, 1965), where R_p is the practical range of the electrons on the phantom material. Values of C_E are tabulated in the protocols mentioned above.

The Exradin ionisation chamber was used in a 10 MeV electron beam, to compare the calorimetry measurements with ionometric measurements. The Exradin chamber was calibrated directly against the Farmer chamber in the 10 MeV electron beam, in terms of absorbed dose to water. This calibration was carried out in the water calorimeter, under exactly the same conditions as existed during measurements with the Exradin chamber, in order to eliminate any errors which might have arisen in changing from calibration to experimental conditions. To perform this calibration it was necessary to construct a jig to hold the Farmer chamber, similar to the one which contained the Exradin chamber. The chambers were irradiated consecutively at identical positions in the water tank, at a depth of 19 mm which was the depth of the calorimetry measurements. During all of the measurements with the Exradin chamber in the electron beam tissue equivalent (TE) gas was flushed through the chamber. This was done because neutron measurements (which necessitated the use of TE gas) were being carried out over the same period as the electron measurements. To ensure that a variable mixture of gas was not present in the chamber TE gas was used routinely in both beams.

A value of C_E appropriate to a depth of 2 cm (or 22 mm, to be precise) and an initial electron energy of 10 MeV is necessary to obtain absorbed dose to water from the reading of the Farmer chamber. The measurements in the electron beam were carried out in 1984 and since then revised values of C_E have been published (HPA 1985). There are significant differences in the methods recommended in this protocol

compared to those recommended in HPA (1971). The method of determining the energy of an electron beam, and consequently the value obtained, has been changed in the new protocol. The photon calibration of the chamber is in terms of air kerma rather than exposure and the value taken for the chamber displacement factor has been reduced by 1.1%. These changes mean that the new protocol does not simply give revised values of C_E, and to signify this the new factors have been given the symbol C_e. Improvements in the basic data used to calculate C_e and the change in the recommended displacement factor mean that measured absorbed doses are significantly different when the new protocol is employed. The maximum change is for electrons with E_d = 8 MeV, where the result of employing the new protocol is to reduce measurements of absorbed dose to water by 4.8%. It is straightforward to calculate new values of C_E (to replace those in HPA (1971)) from the values of C_e given in HPA (1985). From equation 6.10 the value of E_d for electrons of initial energy 10 MeV at a depth of 2 cm in water is 6 MeV. At this energy the value of C_E, calculated from C_e, is 0.857. This compares with the value of 0.90 given in HPA (1971). The value of 0.857 was used in equation 6.9 to determine absorbed dose to water from the reading of the Farmer chamber. Thus, although the method of calibration was as described in HPA (1971), absorbed doses measured with the Farmer chamber, and the Exradin chamber, were the same as would have been obtained had the HPA (1985) protocol been employed.

Corrections to the ionisation chamber measurements were required for ion recombination and polarity. Since the Exradin chamber was calibrated against the Farmer chamber at the same depth as measurements were to be made, corrections were only required to the Farmer chamber readings. In the 10 MeV beam at a depth of 2 cm the polarity correction

was 0.998. The correction for recombination in the electron beam was significant due to the relatively high dose per pulse (290 cGy min^{-1} at 30 pulses per second). The amount of ion recombination, determined by the method described in the HPA (1985) code, was 3.0%.

The uncertainty in determining absorbed dose to water by the methods described in HPA (1985) is quoted as $\pm$3.8%. However, the effect of changing from the 1971 protocol to the 1985 protocol is to reduce measured absorbed doses by up to 4.8%. Uncertainties are not explicitly quoted in HPA (1971) or ICRU (1972) but values of 4–5% would not be unreasonable. This gives some indication of the difficulty in measuring absorbed dose with an exposure calibrated ionisation chamber in an electron beam.

6.2 NEUTRON DOSIMETRY

6.2.1 Additional Considerations with Neutrons

The interaction of neutrons with matter is more complex than that of photons because of the wide variety of charged particles which are produced. In tissue, recoil protons are most predominant but other recoil nuclei, fission fragments, subatomic particles and photons are also produced. The hydrogen content of a material is therefore critical in determining its dosimetry properties. For example, although the hydrogen content of soft tissue is only about 10% by weight, below 7 MeV the hydrogen contributes over 90% of the absorbed dose (Greening, 1981). There are some simplifications in neutron dosimetry, compared to photon dosimetry. The ranges of the recoil protons produced by neutron irradiation are much less than electrons of the same energy. A 1 MeV neutron produces a recoil proton with a mean range of 0.01 mm in tissue

and larger recoil nuclei have ranges considerably less than this. The ranges of the secondary ionising particles are much less than those of the neutrons producing them and for this reason there is a very close approximation to charged particle equilibrium. There is negligible bremsstrahlung production when heavy particles, such as protons, slow down in matter. Finally, the density effect, mentioned in section 6.1.2, is also insignificant, even with very high energy protons.

The short ranges of the secondary charged particles mean that it is impractical to employ ionisation chambers with cavities small enough that the secondary particles lose only a small proportion of their energy in crossing the cavity. In other words the conditions under which the Bragg-Gray equation can be applied are not satisfied. This problem is resolved by the use of homogeneous chambers, as a direct consequence of Fano's theorem. Fano's theorem applies to a material of uniform elemental composition which is exposed to a uniform flux of primary radiation such as neutrons. It states that the flux of secondary radiation is uniform and independent of the density of the medium as well as of the density variations from point to point. This theorem provides the justification for the use of homogeneous ionisation chambers in neutron dosimetry; that is, chambers where the wall material and filling gas have the same elemental composition. The most commonly used chambers are constructed of so-called tissue equivalent (TE) plastic, and filled with tissue equivalent gas. TE plastic contains a large amount of carbon (77%) and this carbon is present at the expense of oxygen since the oxygen content of standard reference tissue is 73% (ICRU, 1964). A correction, discussed in the next section, is therefore required to obtain absorbed dose to tissue from absorbed dose to A-150 plastic.

Another difficulty in neutron dosimetry is the determination of the W value, the average energy required to produce an ion pair in the gas. From equation 6.4 it can be seen that three W values are necessary to obtain absorbed dose from a chamber with an exposure calibration. In the calibration beam, which is a photon beam, the ionising particles are electrons and the W value is constant over a wide range of electron energies. In this case determinations of W have an uncertainty of approximately 1%. It is the W value appropriate to TE gas irradiated by neutrons, known as W_N, which provides the difficulty. As there is a complex assortment of secondary ionising particles the value of W_N is not constant with energy, as is the case with photons, and the value of W_N must be calculated according to the spectrum of the neutron beam. Goodman and Coyne (1980) have calculated values of W_N as a function of neutron energy and the uncertainty in its value is estimated to be 4%.

Some contaminating photons are always present in a neutron beam and more are produced as the neutrons interact with the irradiated material. Any ionisation chamber will respond not only to the neutron component but also to the photon component. In order to separately determine the absorbed dose delivered by the neutrons and that delivered by the photons it is necessary to use two dosimeters having different sensitivities to neutrons and photons. A TE ionisation chamber and a Geiger counter are commonly used for this purpose. The ionisation chamber has roughly the same sensitivity to neutrons and photons and the Geiger counter has a much lower sensitivity to neutrons than to photons. In practice the response of the TE ionisation chamber is considered to be proportional to the total absorbed dose and the validity of this statement is discussed in the next section.

6.2.2 Calibration of TE Chamber

Neutron dosimetry is discussed in ICRU report 26 (ICRU 1977) and a comprehensive protocol (Broerse et al, 1981) has been published by the European Clinical Neutron Dosimetry Group (ECNEU). The methods of calibration and detailed derivations of the required equations are given in the ECNEU protocol and only specific points will be discussed here.

In neutron dosimetry the standard reference material in which absorbed dose is quoted is a tissue composition defined by ICRU (1964), known as ICRU muscle. Water is not used because absorbed dose to water is significantly different from absorbed dose to tissue in neutron beams. To this end ionisation chambers constructed of TE plastic are commonly used to determine absorbed dose to ICRU muscle. However, such a chamber measures absorbed dose to the plastic which has to be converted to absorbed dose to ICRU muscle using the kerma ratio of the two materials. Other materials have also been used to construct ionisation chambers for neutron dosimetry. A polyethylene chamber flushed with ethylene gas (Greene, 1971) and a styrene equivalent chamber flushed with acetylene gas (Williams, 1985) are examples of such chambers. The water calorimeter measures absorbed dose to water. This is a useful quantity because the kerma ratio between water and ICRU muscle is relatively well known compared to the kerma ratio between TE plastic and water. This is because the matching of oxygen content between water and tissue is far better than for TE plastic, and the mismatch of hydrogen is less important due to the accuracy to which the hydrogen cross-section data are known. Table 6.1 gives estimates (Bewley, 1980) of the uncertainties in the kerma ratios between TE plastic and tissue, and water and tissue, for two different neutron

beams. At the higher energy the difference in uncertainties is considerable. However, a great deal of experience has been obtained in the use of TE chambers in neutron dosimetry and current protocols recommend their use (AAPM 1980, Broerse et al, 1981). The ionisation chamber which was employed for neutron measurements (an Exradin chamber) has already been described as it was also used in the photon and electron beams. An identical Exradin chamber was the one upon which clinical neutron dosimetry in Edinburgh was based.

	d(16) + Be	p(66) + Be
K_{TE} / K_{tissue}	2.6	10.6
K_{water} / K_{tissue}	0.4	1.8

Table 6.1. Percentage uncertainties in kerma ratios (Bewley, 1980).

Absorbed dose to ICRU muscle is obtained from a measurement with a TE ionisation chamber from the following equation (Broerse et al, 1981).

$$D_N + D_G = R_T(\prod k_R)_T(k_d)_T \quad \alpha_c \quad \frac{1}{k_T(1+\delta)} \qquad (6.11)$$

$$\text{where } k_T = \frac{W_c}{W_N} \quad \frac{(s_{m,g})_c}{(r_{m,g})_N} \quad \frac{[(\mu_{en}/\rho)_t/(\mu_{en}/\rho)_m]_c}{(K_t/K_m)_N}$$

R_T - the response of the TE ionisation chamber

$(\prod k_R)_T$ - product of several factors to correct to standard experimental conditions.

$(k_d)_T$ - displacement correction factor.

α_c - photon calibration factor.

δ - a factor to account for the unequal sensitivity of the chamber to photons and neutrons.

W_c/W_N - the ratio of average energies required to produce an ion pair in the calibration and neutron beams.

$(s_{m,g})_c$ - the ratio of mass stopping powers in the wall and gas for the calibration beam.

$(r_{m,g})_N$ - the absorbed dose conversion factor for neutrons.

$[(\mu_{en}/\rho)_t/(\mu_{en}/\rho)_m]_c$ - the ratio of mass energy absorption coefficients for tissue and for the wall material in the calibration beam.

$(K_t/K_m)_N$ - the ratio of kerma in tissue to that in the wall material in the neutron beam.

This equation gives the total dose i.e. the sum of the doses from the neutron and photon components. Equation 6.11 is derived from the equation

$$R_T(\prod k_R)_T(k_d)_T\,\alpha_c = k_T D_N + h_T D_G \qquad (6.12)$$

where
$$k_T = \frac{W_c}{W_N}\,\frac{(s_{m,g})_c}{(r_{m,g})_N}\,\frac{[(\mu_{en}/\rho)_t/(\mu_{en}/\rho)_m]_c}{(K_t/K_m)_N}$$

$$h_T = \frac{W_c}{W_G}\,\frac{(s_{m,g})_c}{(s_{m,g})_G}\,\frac{[(\mu_{en}/\rho)_t/(\mu_{en}/\rho)_m]_c}{[(\mu_{en}/\rho)_t/(\mu_{en}/\rho)_m]_G}$$

in which the absorbed dose from the neutrons (D_N) and the absorbed dose from the photons (D_G) are evaluated separately and added together. It

is convenient to rewrite equation 6.12 in the form of equation 6.11 and to assume that the total dose $(D_N + D_G)$ is proportional to the chamber reading. The quantity δ is introduced for this purpose and equations 6.11 and 6.12 define δ as

$$\delta = \frac{D_G}{D_N + D_G} \quad \frac{h_T - k_T}{k_T} \tag{6.13}$$

The photon content of the neutron beam was less than 10% at a depth of 5 cm in water, and a value of 0.001 was used for δ . In fact the approximation that $\delta = 0$ is not uncommon since it introduces only a small error into the evaluation of the total dose. As the calorimeter measured total absorbed dose it was appropriate to use equation 6.11 to determine total absorbed dose from the ionisation chamber measurements.

To obtain absorbed dose in a neutron beam absolutely it is necessary to measure α_c, the photon calibration factor, by calibrating the chamber in a photon beam. This amounts to determining the mass of gas within the cavity of the TE chamber. α_c is defined by

$$(D_t)_c = \alpha_c Q_c \tag{6.14}$$

where D_t is absorbed dose to tissue, Q is the charge collected by the chamber and c indicates the calibration beam. It follows directly that α_c is also given by

$$\alpha_c = \frac{1}{m} \frac{W_c}{e} (s_{m,g})_c \left[\frac{(\mu_{en}/\rho)_t}{(\mu_{en}/\rho)_m} \right]_c \tag{6.15}$$

where m is the mass of gas within the cavity. Hence a measurement of α_c in the photon beam determines m. α_c is measured by calibrating the TE chamber against the secondary standard exposure meter in a photon

beam. If F_c is the exposure calibration factor of the TE chamber, absorbed dose to tissue in the calibration beam is given by

$$(D_t)_c = F_c\, Q_c \left(\frac{W_{air}}{e}\right)_c \left[\frac{(\mu_{en}/\rho)_{tissue}}{(\mu_{en}/\rho)_{air}}\right]_c (k_w)_c\, (k_e)_c \qquad (6.16)$$

where k_w accounts for the attenuation and scatter caused by the chamber wall and k_e is the electrometer factor. Comparing equations 6.14 and 6.16 gives

$$\alpha_c = F_c \left(\frac{W_{air}}{e}\right)_c \left[\frac{(\mu_{en}/\rho)_{tissue}}{(\mu_{en}/\rho)_{air}}\right]_c (k_w)_c\, (k_e)_c \qquad (6.17)$$

The quantities required in equation 6.17 are most accurately known for low energy X-rays. For this reason the photon calibration of the TE chamber was carried out with X-rays generated at 300 kV. Table 6.2 lists the values of the parameters in equation 6.17. The attenuation produced by the chamber wall and the increased scatter tend to cancel each other and the value of k_w at 300 kV is 1.000 (Barnard et al 1959, Franz 1971). The ratio of mass energy absorption coefficients was calculated from the data of Hubbell (1977) assuming an average X-ray energy of 150 keV. The ECNEU protocol lists several correction factors which should be applied to the chamber reading. The only factor which was not taken as unity was k_e which has been included in equation 6.17. This factor is present because the electrometer used for calibration was different from the one used for measurements. The protocol also gives correction factors to be included in equation 6.17, all of which were taken to be unity. Although the wall correction factor, k_w, has been included explicity in equation 6.17, it is also unity at 300 kV.

Quantity	Value
F_c	1.363×10^{-3} C kg^{-1} nC^{-1}
$\frac{W_{air}}{e}$	33.85 J C^{-1}
$\frac{(\mu_{en}/\rho)_{tissue}}{(\mu_{en}/\rho)_{air}}$	1.100
k_w	1.000
k_e	1.002

Table 6.2. Parameters required to evaluated α_c.

Absorbed dose to ICRU muscle was determined from measurements in the neutron beam using equation 6.11. Values of the parameters required in equation 6.11 for the Edinburgh neutron beam, are given in table 6.3. Also included in table 6.3 is an estimate of the uncertainty (one standard error) in these values. Some of the quantitities in table 6.3 are spectrum dependent. They were calculated using a modified version of the spectrum measured by Bonnett (1979) in a d(16)+Be neutron beam. As the deuteron energy at Edinburgh was 15 MeV this measured spectrum was scaled to the lower energy. According to table 6.3 the overall uncertainty in determining absorbed dose to ICRU muscle with the Exradin ionisation chamber is 5.4%. Mijnheer and Williams (1981) have detailed the uncertainties in absorbed dose measurement with TE chambers calibrated by different methods. In particular they quote an uncertainty of 6.5% when an exposure calibrated TE chamber is employed in a d(16)+Be neutron beam. This slightly higher uncertainty arises because they have used a value of 4.3% for the uncertainty in

$(r_{m,g})_N/(s_{m,g})_c$ whereas a value of 2% was given in table 6.3. The ECNEU protocol recommends an uncertainty of 2% although in both cases the source is the same (Bischel and Rubach, 1978). In fact Bischel and Rubach quote uncertainty of 4.3%, and the best estimate of the overall uncertainty with the TE ionisation chamber is probably 6.5%.

Table 6.3. Parameters used in the calculation of absorbed dose from the ionisation chamber measurements.

Parameter	Value	Uncertainty (%)
α_c	5.07×10^{-2} Gy nC^{-1}	1.2
$(k_d)_T$	0.993	0.5
$(1 + \delta)$	1.001	-
W_c/W_N	0.940	4.0
$(r_{m,g})_N/(s_{m,g})_c$	0.99	2.0
$[(\mu_{en}/\rho)_t/(\mu_{en}/\rho)_m]_c$	1.006	0.1
$(K_t/K_m)_N$	0.982	2.6
	* Overall	5.4

* The overall uncertainty is taken as the root of the sum of the squares of the individual uncertainties, including a 0.4% uncertainty in the reading of the chamber.

CHAPTER 7

PHOTON AND ELECTRON MEASUREMENTS

7.1 CORRECTIONS TO CALORIMETRY MEASUREMENTS

Before considering the results of the calorimetry measurements it is necessary to elaborate on the equations used to calculate the absorbed dose. The calorimeter measures the temperature rise induced by the radiation beam at the position of the thermistor. The absorbed dose to the water in the immediate vicinity of the thermistor is given by equation 2.1. This equation gives the absorbed dose under ideal conditions but two small corrections, described in the next two sections, are necessary in practice.

7.1.1 Correction for Power Dissipation in the Thermistor

Equation 2.1 assumes that the temperature rise of the water, ΔT_w, is given by

$$\Delta T_w = \Delta T = \frac{\Delta R_t}{R_t} \frac{T^2}{B} \qquad (7.1)$$

where ΔT is the temperature rise of the thermistor. This is only true if the quantity δT (see section 4.5.2) is constant. However, as the temperature of the thermistor rises during irradiation, its resistance decreases and the power dissipated within it increases. This has the effect of increasing δT and, as it stands, equation 7.1 would therefore overestimate the temperature rise of the water. A correction to equation 2.1 is necessary because it is the temperature rise of the water multiplied by its specific heat which gives the absorbed dose.

The power dissipated in the thermistor (P_t) is given by

$$P_t = \frac{V_t^2}{R_t} \tag{7.2}$$

where V_t is the voltage across the thermistor and R_t is its resistance. Since the variable resistor R_s (see figure 4.2) is altered during the course of a calorimetry run to approximately rebalance the bridge, the voltage across the thermistor remains approximately constant. Differentiating equation 7.2 gives

$$\frac{\Delta P_t}{P_t} = \frac{-\Delta R_t}{R_t} \tag{7.3}$$

showing that the magnitude of the fractional change in P_t is the same as the magnitude of the fractional change in R_t. Since δT is proportional to P_t (see equation 4.9) the magnitude of the fractional change in δT is also equal to the magnitude of the fractional change in R_t.

The initial value of δT was obtained from the power dissipation in the thermistor and the measured self-heating factor for the thermistor (see section 4.5.2). For a given calorimetry run the change in δT was readily evaluated from the measured fractional change in R_t. Under typical conditions the overall temperature change, ΔT, had to be reduced by 0.2%. In practice the appropriate correction was calculated and applied to the measured temperature rise for each calorimetry measurement. Although this correction is considered to be accurately determined, an uncertainty of 0.05% has been included in the measurement of the overall temperature rise to take into account any error in the value of the correction.

7.1.2 Correction for Polyethylene Sheets

The bridge circuit correctly measures the temperature rise of the thermistor but it is the temperature rise of the water immediately surrounding the thermistor which is desired. The absorbed doses in the polyethylene sheets and in the surrounding water are approximately equal but the specific heat of polyethylene is roughly half that of water. If no heat conduction occurred the radiation induced temperature rise of the polyethylene sheets would be approximately twice that of the water, primarily because of the difference in heat capacities. In reality as soon as any temperature differential is established heat will begin to flow from the polyethylene to the water. When the radiation beam is turned off the temperature of the polyethylene sheets is slightly higher than the temperature of the water and this excess temperature gets smaller as heat continues to flow out of the polyethylene. As the thermistor is sandwiched between the two layers of polyethylene its temperature is equal to the temperature of the polyethylene, and therefore slightly overestimates the temperature rise of the water. The excess temperature of the polyethylene sheets was evaluated as a function of the time after the beam was turned off. From this a correction was applied to the temperature rise of the thermistor to give the temperature rise which would have occurred in the water had the polyethylene sheets not been present.

Fortunately a theoretical solution to this heat conduction problem is given by Carslaw and Jaeger (1959). The problem is broken down as follows. Figure 7.1 illustrates the relative temperature rise which would occur in the water and the polyethylene sheets if an instantaneous pulse of radiation was applied. The thermistor is at $x = 0$ and the

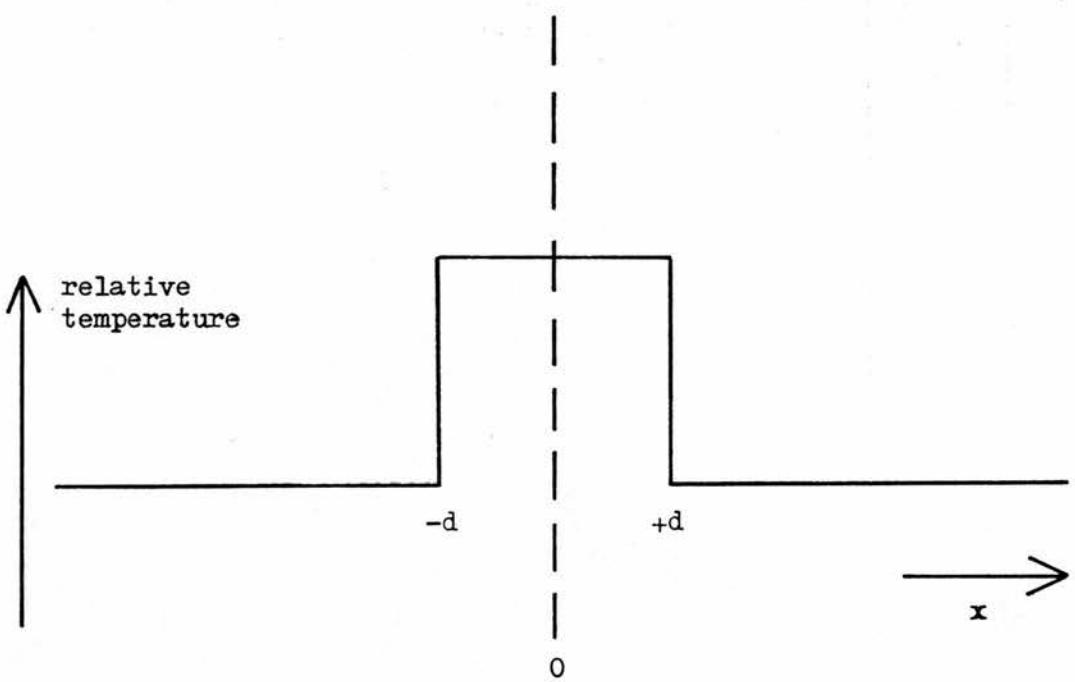

Figure 7.1 Relative temperature rises in water and polyethylene

thickness of the polyethylene is d. The relative temperature rise in the photon beams is given by

$$\frac{\Delta T_{polyethylene}}{\Delta T_{water}} = \frac{(\mu_{en}/\rho)_{polyethylene}}{(\mu_{en}/\rho)_{water}} \quad \frac{c_{water}}{c_{polyethylene}} \qquad (7.4)$$

and this ratio is equal to 1.87 in both the 4MV and 9MV photon beams.

For the solution given by Carslaw and Jaeger to be directly applicable the problem has to be modified slightly. The polyethylene needs to lose a certain amount of excess heat to reach the same temperature as the water. If the polyethylene was replaced by water what would the excess temperature (δT, say) of the water be if it contained the same excess heat? These are related by

$$(\rho.c.\delta T)_{water} = (\rho.c.\delta T)_{polyethylene} \qquad (7.5)$$

where ρ is the density. Since the density of polyethylene is 0.95 gm cm it follows directly that

$$\frac{\delta T_{water}}{\delta T_{polyethylene}} = 0.523 \qquad (7.6)$$

From equation 7.4 the excess temperature of the polyethylene was $0.87\Delta T_{water}$; the excess temperature of the thin layer of water is therefore $0.523.0.87\ \Delta T_{water} = 0.46\ \Delta T_{water}$. Hence the entire region can be considered as water but at the position where the film is normally located the water receives a doserate 46% greater than the rest of the water.

The equation given by Carslaw and Jaeger (1959) is

$$A(t,x) = \frac{2Fk^{\frac{1}{2}}}{K}\left[t^{\frac{1}{2}}\ \text{ierfc}\ \frac{x}{2k^{\frac{1}{2}}t^{\frac{1}{2}}} - (t-T)^{\frac{1}{2}}\ \text{ierfc}\ \frac{x}{2k^{\frac{1}{2}}(t-T)^{\frac{1}{2}}}\right] \qquad (7.7)$$

where A = temperature at time t and position x

t = time

x = distance

T = time when heating ceases

F = heat supplied per unit time per unit area

K = thermal conductivity = 0.602 $Js^{-1}m^{-1}{}^{o}C^{-1}$, for water

k = thermal diffusivity = 1.44×10^{-7} m^2s^{-1}, for water

and ierfc = the error function.

This equation gives the temperature as a function of position and time (for times $t > T$), for the situation depicted in figure 7.2. Figure 7.3 depicts the situation in the calorimeter. Since heat flow about $x = 0$ is symmetrical this is identical to the situation where the region $x < 0$ is a perfect insulator. Apart from the fact that heat is supplied uniformly to a film of thickness d equation 7.6 is now applicable. Since it is the temperature at $x = 0$ in which we are interested equation 7.7 reduces to

$$A(t) = \frac{2Fk^{\frac{1}{2}}}{K\sqrt{\pi}} \left[t^{\frac{1}{2}} - (t - T)^{\frac{1}{2}} \right] \qquad (7.8)$$

Under the conditions assumed irradiation results in a temperature rise of the bulk of the water and a 46% greater temperature rise in the thin water films. The dose gradient in the water is a secondary effect and is ignored in this analysis. Since the principle of superposition is valid with heat sources, the excess heating in the films and the bulk heating of all of the water can be considered independently. For simplicity irradiation can be considered to raise the temperature of the

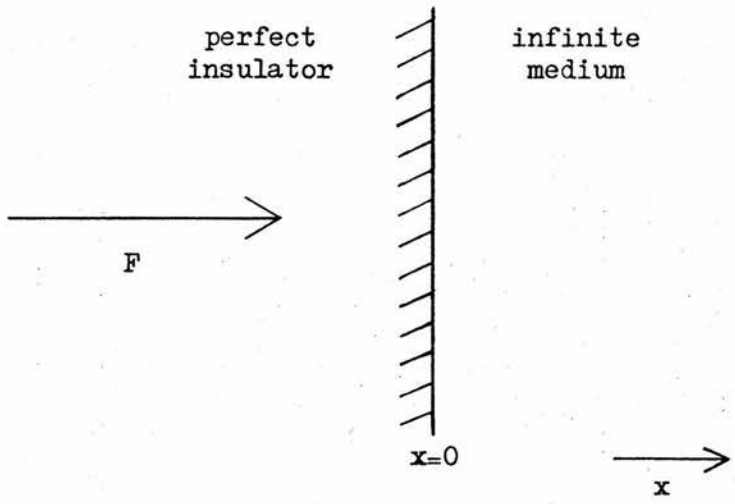

Figure 7.2 Conditions under which equation 7.7 applies

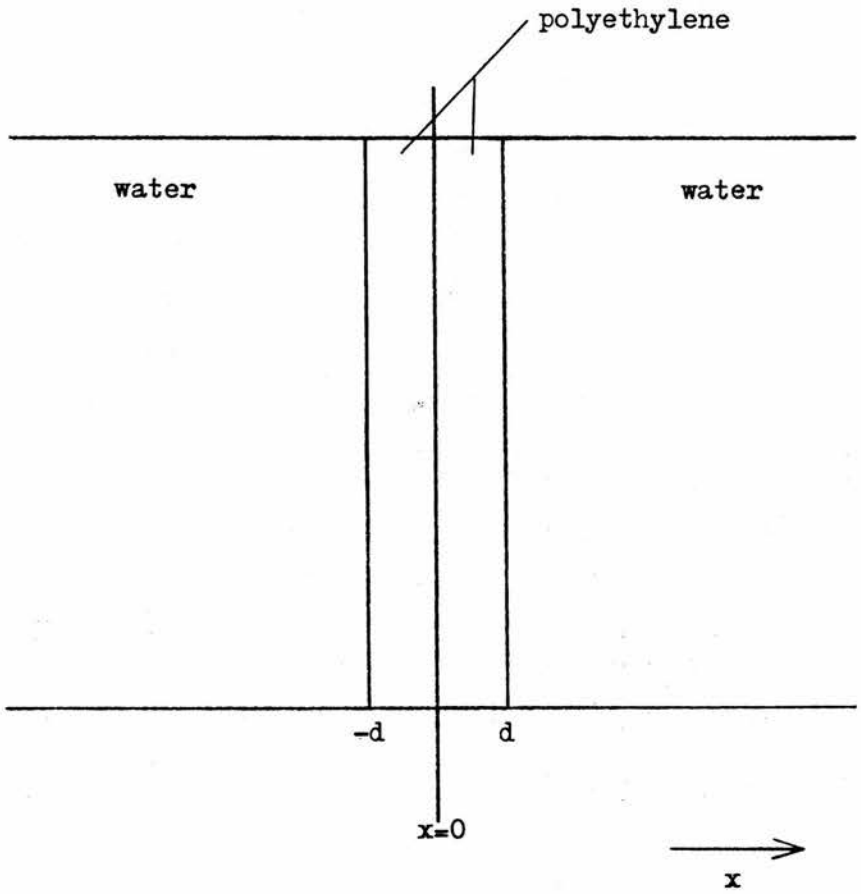

Figure 7.3 Situation in the calorimeter

water by $1^{o}Cs^{-1}$, i.e. 4.18×10^{6} J $s^{-1}m^{-3}$ is supplied to the water. In this case F is given by

$$F = 4.18 \times 10^{6} \cdot 0.46 \cdot d \qquad (7.9)$$

where d, the thickness of the film, is 25×10^{-6}m. A typical irradiation in the photon beams lasted 90 seconds, in which time the temperature rise of the bulk of the water would be $90^{o}C$ under the assumed conditions. The excess temperature at x = 0, given by equation 7.8 has been plotted in figure 7.4 as a percentage of $90^{o}C$, starting at the point where the beam is switched off. Also plotted are the corrections corresponding to T = 180 s and T = 20 s which were the two extremes in the 9MV photon beam. After a calorimetry run the temperature drifts which were extrapolated back to mid-run lasted between 1 and 5 minutes. The correction which should be applied does not therefore correspond to the excess temperature which exists at the instant the beam is turned off, but at some time thereafter. From figure 7.4 it can be seen that 30 to 60 seconds after beam turn off the excess temperature is approximately 0.2%, irrespective of the duration of the calorimetry run. A correction of 0.2% was therefore applied to all of the measurements in the photon beams. The precise corrections applied in the electron and neutron beams are given in the relevant sections. An uncertainty of 0.1% was associated with the measurement of the overall temperature rise, to take into account any possible error in the determination of this correction.

The thermal effects of the thermistor and its leads were also investigated using solutions for heat flow from point and line sources respectively. For both the thermistor and its leads corrections of less than 0.01% would be required and these were ignored.

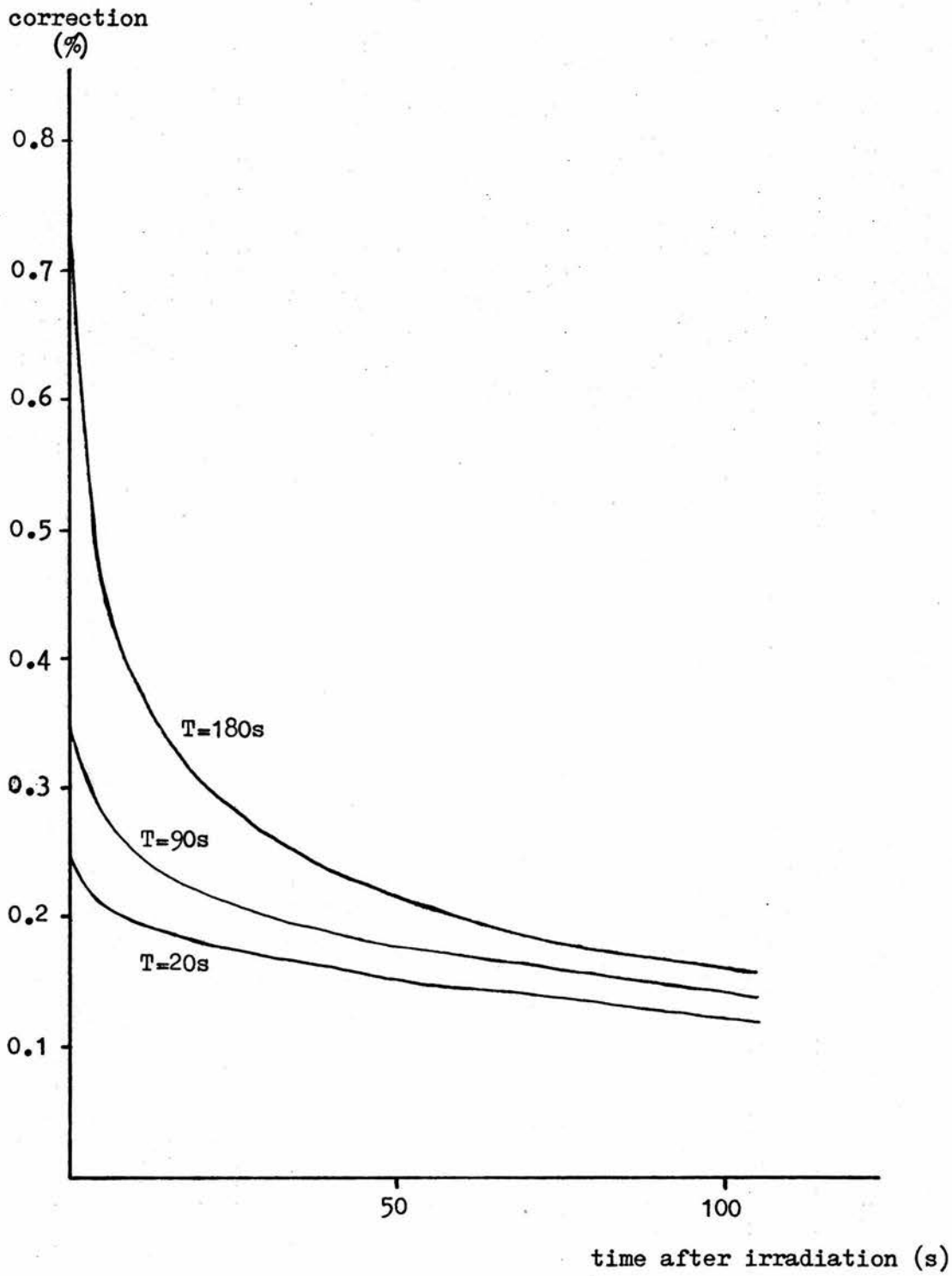

Figure 7.4 Excess temperature of thermistor

7.2 9 MV PHOTON BEAM

All of the measurements carried out were comparisons between the calorimeter and an ionisation chamber. Since it was not possible to carry out measurements with the calorimeter and the ionisation chamber simultaneously, it was necessary to have a method of monitoring the radiation beam. A transmission ionisation chamber in the head of the linear accelerator, with a display on the control panel, provided one means of monitoring the beam. However, temperature changes in the head of the accelerator could have produced variations in the reading of this ionisation chamber. The arrangement illustrated in figure 7.5 was therefore adopted as a more accurate method of monitoring the beam. A small waterproof ionisation chamber (manufactured by PTW), held in a Perspex tube, was positioned 3 cm deeper than the thermistor (or the Exradin chamber which replaced it) as shown in figure 7.5. This chamber remained in the same position throughout both the calorimetry and the ionisation chamber measurements, and all readings were normalised to the reading of this chamber.

The calorimeter was situated under the head of the linear accelerator with the thermistor at the centre of the radiation field. The size of the field was 35 x 35 cm at a distance of 100 cm from the target, which was the approximate position of the thermistor. The thermistor was at a depth of 5 cm in the water, where the doserate was typically 320 cGy min^{-1}. The signal leads from the calorimeter passed through a channel in the wall of the treatment room and the bridge and associated electronics were situated adjacent to the control panel of the linear accelerator. The calorimeter was normally set up the evening before the day on which measurements were to take place. This

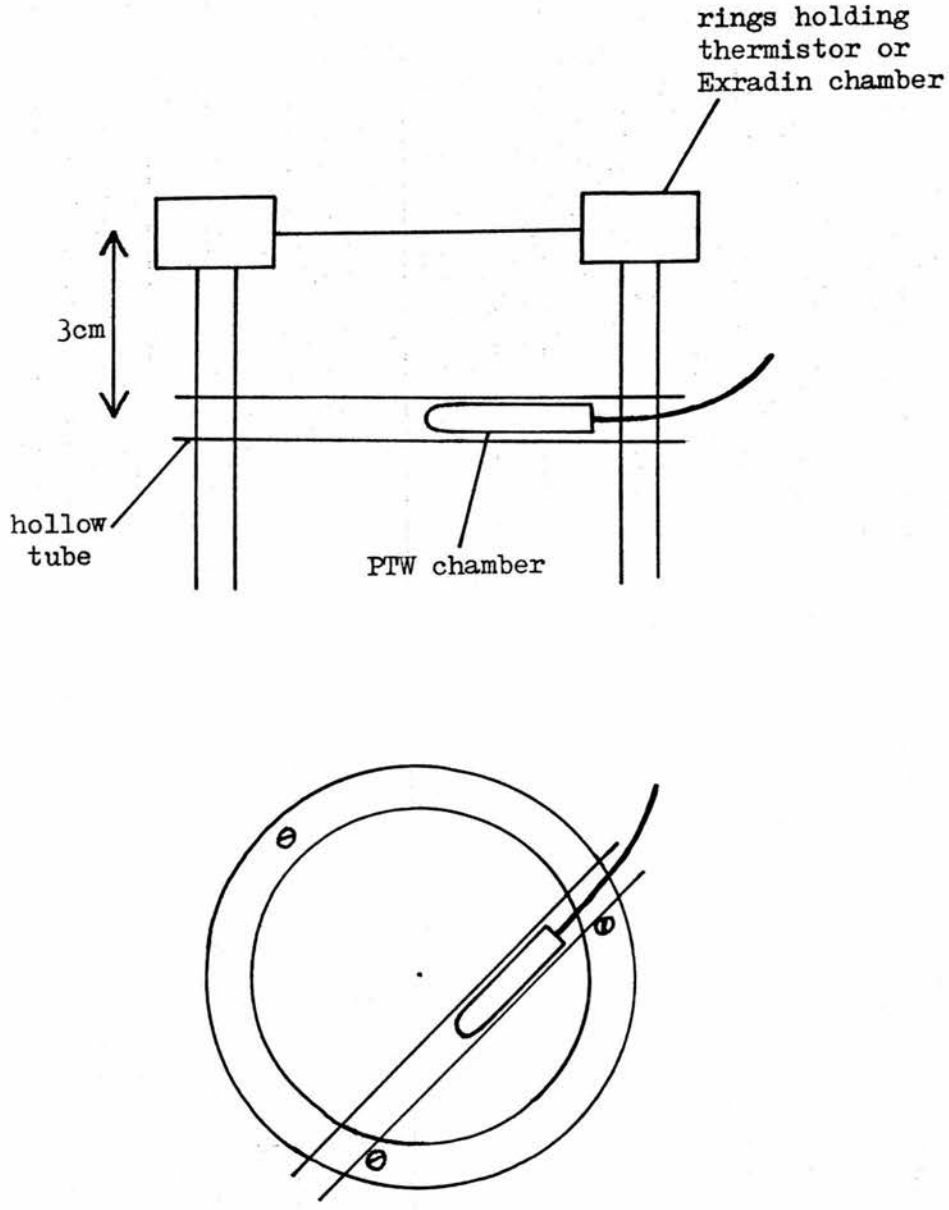

Figure 7.5 Position of PTW ionisation chamber

allowed a long period for the calorimeter to settle although it was possible to make measurements a few hours after setting it up. Examples of calorimetry runs in the 9 MV photon beam are given in figure 7.6. The results are detailed in table 7.1 where the headings have the following meanings.

(i) Panel Units. This is the number of panel units displayed on the control panel and is approximately equal to the absorbed dose at the position of the thermistor.

(ii) N. This is the number of calorimetry runs in a set of measurements.

(iii) R_s. This is the resistance of the balancing resistor R_s. The resistance of the thermistor is given by $R_s/9.168$, since 9.168 was the exact value of the bridge ratio.

(iv) ΔR_s. This is the overall change in R_s which corresponds to the change in the resistance of the thermistor.

(v) ΔT. This is the temperature rise of the thermistor.

(vi) Power Dissipation. This is the level of power dissipation in the thermistor.

(vii) S.D. This column gives one standard deviation of the set of N runs which were carried out.

(viii) D_{cal}/PTW. This is the absorbed dose measured by the calorimeter, before any corrections have been applied, divided by the reading of the ionisation chamber monitor.

(ix) D_{Ex}/PTW. This is the absorbed dose measured by the Exradin chamber divided by the reading of the ionisation chamber monitor.

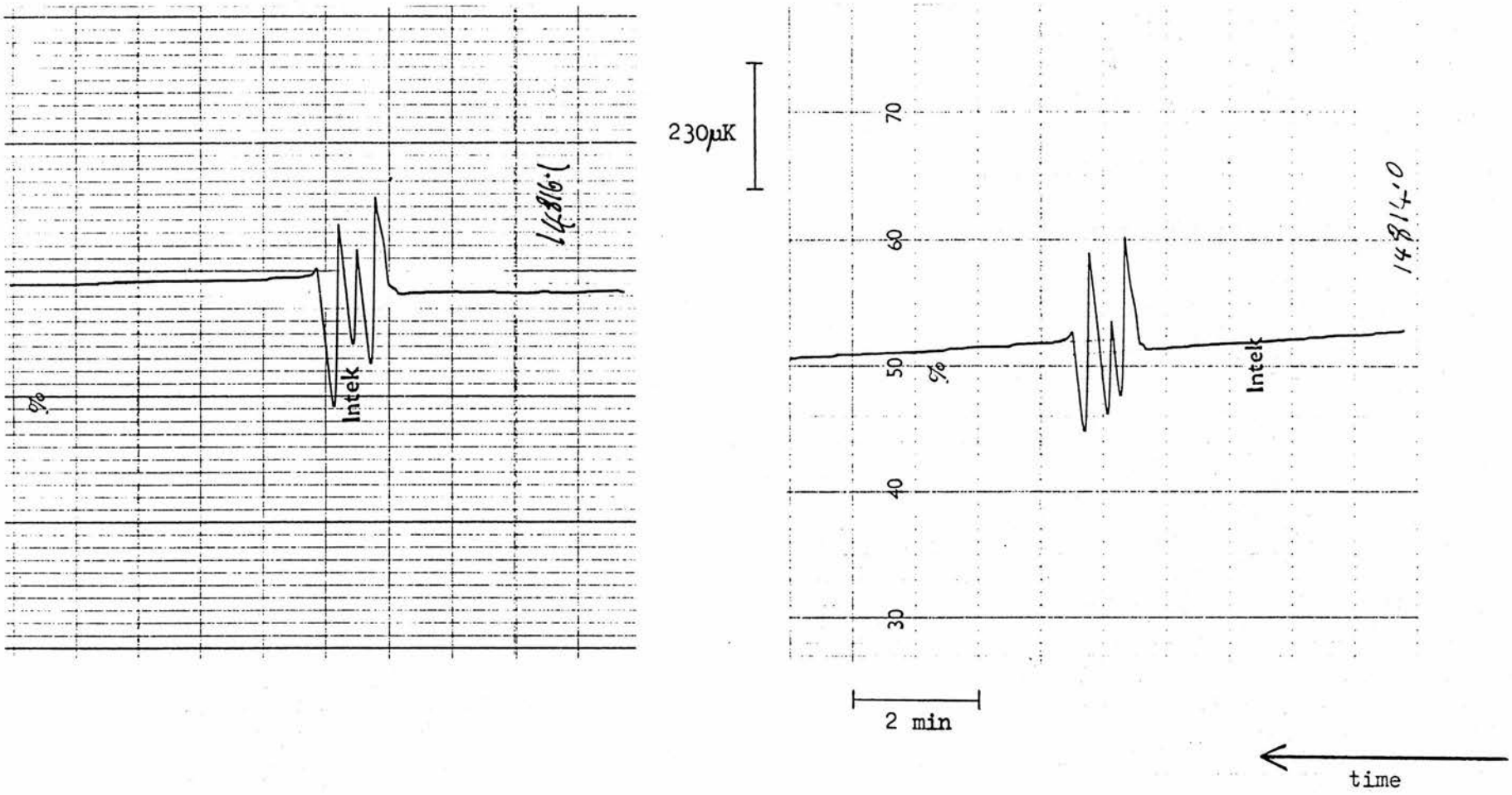

Figure 7.6 Calorimetry runs in the 9 MV photon beam

Measurement	Panel Units	N	R_s (Ω)	ΔR_s (Ω)	ΔT (mK)	Power Dissipation (μW)	SD (%)	$\frac{D_{cal}}{PTW}$ (Gy/monitor unit)	$\frac{D_{Ex}}{PTW}$ (Gy/monitor unit)	$\frac{D_{cal}}{D_{Ex}}$
1	100	15	15359	0.132	0.27	16	1.0	0.4292	0.4041	1.057
2	100	10	14841	0.128	0.27	17	0.6	0.4379	0.4205	1.036
3	100	10	14985	0.128	0.27	17	0.4	0.4307	0.4141	1.035
4	400	10	14898	0.523	1.09	17	0.6	0.4508	0.4218	1.064
5	400	10	14865	0.522	1.09	17	0.7	0.4455	0.4217	1.052
6	1000	10	15574	1.34	2.65	16	0.6	1.195	1.144	1.040
7	1000	9	15794	1.38	2.68	16	0.2	1.218	1.158	1.047
8	1000	5	15995	1.35	2.60	16	0.3	0.4180	0.4036	1.031
9	500	6	15995	0.69	1.33	16	1.0	0.4254	0.4036	1.049
10	1000	6	15379	1.32	2.66	16	0.8	0.4222	0.4033	1.042
11	500	6	15379	0.67	1.36	16	1.3	0.4274	0.4033	1.055
12	300	6	15379	0.40	0.81	16	1.2	0.4253	0.4033	1.050
13	200	10	15833	0.27	0.53	21	1.3	0.4123	0.3977	1.031

mean = 1.045

Table 7.1. Results of measurements in the 9 MV photon beam.

(x) D_{cal}/D_{Ex}. This column gives the ratio of the absorbed dose measured by the Exradin ionisation chamber, divided by the reading of the monitor, when both the correction for changes in the thermistor power dissipation and the correction for the polyethylene films have been included in the calorimetry results.

The calculation of absorbed dose to water from the Exradin chamber measurements has already been described in chapter six. The absorbed dose to water was calculated from the calorimetry measurements using equation 2.1. The two corrections described in section 7.1 were then applied. The correction applied for the polyethylene sheets was a reduction of 0.2% (see section 7.1.1). The average ratio D_{cal}/D_{Ex} is 1.045 and one standard error on the mean (s.e.m.) of the thirteen ratios in table 7.1 is 0.3%.

7.3 4 MV PHOTON BEAM

Measurements in the 4 MV beam were virtually identical to those in the 9 MV beam. The PTW ionisation chamber was again used as a monitor and was in the position illustrated in figure 7.5. The profile of the 4 MV beam was not perfectly flat. Due to an obstruction in the beam path there was a small dip in the beam profile on the central axis. For this reason the thermistor was offset approximately 5 cm from the central axis of the beam so that measurements were carried out on a flat part of the beam. This eliminated any possibility of a difference in the responses of the calorimeter and the ionisation chamber due to the difference in their sizes. The thermistor was approximately 100 cm from the target (at a depth of 5 cm) where the size of the radiation field was 30 x 30 cm. The doserate at the thermistor was 220 cGy min^{-1}

and most of the calorimetry runs lasted around 90 seconds. Examples of calorimetry runs in the 4 MV photon beam are given in figure 7.7.

The results of measurements in the 4 MV beam are detailed in table 7.2. The headings in table 7.2 have the same meanings as those of table 7.1. A correction of 0.2% was applied to allow for the polyethylene films. Calorimetry runs lasted between 20 and 100 seconds and figure 7.4 illustrates that a correction of 0.2% was appropriate. The average ratio D_{cal}/D_{Ex} is 1.040, and one s.e.m. of the six ratios in table 7.2 is 0.3%.

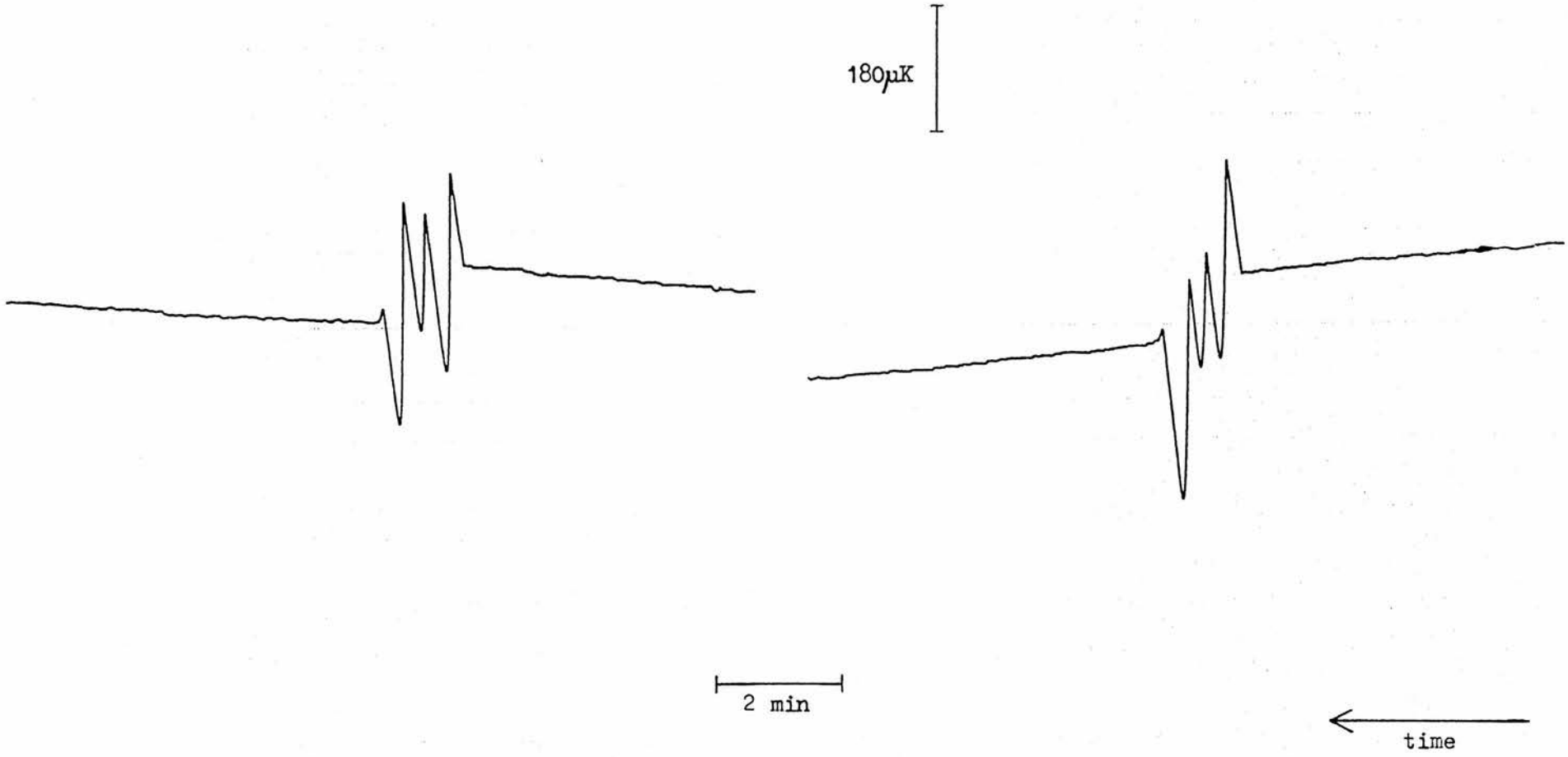

Figure 7.7 Calorimetry runs in the 4 MV photon beam

Measurement	Panel Units	N	R_s (Ω)	ΔR_s (Ω)	ΔT (mK)	Power Dissipation (μW)	SD (%)	$\frac{D_{cal}}{PTW}$ (Gy/monitor unit)	$\frac{D_{Ex}}{PTW}$ (Gy/monitor unit)	$\frac{D_{cal}}{D_{Ex}}$
1	350	16	15887	0.464	0.90	21	0.5	0.4412	0.4166	1.053
2	300	10	16201	0.403	0.76	20	0.6	0.4310	0.4140	1.036
3	300	10	16930	0.435	0.78	19	1.0	0.4371	0.4183	1.039
4	300	10	17192	0.448	0.79	19	1.0	0.4337	0.4162	1.037
5	250	9	16480	0.337	0.62	20	1.0	0.4180	0.4031	1.032
6	70	10	15069	0.0856	0.18	22	0.9	0.4242	0.4059	1.040

mean = 1.040

Table 7.2. Results of measurements in the 4 MV photon beam.

7.4 10 MEV ELECTRON BEAM

The absorbed dose falls off much more steeply with depth in the electron beam than it does in the photon beams. Measurements were carried out at the depth of maximum absorbed dose, d_{max}, which was 19 mm deep in the water when the effect of the expanded polystyrene "lid" of the calorimeter was taken into account. At the position d_{max}, on the top of the depth dose curve, the dose is varying least with depth. Making measurements at this depth minimised any error due to the depths of the thermistor and the Exradin ionisation chamber not being equal. The PTW chamber monitored the beam and was also positioned at d_{max} using the arrangement of figure 7.8. The thermistor was placed in the centre of the radiation field, 110 cm from the source. No horn or applicator was used on the accelerator head so that the whole calorimeter was irradiated. The doserate in the electron beam, at the position of the thermistor, was typically 290 cGy min^{-1}.

Figure 7.9 illustrates two typical calorimetry runs in the electron beam. It can be seen in figure 7.9 that the final drifts are not quite parallel to the initial drifts. This was a characteristic of measurements in the electron beam. The explanation for this is probably that heat was flowing away from the thermistor due to the relatively steep temperature gradients produced by the electron beam. The depth dose falls off much more rapidly in the electron beam than it does in the photon beams. In the electron beam measurements were carried out at the peak of the depth dose curve and heat therefore flowed away from the thermistor in both vertical directions. In the photon beams measurements were carried out at a depth of 5 cm and heat flow at the thermistor was therefore in the downward direction only. In this case approximately as much heat flowed into the plane of the thermistor as

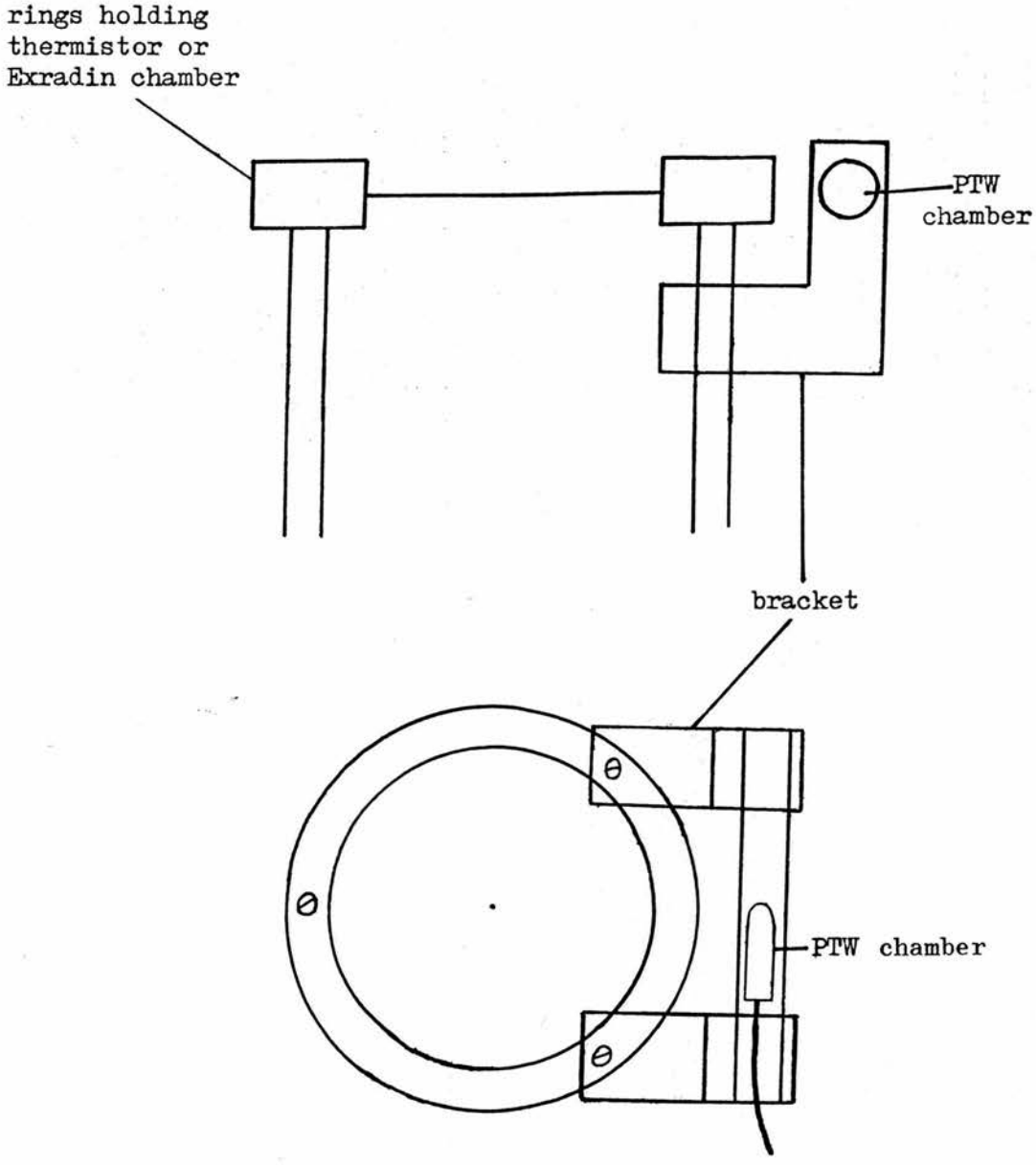

Figure 7.8 Position of PTW chamber in the electron beam

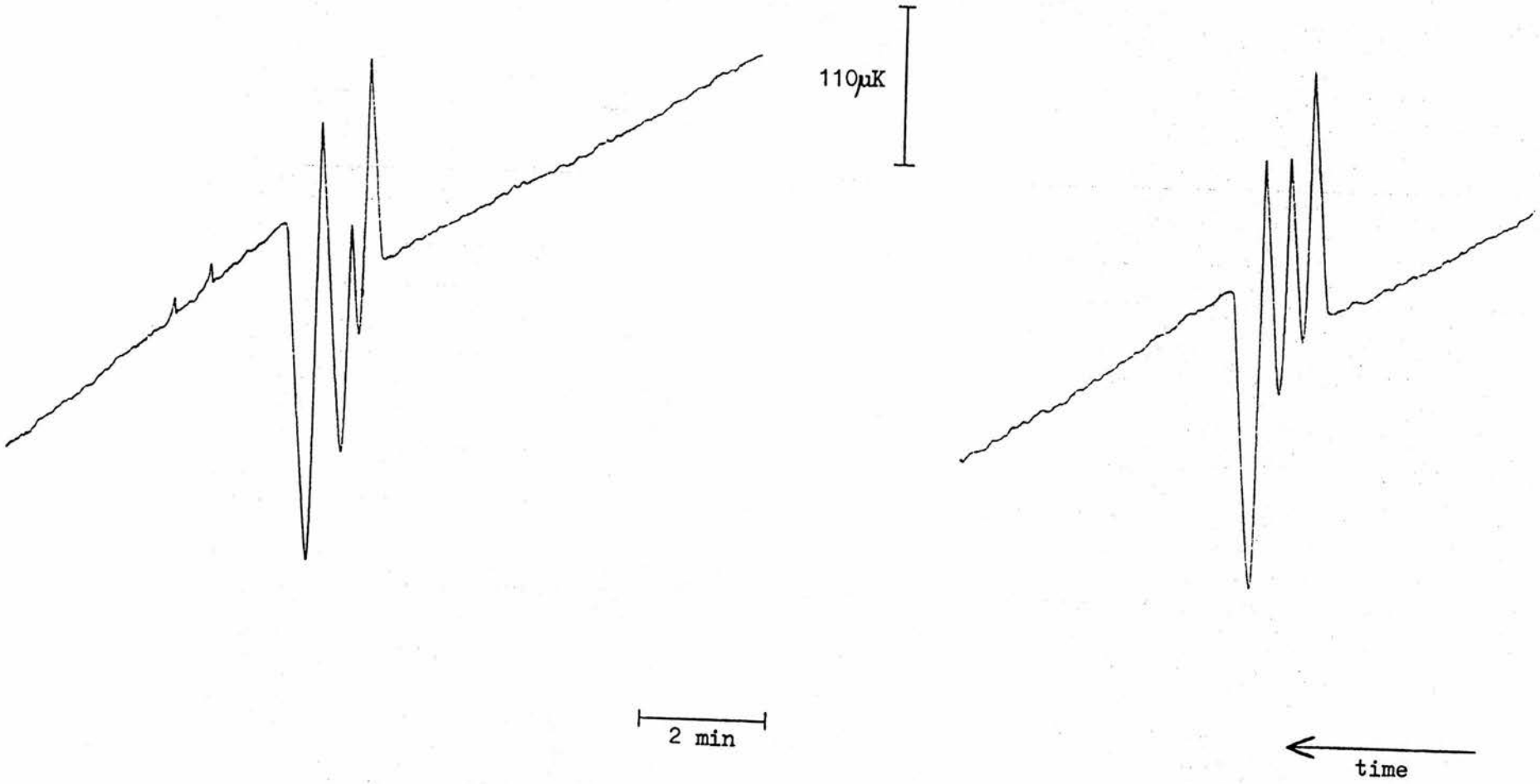

Figure 7.9 Calorimetry runs in the electron beam

flowed out of this plane. For these reasons the effect observed in the electron beam would not have been expected in the photon beams. In the analysis of a calorimetry run there are two effects to consider. Firstly, the fact that the final drift is at an angle relative to the initial drift means that in extrapolating the drifts to mid-run the change in R_s is overestimated. Secondly, heat flow away from the thermistor during the course of a run means that the temperature rise of the thermistor underestimates the absorbed dose delivered at the position of the thermistor. These two effects tend to cancel. In practice the analysis of calorimetry runs in the electron beam was carried out by extrapolating the initial and final drifts, and any error introduced by the effect described above was ignored.

The results of measurements in the 10 MeV electron beam are given in table 7.3, where the headings have the same meanings as those of tables 7.1 and 7.2. The correction for the excess heat generated in the polyethylene films was calculated by the method outlined in section 7.1.1. The ratio of mass stopping powers between polyethylene and water is 1.03 in the electron beam (E_d = 6 MeV). This is the same as the ratio of mass absorption coefficients in the photon beams, used in equation 7.4. The value of F used in equation 7.8 was therefore that given by equation 7.9. Calorimetry runs in the electron beam all lasted approximately 90 seconds and the correction applied for the polyethylene sheets was therefore 0.2% (see figure 7.4).

The Exradin ionisation chamber measurements were converted to absorbed dose as described in chapter six. The data used were those given in the HPA protocol for electron dosimetry (HPA 1985). It was mentioned in section 6.1.4 that the effective point of measurement when

Measurement	Panel Units	N	R_s (Ω)	ΔR_s (Ω)	ΔT (mK)	Power Dissipation (μW)	SD (%)	$\frac{D_{cal}}{PTW}$ (Gy/monitor unit)	$\frac{D_{Ex}}{PTW}$ (Gy/monitor unit)	$\frac{D_{cal}}{D_{Ex}}$
1	400	10	16437	0.496	0.92	24	0.8	0.5692	0.5376	1.053
2	400	10	16862	0.517	0.93	23	0.6	0.5522	0.5224	1.051
3	480	9	14913	0.587	1.23	26	0.4	0.5712	0.5329	1.066
4	470	10	15215	0.586	1.19	26	0.7	0.5649	0.5231	1.075
5	480	10	15469	0.568	1.13	25	0.5	0.5667	0.5356	1.052
6	450	10	15925	0.581	1.12	25	0.5	0.5682	0.5463	1.035

mean = 1.055

Table 7.3. Results of measurements in the 10 MeV electron beam.

using an ionisation chamber is not at the centre of the chamber, but is displaced towards the source of the radiation. For the Exradin chamber the effective point of measurement is 2 mm from the centre of the chamber. At this point the absorbed dose, determined from the depth dose curve, is 99.2% of the absorbed dose at the position of the centre of the chamber. In order to obtain the absorbed dose at the position of the thermistor the Exradin chamber measurements were increased by the factor 1/0.992. This factor has been included in the results given in table 7.3. The average ratio D_{cal}/D_{Ex} is 1.055, and one s.e.m. of the six ratios in table 7.3 is 0.5%.

7.5 UNCERTAINTIES

The uncertainty in determining the absorbed dose to water in the vicinity of the thermistor, with the calorimeter, is discussed in this section. It was mentioned in section 2.1.7 that one of the principal uncertainties is the heat defect. It is necessary to know the heat defect in order to obtain absorbed dose from the measured temperature rise. The heat defect has not been included in the results given in the previous sections; the implications of the heat defect will be discussed in chapter nine. The uncertainties presented here therefore represent the uncertainties in determining the overall temperature rise induced by irradiation.

A breakdown of the uncertainties involved in a calorimetric measurement is given in table 7.4. Tables 7.1 to 7.3 give the standard deviation of the measured values of ΔR_s for each set of calorimetry runs. From the standard deviation and the value of N the s.e.m. was calculated for each calorimetry measurement. This was then multiplied by three to give an estimate of the experimental uncertainty in the

measurement. The average value of this quantity, for the three radiation beams, was between 0.6% and 0.9%. This has been rounded up to 1.0% to give the experimental uncertainty quoted in table 7.4. The accuracy of the calibration of the thermistor was discussed in chapter four. The uncertainties in the corrections for power dissipation in the thermistor and for the polyethylene sheets were given in section 7.1. The specific heat of water is listed to five significant figures in Kay and Laby (1973) and the uncertainty in c was therefore assumed to be negligible. The overall uncertainty, taken as the root of the sum of the squares of the contributory uncertainties, is 1.0%.

Quantity	Uncertainty (%)
$\Delta R_s/R_s$	1.0
Thermistor sensitivity	0.2
Correction for power dissipation	0.05
Correction for polyethylene films	0.1
c	-
Overall uncertainty	1.0

Table 7.4. Uncertainties in calorimetry measurements.

CHAPTER 8

NEUTRON BEAM MEASUREMENTS

8.1 CORRECTIONS TO CALORIMETRY MEASUREMENTS

Corrections for power dissipation in the thermistor and for excess heat generation in the polyethylene films are also required in the neutron beam. The calculation of the correction for power dissipation in the thermistor is identical to that described in section 7.1.1. The correction was determined for each calorimetry measurement, from the thermistor power dissipation which was present during the measurement. The value of the correction was 0.2-0.3%.

The correction required to account for the presence of the polyethylene films was in principle the same as that described in section 7.1.2. However, the ratio between absorbed dose in polyethylene and absorbed dose in water is larger in the neutron beam than in the photon or electron beams. The excess heat generated in the polyethylene films is therefore greater in the neutron beam. The kerma ratio between polyethylene and water is 1.287, assuming a mean neutron energy of 6 MeV. Equation 7.4, with the ratio of mass energy absorption coefficients replaced by this kerma ratio, gives the relative temperature rise;

$$\frac{\Delta T_{polyethylene}}{\Delta T_{water}} = 1.287 \cdot \frac{4180}{2300} = 2.34 \qquad (8.1)$$

Using equation 7.6 the excess heat in the imaginary layer of water which replaces the polyethylene films is 0.70 ΔT_{water}. Hence the

excess heating in this thin layer of water is 70%, which compares with a value of 46% obtained in the photon beams. The value of F (see equation 7.9) which was used in equation 7.8 was therefore

$$F = 4.18 \times 10^6 \cdot 0.70 \cdot d \qquad (8.2)$$

Calorimetry runs in the neutron beam all lasted approximately 5 minutes. The correction for the polyethylene films was determined from equation 7.8 with T = 300 seconds. This correction has been plotted in figure 8.1 as a function of time after beam turn-off. For the same reasons mentioned in section 7.1.2 the correction was taken to be 0.2%, which is identical to the value obtained for the photon and electron beams. Although the excess heat in the polyethylene is greater in the neutron beam, the duration of the runs is longer and these two effects cancel.

8.2 RESULTS

The calorimeter was placed on the treatment couch under the isocentric head which delivered the neutron beam. It was positioned as close as possible to the head and the thermistor was 124 cm from the target. The thermistor was at the centre of the neutron field at a depth of 5 cm in the water. The vertically downward beam was circular and had a diameter of approximately 25 cm at the depth of the thermistor. The neutron beam was produced by a 15 MeV deuteron beam on a beryllium target and the doserate was typically 25 cGy min^{-1} at the depth of the thermistor. The bridge circuit and associated equipment was adjacent to the control console and the signal leads passed through a channel under the floor into the treatment room. At times the calorimeter was left in the treatment room, with the air temperature

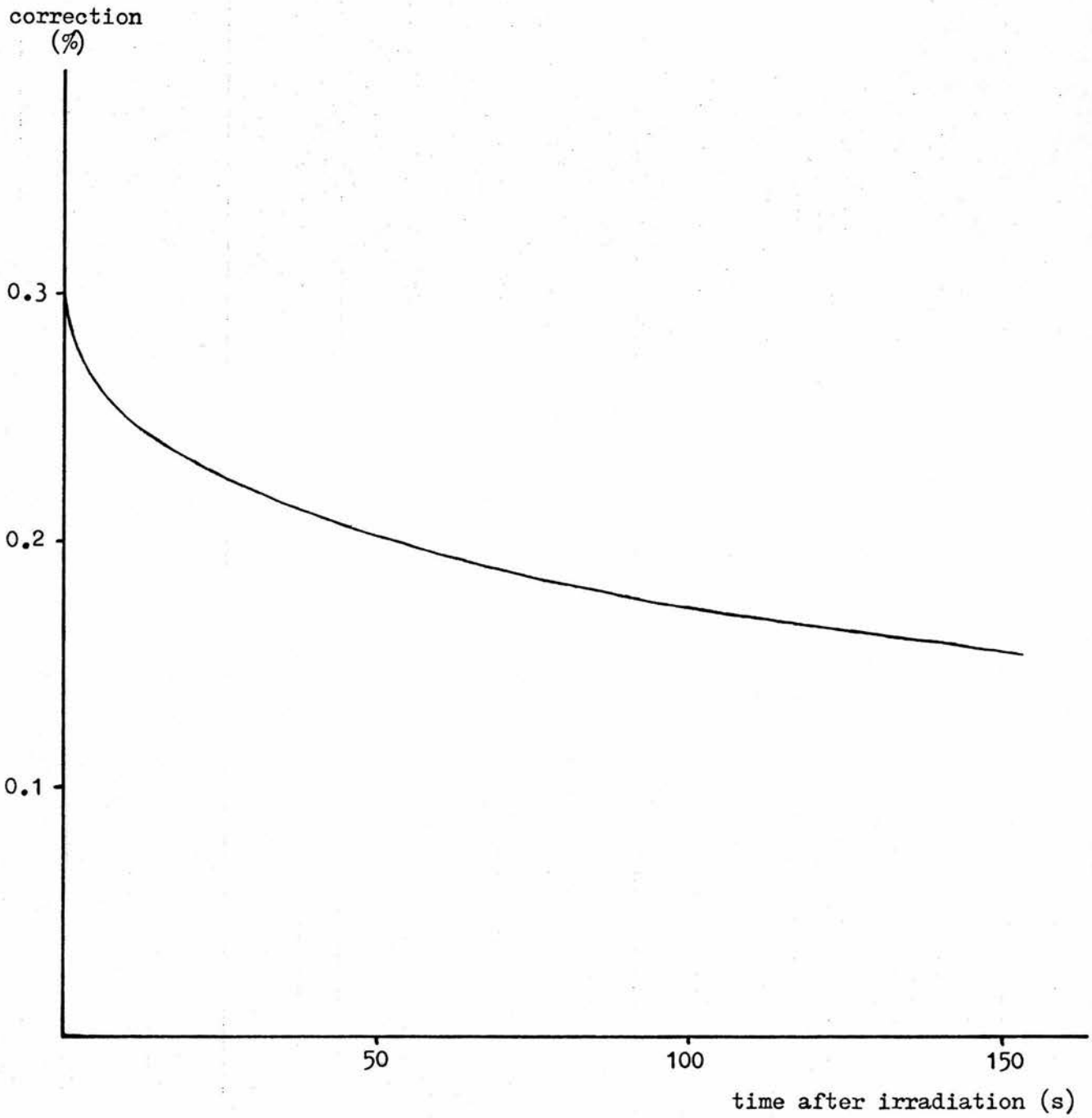

Figure 8.1 Excess thermistor temperature in the neutron beam

controller switched on, so that the calorimeter was at equilibrium. When the neutron beam became available the calorimeter was moved into position under the head. This minimised the time required to set up the equipment and allowed measurements to commence less than an hour after the beam became available. Monitoring of the beam was by the transmission ionisation chamber situated in the isocentric head. A thermistor monitored the temperature of this ionisation chamber and a control on the console allowed a correction to be directly applied so that changes in temperature did not affect the reading of this chamber. The setting of this control was checked at regular intervals during calorimetry measurements. With this modification the transmission ionisation chamber was known to be very consistent and was therefore used to monitor the beam.

Figure 8.2 shows typical chart recorder traces from calorimetry runs in the neutron beam. Doses delivered at the position of the thermistor were 1.2 to 1.4 Gy and irradiation lasted approximately five minutes. Calorimetry runs lasted 10-15 minutes and resistance calibration 5-10 minutes; resistance calibrations were carried out in between calorimetry runs. The results of measurements in the neutron beam are detailed in table 8.1. The headings have the same meanings as those of table 7.1 except the columns headed D_{cal} and D_{Ex}. The beam was terminated when the monitoring ionisation chamber reached the preset number of panel units. Since the reading of this ionisation chamber did not vary during a set of measurements the columns D_{cal} and D_{Ex} are in absorbed dose rather than absorbed dose per monitor unit. Both these columns are in absorbed dose to tissue (ICRU muscle). The final column gives the ratios D_{cal}/D_{Ex} which include the two corrections described in

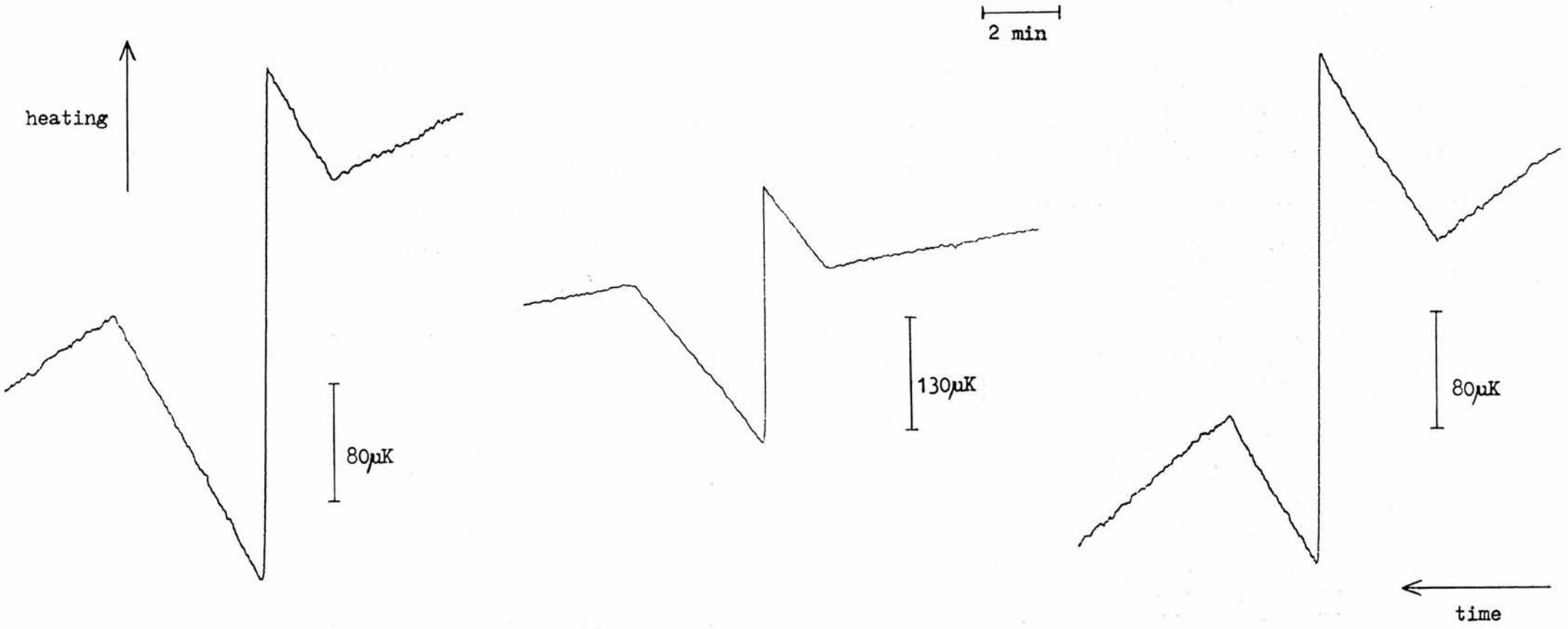

Figure 8.2 Examples of calorimetry runs in the neutron beam

section 8.1. The mean of the nine ratios is 0.956 with a s.e.m. of 0.25%. The results are also shown graphically in figure 8.3 where the error bars are the standard deviations quoted in column eight of table 8.1.

Ionisation measurements were carried out with the Exradin ionisation chamber, flushed with TE gas, immediately after the calorimetry measurements. Details of the calibration of the Exradin chamber are given in chapter six. Absorbed dose to tissue (ICRU muscle) at the position previously occupied by the thermistor was calculated from the Exradin chamber measurements. The calorimeter measured absorbed dose to water and this was converted to absorbed dose to tissue using the kerma ratio for the two materials. The ratio of kerma in tissue to kerma in water was calculated from the neutron spectrum (see section 6.2.2) and the kerma data of Caswell et al (1980) to be 0.930. In converting the calorimetry results to absorbed dose to tissue more work is being done than is required. Since the calorimeter measures absorbed dose to water and the Exradin chamber measures absorbed dose to TE plastic (see equation 6.11) it is not necessary to convert both measurements to absorbed dose to tissue in order to compare them. The ionisation measurements could have been converted directly from absorbed dose to TE plastic to absorbed dose to water, and then compared with the calorimetry results. However, the two approaches are equivalent since a common set of kerma data and a common neutron spectrum were used to calculate the kerma ratios.

Measurement	Panel Units	N	R_s (Ω)	ΔR_s (Ω)	ΔT (mK)	Power Dissipation (μW)	SD (%)	D_{cal} (Gy)	D_{Ex} (Gy)	$\frac{D_{cal}}{D_{Ex}}$
1	100	10	16433	0.172	0.320	24	1.8	1.242	1.280	0.965
2	100	10	16436	0.171	0.318	24	2.6	1.235	1.280	0.960
3	100	8	16119	0.168	0.320	24	1.6	1.245	1.285	0.964
4	100	13	16533	0.176	0.325	24	1.3	1.265	1.310	0.961
5	90	14	16201	0.163	0.307	13	2.1	1.195	1.248	0.954
6	90	15	15888	0.152	0.294	14	1.3	1.142	1.201	0.947
7	90	9	16172	0.159	0.301	13	2.4	1.170	1.221	0.955
8	100	11	14618	0.162	0.346	15	0.8	1.345	1.416	0.946
9	110	12	14001	0.166	0.375	14	1.0	1.456	1.519	0.955

mean = 0.956

Table 8.1. Results of measurements in the neutron beam.

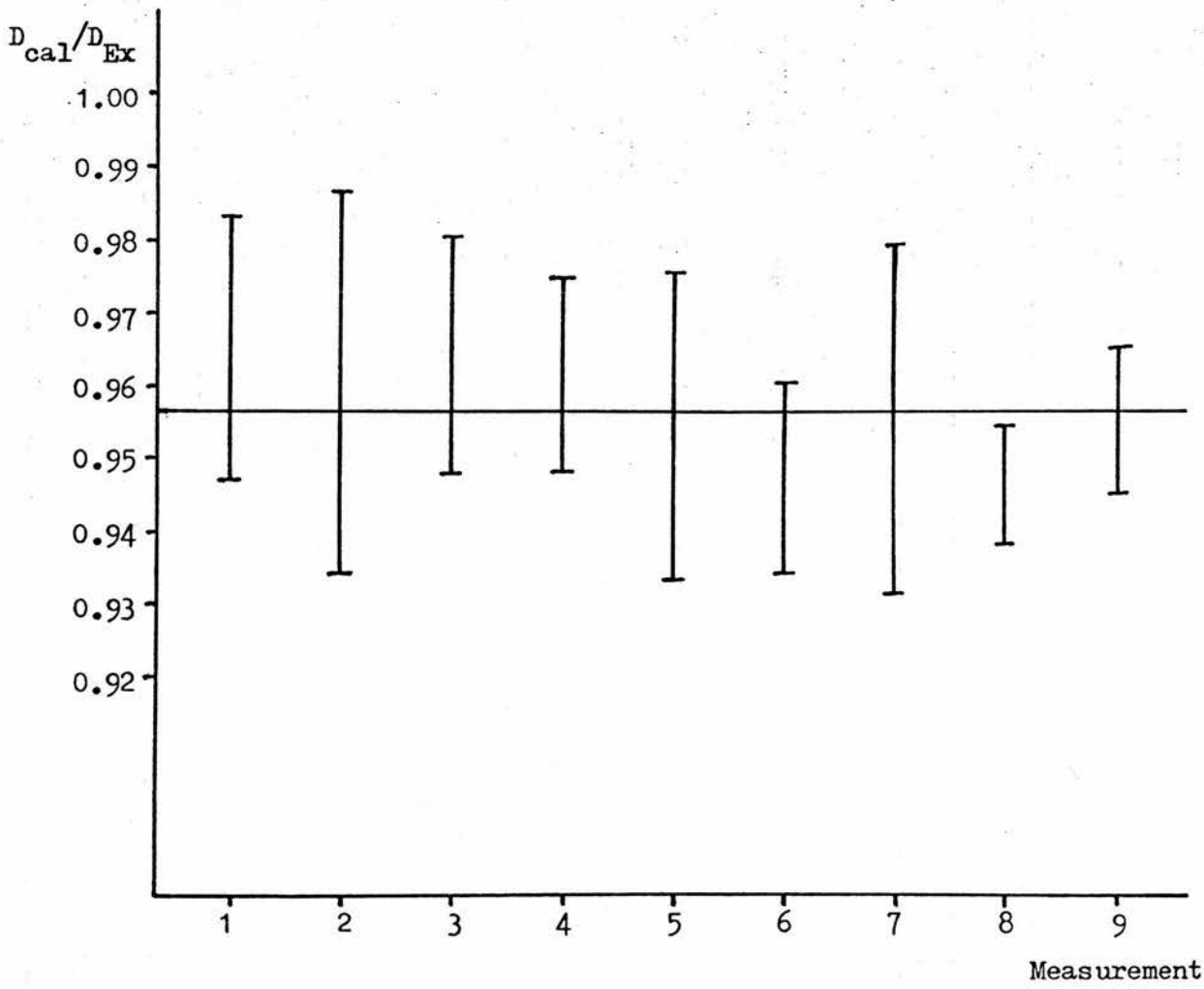

Figure 8.3 Results of measurements in the neutron beam

8.3 UNCERTAINTIES

The uncertainty associated with a calorimetric measurement in the neutron beam is in principle the same as that described in section 7.5 for the photon and electron beams. The doserate in the neutron beam was approximately a factor of ten lower than that in the photon and electron beams. Consequently the experimental uncertainty in the neutron measurements is slightly higher. Three times the s.e.m. of a set of calorimetry runs was again taken as an estimate of the experimental uncertainty. The average value of this quantity was 1.6%. The contributory uncertainties are given in table 8.2. These are identical to those of table 7.4 except for the experimental uncertainty, and the inclusion of the uncertainty in the kerma ratio. No uncertainty has been assigned to account for the heat defect.

Quantity	Uncertainty (%)
$\Delta R_s/R_s$	1.6
Thermistor sensitivity	0.2
Correction for power dissipation	0.05
Correction for polyethylene films	0.1
c	-
Kerma ratio	0.4
Overall uncertainty	1.7

Table 8.2. Uncertainties in a calorimetric measurement in the neutron beam.

CHAPTER 9

DISCUSSION AND CONCLUSIONS

9.1 THE HEAT DEFECT

Before considering the results of the calorimetry measurements it is worth discussing the heat defect. The reasons for the existence of a heat defect have already been outlined in section 2.1.7. The heat defect is a fundamental problem in all radiation calorimeters and it must be determined if the calorimeter is to be a useful dosimetric tool. There have been two recent investigations of the heat defect in water inspired by the current interest in water calorimetry (Fletcher 1982, Ross et al 1984).

Fletcher (1982) developed a theoretical model to predict the heat defect in water irradiated by low LET radiation. Reactions induced in the water by radiation are well known. The rate constants of these reactions and the heats of formation of the various species are also known. Even in pure water the radiation chemistry is complex; Fletcher lists thirty-nine possible reactions, all of which potentially contribute to the overall energy balance. The yields of the radiolytic products were calculated by a computer and the chemical energy balance was determined as a function of dose and initial concentrations of hydrogen (H_2), oxygen (O_2) and hydrogen peroxide (H_2O_2).

For pure, deoxygenated water at a pH of 7 the overall reaction was endothermic. At a doserate of 300 cGy min^{-1} the overall endothermicity was 2.5% at a cumulative dose of 100 cGy, decreasing to 1% at a cumulative dose of 500 cGy. This disagrees with the results of several

water calorimetry measurements in photon beams (see next section), which suggest an overall exothermicity of 3-5% in pure water at these dose levels. However the water used in water calorimeters may not be "pure" in the sense meant by Fletcher, i.e. having no dissolved H_2, O_2 or H_2O_2. Under normal conditions water will inevitably contain dissolved oxygen. Fletcher considered water containing dissolved O_2, at a concentration of 3×10^{-4} molar. At the same doserate as above (300 cGy min^{-1}) and a cumulative dose of a few hundred cGy, an overall endothermicity of approximately 2.5% was predicted. For pure water, or water containing dissolved O_2 or H_2, endothermicities between 2% and 5% were predicted. If hydrogen peroxide or both H_2 and O_2 were present then the overall reaction was exothermic. The presence of hydrogen peroxide could also lead to chain reactions resulting in large overall exothermicities. Fletcher suggested that for particular initial conditions the chain reaction could produce a ten-fold increase in the sensitivity of the calorimeter.

Ross et al (1984) compared predictions of a radiochemical model (Boyd et al 1980) with water calorimetry measurements using water containing different dissolved gases. This model was essentially the same as that employed by Fletcher (1982). As the calorimetry measurements were not absolute, the results were normalised to the predicted exothermicity of 2.1% for water containing a 50/50 mixture of H_2 and O_2. The model predicts a zero heat defect for N_2 saturated (i.e. pure) water, and approximately 2% endothermicity for O_2 or air saturated water. Measurements agreed well with these predictions. The doserate employed was 2500 cGy min^{-1} and cumulative doses were up to 500 Gy. This doserate is much higher than the doserates used with calorimeters which have been irradiated in medical therapy beams. However, the

predicted effects are virtually identical at a doserate of 100 cGy min^{-1}. In initial radiation periods for N_2 saturated water a small unexpected exothermicity was noted. This was attributed to the presence of trace impurities in the water, the effect of which was removed by further irradiation. The presence of impurities, particularly organic, was suggested as the reason for the 3-5% exothermicity which has been found with several water calorimeters (see next section). The results of Schulz and Rothman (1983) indicated an exothermic heat defect of 3-5%. Their calorimeter was of similar construction to the other calorimeters discussed in section 9.2; in particular perspex was used in its construction. Schulz (1985) constructed a calorimeter with glass walls, which had no organic materials in contact with the water. Preliminary results with this calorimeter indicated positive (or endothermic) heat defects of 3.1% with aerated water and 2.2% with hypoxic water. These findings are in reasonable agreement with the 2.1% endothermicity predicted by the radiochemical model, and support the proposal that organic impurities induce chemical reactions which result in a small exothermicity at low doses. Unfortunately there have been no attempts to determine the heat defect with high LET radiation.

9.2 PHOTON BEAM RESULTS

Radiation Beam	$D_{calorimeter}/D_{ionisation\ chamber}$
d(15)+Be neutrons	0.956
4 MV X-rays	1.040
9 MV X-rays	1.045
10 MeV electrons	1.055

Table 9.1. Summary of results.

The results of all of the calorimetry measurements in the different radiation beams are summarised in table 9.1. It must again be stressed that these results take no account of the heat defect in water. Table 9.2 is a summary of the results of other water calorimetry measurements in photon beams. The ratio given in table 9.2 is the ratio of absorbed dose measured by the calorimeter to absorbed dose measured with a reference dosimeter. In the cases of de Marles, Kubo and Schulz and Rothman the reference dosimeter was an ionisation chamber, whereas Domen employed a graphite calorimeter. Mattsson's calorimetry measurements were compared with an ionisation chamber which had been calibrated using the same graphite calorimeter employed by Domen. This measurement was therefore essentially a repeat of that made by Domen.

Reference	Radiation Beam	Ratio
Domen (1982)	cobalt-60	1.035
de Marles (1981)	1.25 MV X-rays	1.034
	6 MV X-rays	1.033
	18 MV X-rays	1.055
	25 MV X-rays	1.030
Kubo (1983)	cobalt-60	1.038
	10 MV X-rays	1.030
	25 MV X-rays	1.019
Schulz & Rothman (1983)	25 MV X-rays	1.03 - 1.05
Mattsson (1984)	cobalt-60	1.033
Kubo (1985)	orthovoltage X-rays	1.07 - 1.09

Table 9.2. Water calorimetry measurements in photon beams.

Calorimeter to ionisation chamber ratios in the 4 and 9 MV photon beams in this work are in good agreement with similar results of other workers, as can be seen from table 9.2. The consistency of these results proves the water calorimeter as a reliable instrument for determining absorbed dose. To compare directly the calorimeter to ionisation chamber ratios of different workers assumes that the ionisation chamber dosimetry is consistent throughout. Different workers have employed different codes of practice, such as AAPM (1983), NACP (1980) or HPA (1983), for their ionisation chamber dosimetry. However, a recent study, Mijnheer and Wittkämper (1986), has shown that absorbed dose measurements using these codes of practice agree to within

±1%. It is therefore reasonable to make a direct comparison between the ratios obtained with different calorimeters. For example, comparing the AAPM (1983) and HPA (1983) protocols, differences of up to 0.8% in the determination of absorbed dose are evident under identical radiation conditions, using identical ionisation chambers. A common international protocol would avoid such anomalies. The uncertainties in the calorimetry measurements of table 9.2 were similar to those of this work, at around 1%. Within these uncertainties there is good agreement amongst all of the results for photon beams.

The 3-5% discrepancy between the calorimeter and ionisation chamber measurements is almost certainly due to the heat defect in water. This has been demonstrated by Domen (1983) using a polystyrene-water calorimeter. In this calorimeter the thermistors were not sandwiched between polyethylene films but were cemented between two polystyrene discs which were immersed in the water tank. Absorbed dose to water measured with the polystyrene-water calorimeter was 3% lower than that measured with a water calorimeter. Since the heat defect in polystyrene is less than 1% (ICRU 1969, Weimer 1972), this suggests a heat defect of -3% for water irradiated by megavoltage X-rays. In his original work Domen (1982) found a discrepancy (or heat defect) of 3.5% when water calorimetry measurements were compared with a graphite calorimeter.

A value of about -3% for the heat defect does not agree with the predictions of the radiochemical model discussed in section 9.1. The model predicts a positive heat defect of approximately 2% for air saturated water. Ross et al (1984) suggested that the negative heat defect may be due to organic impurities in the water. However the water calorimetry results cited in table 9.2 and those of this work all point to a heat defect in the range -3 to -5% for water irradiated by

megavoltage photons. It is highly unlikely that these calorimeters all contained water which had the same degree of impurity, and therefore it is probable that the purity, within certain limits, is not critical for consistent results to be obtained. Domen (1982) also compared the effect of using water which had been stored in a glass contained with water which had been stored in a polyethylene container, and found no detectable difference.

9.3 ELECTRON BEAM RESULTS

The results of other water calorimetry measurements in electron beams are presented in table 9.3. The ratio quoted is that of absorbed dose measured with the calorimeter to that measured with an ionisation chamber: the ratio measured in a 10 MeV beam in this work was 1.055.

Reference	Nominal Energy	Ratio
de Marles (1981)	13 MeV	0.995
	17 MeV	0.975
	20 MeV	1.005
Kubo (1983)	18 MeV	1.036
	23 MeV	1.034

Table 9.3. Water calorimetry measurements in electron beams.

All of these calorimetry measurements (including those of this work) were referenced to ionisation chamber dosimetry. de Marles followed the NACP (1980) protocol to determine absorbed dose from the ionisation chamber measurement. Kubo used the equations given by Loevinger (1981) which were a precursor to the AAPM (1983) code. The

HPA (1985) code was employed in this work. Although these are current protocols in their respective countries of origin there are significant differences between them. This is a complication when comparing the calorimeter to ionisation chamber ratios of different workers. As with photons, a common international protocol would remove these differences. Had the AAPM (1983) protocol been used for the ionisation chamber measurements in this work the ratio would be 1.049 instead of 1.055. Had the NACP (1980) protocol been used the ratio would be 1.037. Taking this into account the ratio obtained by Kubo is in good agreement with that obtained in this work. However the ratios obtained by de Marles are significantly lower.

There is an intrinsic difficulty in comparing calorimetry and ionisation chamber measurements in electron beams due to the presence of steep dose gradients. It is essential either that the positions of the thermistor and the ionisation chamber are identical, or that the difference between their positions is accurately known, and is corrected for. Small positional errors will result in relatively large errors in the comparison between the calorimeter and the ionisation chamber. In this work, and that of Kubo, two jigs were constructed, one containing the thermistor and the other containing the ionisation chamber. The ionisation chamber jig was substituted for the jig holding the thermistor ensuring that their positions were identical and obviating the need for depth measurements. de Marles, on the other hand, irradiated the ionisation chamber in a dummy calorimeter, and depth measurements were therefore required. However measurements were carried out at the depth of maximum ionisation, where the dose is varying least with depth, and it is unlikely that any positional error would be large

enough to explain the different calorimeter to ionisation chamber ratios obtained.

Since the way in which photons and electrons deposit their energy is similar it is likely that the heat defect with the two radiations is the same. The results of Kubo, and this work, support this conclusion since they are in fairly good agreement with the heat defect of -3 to -5% found in photon beams. This is encouraging as it points to a stable heat defect for low LET radiation. Additional measurements in electron beams are necessary to confirm these conclusions.

9.4 NEUTRON BEAM RESULTS

The calorimeter to ionisation chamber ratio obtained in the d(15)+Be neutron beam was 0.956. To date no other water calorimetry measurements in neutron beams have been reported. This ratio does not include any correction to account for the heat defect in water. It is difficult to draw any firm conclusions from the result without any information on the heat defect. If the ionisation chamber measurements are assumed to be correct then the heat defect is equal to +4.4% (i.e. an endothermic effect). This is in contrast to the heat defect found with photon irradiation which was -3 to -5% (i.e. exothermic). There has been no study of the heat defect in water irradiated by high LET radiation. The negative heat defect with photons may be due to impurities in the water (Ross et al 1984). It is possible that water containing the same impurities exhibits a different heat defect when irradiated by neutrons. However, it seems unlikely that the difference in heat defects is as large as the present result would suggest. One material in which the heat defect has been measured for beams of different LET is A-150 plastic. It exhibits a heat defect of 4.2% when

irradiated with 1.7 MeV protons and 4.1% with low energy X-rays (Fleming and Glass 1969, Säbel et al 1972). Although the heat defect in A-150 plastic is constant over a wide range of LET this is not necessarily the case for water. In plastics irradiation results in permanent changes which involve cross linking, a reduction in the saturation of chemical bonds, chain breakage and hydrogen evolution. In water the mechanism is different; the most important chemical effect is the production of free radicals, and this is a temporary effect. It is therefore unclear how the heat defect in water will vary with radiation of differing LET and what part the presence of impurities plays in determining the heat defect.

The results of measurements with photons at 4 and 9 MV show an average calorimeter to ionisation chamber ratio of 1.042. A comparison of the photon beam results and the neutron beam results demonstrates a discrepancy of approximately 9% in the ratio of calorimeter to ionisation chamber results. The operation of the calorimeter was essentially identical in the photon and neutron beams. The only significant difference was that the doserate in the neutron beam was lower, which necessitated longer irradiation periods, and resulted in a slightly higher experimental uncertainty. It seems unlikely that there is any error in the calorimetry measurements with neutrons which would not also be present with photons.

The uncertainty in determining absorbed dose to tissue with the ionisation chamber is 6.5% (Mijnheer and Williams 1981) and with the calorimeter 1.7%. These uncertainties are not large enough to explain the 9% discrepancy. McDonald et al (1981) and Caumes et al (1984) have carried out comparisons between A-150 calorimeters and A-150 ionisation

chambers in several neutron beams ranging in energy from d(4)+Be to p(67)+Be. These have shown agreement, but the results are dependent on the data used in each case to calculate absorbed dose from the ionisation chamber measurements. Williams (1984) recalculated these intercomparisons using a common set of data to calculate the ionisation chamber results. This demonstrated a good agreement between the calorimetric and the ionometric measurements (within approximately 2%), which implies that such chambers are capable of accurate measurements of absorbed dose to A-150 plastic. Although the uncertainty in determining absorbed dose to A-150 plastic with an A-150 ionisation chamber is 6% these intercomparisons show that the net error in the factors required to convert the response of the ionisation chamber to absorbed dose to A-150 plastic is in fact less than 2%. However, the ionisation chamber measurement has to be converted from absorbed dose to A-150 plastic to absorbed dose to tissue using the kerma ratio of the two materials. The water calorimetry results may therefore indicate an error in this kerma ratio. This is unlikely to be a complete explanation of the 9% discrepancy since the uncertainty in the kerma ratio for a d(15)+Be spectrum is only 2.6% (Bewley, 1980).

Although kerma ratios are essential in neutron dosimetry their accuracy has not really been well tested. Kerma factors are generally obtained from the basic nuclear data by calculation. Where these data are not available it is difficult to estimate kerma factors due to the complexity of the interactions. The deposition of energy in tissue is dominated by hydrogen interactions and, because of the simplicity of this interaction, hydrogen kerma factors are fairly well known (to about 2%). For other elements the uncertainty, in the energy region below 20 MeV, is generally about $\pm$10%. Above 20 MeV kerma factors can only be

considered as rough estimates (Caswell et al, 1980). It is therfore important for accurate neutron dosimetry, particularly at energies above 20 MeV that the uncertainties in kerma factors and kerma ratios are reduced. If the heat defect in water can be determined, water calorimetry measurements will provide a useful check on kerma ratios.

There are therefore three potential explanations for the calorimetry result in the neutron beam. Firstly there may be a systematic error in the calorimetry measurements. However this does not explain the 9% difference between the results in the neutron and photon beams, unless there is a significant difference in the operation of the calorimeter in the two beams which has been overlooked. Secondly there may be an error in the ionisation chamber dosimetry in the neutron beam. The results with A-150 calorimeters point to the only possible source of error being the kerma ratio between A-150 plastic and tissue. Lastly the heat defect in water may be responsible for the result obtained in the neutron beam. A heat defect which varies with LET, possibly due to impurities in the water, could explain the difference between the neutron and photon results. Since the mechanism whereby photons and neutrons deposit their energy is fundamentally different, the radiochemical effects of the two radiations, and consequently the heat defects, may also be significantly different. At present this seems to be the most likely explanation of the results but until the heat defect with neutrons is determined it is not possible to draw any firm conclusions.

9.5 SUMMARY

Absorbed dose measurements in a d(15)+Be neutron beam have been carried out using a water calorimeter. These were directly compared with measurements using a TE ionisation chamber. The ratio of absorbed dose to tissue measured with the calorimeter to that measured with the ionisation chamber was 0.956, if the heat defect in water is ignored. Relative to ionisation chamber dosimetry, absorbed dose measurements with the calorimeter in the neutron beam were 9% lower than similar measurements in 4MV and 9MV photon beams.

The current state of neutron dosimetry is less than satisfactory. Firstly there is a large uncertainty in the determination of absorbed dose to tissue, and secondly, there is significant discrepancy between the neutron dosimetry protocols in Europe and the USA. The American protocol (AAPM, 1980) recommends a tissue equivalent liquid as the phantom material whereas the European protocol (Broerse et al, 1981) recommends water. The recommended values for the parameters required to convert an ionisation chamber measurement to a measurement of absorbed dose to tissue differ between the two protocols and the type of ionisation chamber recommended also differs. In the neutron beam used in this work (d(15)+Be), at a depth of 5 cm, following the European protocol would give a measurement of absorbed dose to tissue 4.8% higher than the American protocol (Mijnheer et al, 1984). Since, in fast neutron therapy, the occurrence of normal tissue complications and the probability of tumour control are steep functions of absorbed dose (Battermann et al 1981, Cohen 1982), it is important that neutron dosimetry is consistent if results from different centres are to be compared. Even if a unified protocol were to be agreed the relatively

large uncertainty in the absolute measurement of absorbed dose to tissue would still remain. If the heat defect in water can be determined water calorimeters will provide a more accurate method of determining neutron absorbed dose.

The advantage of the water calorimeter in measuring absorbed dose is that the uncertainty (1.7%) is lower than that associated with ionometric methods (6.5%). However, at present the unknown heat defect must also be included as an uncertainty in the calorimetric measurement. If the heat defect with neutrons can be determined the water calorimeter will provide a useful check on the accuracy of ionisation chamber measurements of absorbed dose. This is particularly important at high neutron energies where the uncertainty in the kerma ratio between A-150 plastic and tissue is large. For example, Bewley (1980) estimates the uncertainty in this kerma ratio to be 10.6% for a p(66)+Be spectrum, making the overall uncertainty in absorbed dose to tissue 12.6%. At this energy the kerma correction for the water calorimeter (i.e. from water to tissue) is only 1.8%. In order to improve the efficacy of neutron radiotherapy there is an increasing use of high energy neutron beams. The water calorimeter could have an important part to play in improving the accuracy of the dosimetry of such beams.

APPENDIX A

THE AIR TEMPERATURE CONTROLLER

Figure A.1 is a circuit diagram of the air temperature controller and table A.1 gives the component details. The circuit was powered by a 50W transformer giving $\pm$12V and $\pm$15V d.c. The heating coils (R14 and R16) were wound from "Nichrome" resistance wire and were mounted directly in front of the fan.

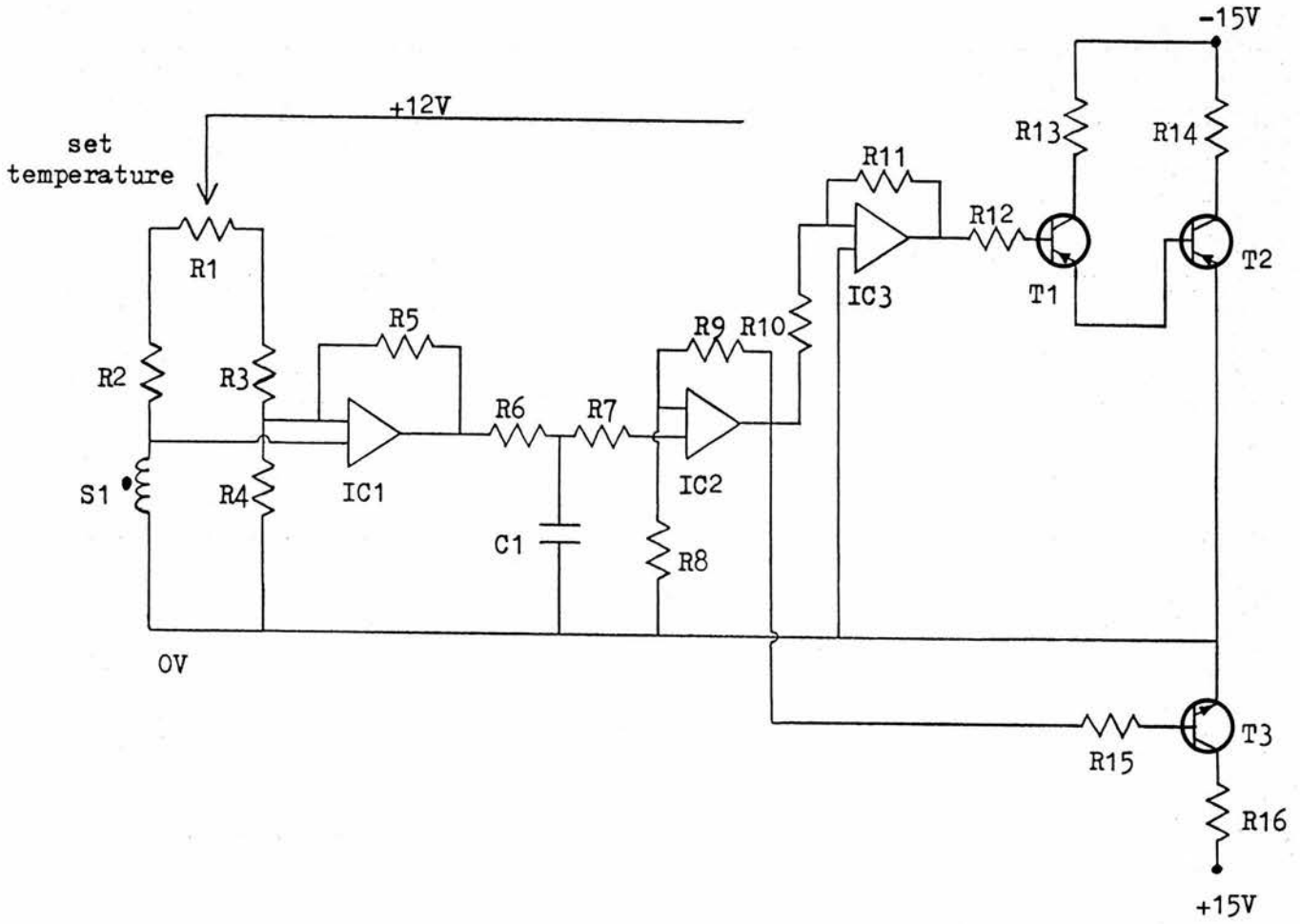

Figure A.1 Circuit diagram of air temperature controller

Component	Details
R1	20 k
R2	270 k
R3	270 k
R4	100 k
R5	10 M
R6	470 k
R7	470 k
R8	3.3 M
R9	1.2 M
R10	1 k
R11	1 k
R12	1 k
R13	150 R
R14	9 R
R15	82 R
R16	9 R
C1	1 μF
IC1	741
IC2	741
IC3	741
S1	100 k thermistor
T1	BC 461
T2	TIP 2955
T3	TIP 3055

Table A.1. Component list for air temperature controller.

APPENDIX B

THE RESISTANCE BRIDGE

Figure B.1 is a circuit diagram of the resistance bridge. Component values are given in table B.1. The circuit was powered by a 12V, smoothed and regulated supply.

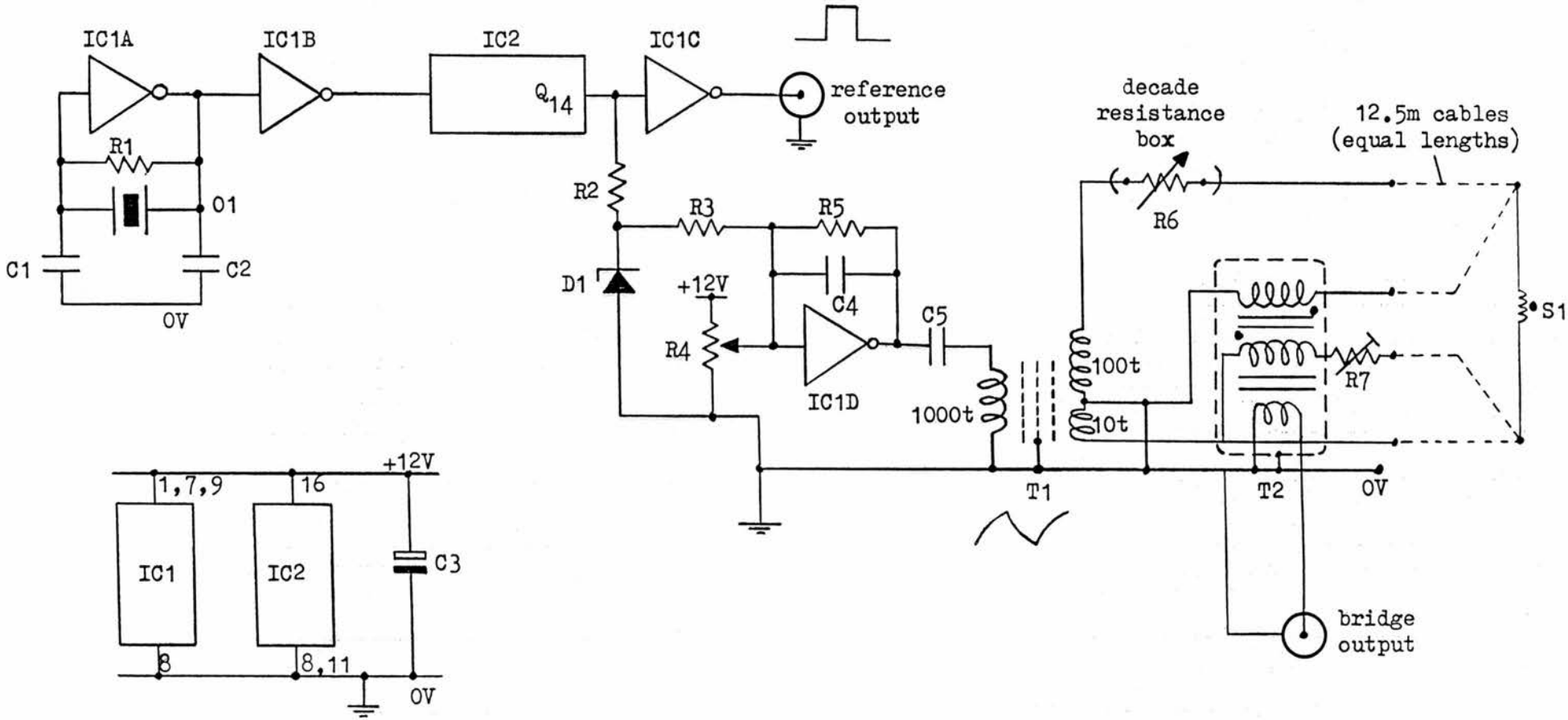

Figure B.1 Circuit diagram of resistance bridge

	Component	Details
	IC1	CD 4049
	IC2	CD 4020
	O1	6.144 MHz crystal oscillator
	D1	BZY 88
	R1	10 M
	R2	1 k
	R3	4 k7
	R4	20 k
	R5	33 k
	R6	100 k decade box
	R7	5 k
	C1	33 pF
	C2	33 pF
	C3	10 μF
	C4	0.1 μF
*	C5	10 nF - 10 μF
	T1	transformer; grounded core
	T2	transformer; contained mumetal case
	S1	2000 k thermistor

Table B.1. Component list for resistance bridge circuit.

* The value of this capacitor was altered in order to vary the amplitude of the voltage exciting the bridge (see section 5.2).

REFERENCES

AAPM 1980. Protocol for Neutron Beam Dosimetry, Report No. 7 (New York: American Institute of Physics for AAPM).

AAPM 1983. Med. Phys. 10, 741.

Awschalom, M., Rosenberg, I. and Ten Haken, R.K. 1983. Med. Phys. 10, 436.

Barnard, G.P., Axton, E.J. and Marsh, A.R. 1959. Phys. Med. Biol. 3, 366.

Batterman, J.J., Hart, A.A.M. and Breur, K. 1981. Br. J. Radiol. 54, 899.

Bewley, D.K. 1963. Br. J. Radiol. 36, 865.

Bewley, D.K. 1980 in Proc. Workshop on Ion Chambers for Neutron Dosimetry (Brussels: CEC) p.209.

Bewley, D.K., McCullough, E.C., Page, B.C. and Sakata, S. 1974. Phys. Med. Biol. 19, 831.

Bischel, H. and Rubach, A. 1978 in Proc. 3rd Symp. on Neutron Dosimetry in Biology and Medicine, EUR 5848, Ed. by G Burger and H G Ebert (Brussels: CEC) p.549.

Bonnett, D.E. 1979. Ph.D. Thesis. University of London.

Boyd, A.W., Carver, M.B. and Dixon, R.S. 1980. Radiat. Phys. Chem. 15, 177.

Bradshaw, A.L. 1965. Phys. Med. Biol. 10, 355.

Broerse, J.J., Mijnheer, B.J., and Williams, J.R. 1981. Br. J. Radiol. 54, 882.

Burlin, T.E. 1966. Br. J. Radiol. 39, 727.

Callendar, H.A. 1911. Proc. Phys. Soc. 23, 1.

Calverd, A.M. 1982. J. Phys. E: Sci. Instrum. 15, 414.

Carslaw, H.S. and Jaeger, J.C. 1959. Conduction of Heat in Solids. 2nd ed. (Oxford: Clarenden Press).

Caswell, R.S., Coyne, J.J. and Randolph, M.L. 1980. Radiat. Res. 83, 217.

Caumes, J., Ostrowsky, A., Steinschaden, K., Mancaux, M., Cance, M., Simoen, J.P., Sabattier, R. and Breteau, N. 1984. Strahlentherapie 160, 127.

Cohen, L. 1982. Int. J. Radiat. Oncol. Biol. Phys. 8, 2173.

Domen, S.R. 1980. Med. Phys. 7, 157.

Domen, S.R. 1982. J. Res. NBS, 87, 211.

Domen, S.R. 1983. Int. J. Appl. Radiat. Isot. 34, 643.

Fleming, D.H. and Glass, W.A. 1969. Radiat. Res. 37, 316.

Fletcher, J.W. 1982. AECL 7834 (Chalk River Nuclear Laboratories, Ontario, Canada).

Franz, H. 1971. Phys. Med. Biol. 16, 57.

Genna, S. and Laughlin, J.S. 1956. Radiat. Res. 5, 604.

Goodman, L.J. and Coyne, J.J. 1980. Radiat. Res. 82, 13.

Greene, D. 1962. Phys. Med. Biol. 7, 213.

Greene, D. 1971. Phys. Med. Biol. 16, 489.

Greene, D., Massey, J.B. and Meredith, W.J. 1962. Phys. Med. Biol. 6, 551.

Greene, D., Major, D. and Redpath, T. 1975. Phys. Med. Biol. 20, 244.

Greening, J.R. 1981 in Fundamentals of Radiation Dosimetry (Bristol: Adam Hilger).

Gunn, S.R. 1964. Nucl. Instrum. Meth. 29, 1.

Harder, D. 1965. Symposium on High-Energy Electrons (Montreux) ed. A Zuppinger and G Poretti (Berlin: Springer) p.26.

Hohlfeld, K. 1975. J. Belge de Radiologie, 58, 475.

Holm, N.W., Brynjolfsson, A. and Maul, J.E. 1961 in Selected Topics in Radiation Dosimetry (IAEA, Vienna) p.371.

HPA 1969. Phys. Med. Biol. 14, 1.

HPA1971.ReportSeries No. 4(London:Hospital Physicists' Association).

HPA 1983. Phys. Med. Biol. 28, 1097.

HPA 1985. Phys. Med. Biol. 30, 1169.

Hubbell, J.H. 1977. Radiat. Res. 70, 58.

ICRU 1951. Br. J. Radiol. 24, 54.

ICRU 1954. Br. J. Radiol. 27, 243.

ICRU 1957. Rep. 8 (Washington, DC: ICRU Publications).

ICRU 1962. Rep. 10a (Washington, DC: ICRU publications).

ICRU 1964. Rep. 10b (National Bureau of Standards Handbook, Washington, DC).

ICRU 1969. Rep. 14 (Washington, DC: ICRU Publications).

ICRU 1972. Rep. 21 (Washington, DC: ICRU Publications).

ICRU 1977. Rep. 26 (Washington, DC: ICRU Publications).

ICRU 1980. Rep. 33 (Washington, DC: ICRU Publications).

Inada, T., Sakata, S., Hoshino, K. and Hiraoka, T. 1974. Int. J. Appl. Radiat. Isot., 25, 377.

Kaye, G.W.C. and Laby, T.H. 1973. Tables of Physical and Chemical Constants, 14th ed. (Longman, London).

Kubo, H. 1983. Phys. Med. Biol. 28, 1391.

Kubo, H. 1985. Radiother. Oncol. 4, 275.

Laughlin, J.S. and Beattie, J.W. 1951. Rev. Sci. Instr. 22, 572.

Laughlin, J.S. and Genna, S. 1966 in Radiation Dosimetry Vol. III. Ed. F H Attix and E Tochilin (New York: Academic Press), p.389.

Loevinger, R. 1981. Med. Phys. 8, 1.

McDonald, J.C., Laughlin, J.S. and Freeman, R.E. 1976. Med. Phys. 3, 80.

McLaughlin, E. 1964. Chem. Rev. 64, 389.

Mann, W.B. 1954. J. Res. NBS, 52, 277.

de Marles, A.E.M. 1981. Ph.D. Dissertation, University of Texas, Houston.

Mattsson, O. 1984. Ph.D. Thesis. University of Göteborg, Sweden.

Mijnheer, B.J. and Williams, J.R. 1981. Phys. Med. Biol. 26, 57.

Mijnheer, B.J., Williams, J.R. and Broerse, J.J. 1984. J. Eur. Radiother. 5, 195.

Mijnheer, B.J. and Wittkämper, F.W. 1986. Phys. Med. Biol. 31, 407.

Mitacek, P. and Frigerio, N.A. 1965. Ann. Rept., Biol. Med. Res. Div., Argonne Nat. Lab., ANL-6971, p.112.

Moss, W.T., Brand, W.N. and Battifora, H. 1973 in Radiation Oncology, 4th ed. (C V Mosby, St. Louis, USA), p.33.

NACP 1980. Acta Radiol. Oncol. 19, 55.

Nahum, A.E. 1978. Phys. Med. Biol. 23, 24.

Petterson, C. 1967. Arkiv. for Fysik. 34, 385.

Pinkerton, A.P. 1969. Ann. NY Acad. Sci. 161, 63.

Pruitt, J.S. and Domen, S.R. 1962. J. Res. NBS, 66A, 471.

Redpath, T. 1967. Ph.D. Thesis, University of Edinburgh.

Ross, C.K., Klassen, N.V. and Smith, G.D. 1984. Med. Phys. 11, 653.

Rothman, A. and Nath. R. 1983. Med. Phys. 10, 537.

Rump, W. 1927. Physik 44, 396.

Sabel, M., Schmidt, T. and Pauly, H. 1972. Health Phys. 23, 744.

Schleiger, E.R. and Goldstein, N. 1964. Rev. Sci. Instr. 35, 890.

Schmidt, E. 1924. On the Application of the Calculus of Finite Differences to Heating and Cooling Problems in Engineering, Frappls Fetschrift, Springer, Berlin, p.179.

Schmidt, K. and Buck, W. 1969. Radiat. Res. 40, 473.

Schulz, R.J. 1985. Private communication.

Schulz, R.J. and Rothman, A. 1983. Med. Phys. 10, 538.

Schulz, R.J. and Weinhous, M.S. 1985. Phys. Med. Biol. 30, 1093.

Spencer, L.W. and Attix, F.H. 1955. Radiat. Res. 3, 239.

Tedman, B.N. 1975. Ph.D. Thesis, University of Edinburgh.

Thompson, A.M. and Small, B.E. 1971. Proc. IEE, 118, 1662.

Verlarde, M.G. and Normand, C. 1980. Sci. Am. 243, 93.

Weimer, G. 1972. Atomkernenergie, 20, 327.

Williams, J.R. 1985 in Proc. 5th Symposium on Neutron Dosimetry in Biology and Medicine, EUR 9762, ed. H Schraube and G Burger, Vol. II, p.695 (CEC, Luxembourg).

Williams, J.R. 1984. Private communication.